Temperature-Dependent Studies of Condensed Phase Reaction Dynamics

By

Michael B. Orozco

A dissertation submitted in partial fulfillment
of the requirements for the degree of
Doctor of Philosophy
(Chemistry)
in The University of Michigan
2011

Doctoral Committee:

Professor Roseanne J. Sension, Chair
Professor Eitan Geva
Professor Raoul Kopelman
Professor Duncan G. Steel
Assistant Professor Barry Dunietz

ACKNOWLEDGEMENTS

Looking back, I have come to realize that I never would have made it through this program without the support of a great many individuals. First and foremost I must thank my advisor Dr. Roseanne J. Sension. Without her patience, support and willingness to teach there is no way I could have accomplished what I have. Second, I thank my family and friends for their support and belief in me. Lastly, I would like to thank my colleagues. If it wasn't for their willingness to teach and lend a helping hand I would still be burning my hands in the amplifier.

TABLE OF CONTENTS

LIST OF FIGURES

LIST OF TABLES

ABSTRACT

Transient absorption spectroscopy was used to perform temperature-dependent studies of the reaction dynamics of *cis*-1,3,5-hexatriene (Z-HT), 7-dehydrocholesterol (DHC) and iso-bromoiodomethane (iso-CH_2BrI) in various solvents.

The activation barrier for the ground-state isomerization of cZt-1,3,5-hexatriene to tZt-1,3,5-hexatriene was measured in methanol/propanol (17.4 ± 2.4 kJ/mol), and in cyclohexane/hexadecane (23.5 ± 2.5 kJ/mol). It was found to be independent of which alcohol or alkane was used but dependent on solvent type. Calculations to replicate experimental results were performed in Gaussian 03. In methanol the calculations accurately predicted the barrier height within the error bars of the measurement, while in cyclohexane the calculated results were lower than experimental results. The discrepancy suggested that a more complex calculation was needed in order to explain the experimental results.

The decay of the excited-state absorption (ESA) of DHC was studied in methanol, ethanol, 1-propanol, 1-butanol, 2-butanol, n-heptane and n-hexadecane. The decay of the ESA is biexponential, with a fast component of *ca*. 0.4 – 0.65 ps and a slow component 1.0 - 1.8 ps depending on the solvent. The relative amplitudes are also influenced by the solvent. Temperature dependent results suggested an intrinsic

intramolecular barrier to ring-opening and a solvent dependent barrier arising from friction of the environment on the reaction coordinate. The low viscosity solvents set an upper limit for the intrinsic barrier of *ca*. 4 kJ/mol. A more complete analysis suggests that the intrinsic barrier is *ca.* 2 kJ/mol

The decay of iso-CH_2Br—I was studied in 1-butanol, 2-butanol, methanol and acetonitrile. The results are interpreted using a model consisting of a bimolecular reaction between iso-CH_2Br-I and CH_2BrI and a solvent-assisted unimolecular decay. Rate constants are calculated for the diffusion-controlled bimolecular reaction using three approximations for the diffusion coefficient of the solute particles. Comparison of calculated and measured values suggested that at ≤135 mM, iso-CH_2Br--I decays primarily through a solvent-assisted isomerization in 2-butanol and ≥135 mM the decay is dominated by a diffusion-limited bimolecular collision with another species in 1-and 2-butanol. In methanol and acetonitrile, the decay is presumed to be a bimolecular reaction between contact-pairs and is essentially temperature independent.

Chapter 1. **INTRODUCTION**

Transient absorption spectroscopy (TA) has proven to be a valuable tool for multiple fields of investigation. This technique has been used to study photo-initiated reactions in biology, atmospheric chemistry, organic chemistry and physical chemistry. In chemistry, it has been used to study photo-initiated chemical syntheses[1] in the condensed phase, atmospheric gas-phase radical formation in both the atmosphere and marine layers[2-5] and photodissociation reactions[5-8] in both phases. At the boundary between chemistry and physics, transient absorption has shown promise as a means of coherent control and bond-selective chemistry.[9-11] When TA is paired with temperature control and solvent variation a whole new realm of experiments and measureable quantities are made available. One of the measurable quantities made available through temperature-dependent transient absorption spectroscopy (TD-TA) is the investigation of reaction barriers.

With the use of TD-TA it is possible to determine the presence and relative height of both intrinsic and extrinsic reaction barriers in a reactive system. The first of these barrier types, intrinsic, are a fundamental property of the system being studied. These barriers are expected to be relatively independent of the reaction environment. As a result of this independence the study of the intrinsic reaction barriers provides

valuable information about the molecular energy surface and the dynamics occurring on the surface. Extrinsic barriers, on the other hand, can be heavily influenced by the solvent environment. In particular, the nature of solvent environment will affect the potential energy surface in different ways. In the studies presented here both solvent polarity and viscosity have been varied in a precise, controlled manner to determine how each solvent property affects the relative barriers on the potential energy surface. In order to extract these barrier heights, rate constants are measured at various temperatures in each of the solvents explored.

Once rate constants have been measured for a series of temperatures with in a solvent it is possible to extract the barrier heights using an Arrhenius-type plot. In this plot the natural log of the rate constants is plotted against inverse temperature. The plot, if the process is temperature dependent, can typically to a line using a simple least-squares linear regression. In some cases, the inherent "noise" of the measurements may call for a more complicated weighted least-square which discounts values with larger error bars. In either case, the linear plot created is fit to a line whose slope represent reaction barrier and the intercept the Arrhenius prefactor. When these plots are compared for solvent of varying polarity and viscosity it is possible compare the effect of each on the system.

In the following chapters, the results of temperature-dependent transient absorption measurements are presented for three systems. In each case, experiments were performed to measure extrinsic barriers as well as intrinsic barriers if present. It

was determined that in all of the systems investigated there is some form of an isomerization element with a corresponding barrier. To extract the relative barrier heights in each of the systems an Arrhenius-type plot, as previously described, was made. The dependence of the extrinsic barrier on the reaction environment was then determined in each system though careful variation of the solvent environment. In particular, the effects of solvent polarity and viscosity were explored for each barrier.

Chapter 2 reports on the influence of solvent on the ground state conformational relaxation of cis-1,3,5-hexatriene (Z-HT). Originally, Z-HT comes from the ring-opening reaction of the cyclohexadiene (CHD) following UV excitation [12,13]. CHD is the chromophore of 7-dehydrocholesterol (DHC) which, in turn, is the precursor to vitamin D production in vivo. To study the influence of solvent the decay of cZt-HT through single-bond isomerization to tZt-HT (Figure 1.1), following solvent-aided thermalization, was measured in methanol, 1-propanol, cyclohexane, and hexadecane. Activation barriers for the isomerization were extracted from the data in each solvent and compared to determine the effects of different solvent types. Calculations were performed in an attempt to replicate and provide insight into the observed solvent dependence. The measurements were then compared to earlier studies of the conformational relaxation dynamics of Z-HT produced from 1,3-cyclohexadiene (CHD) in methanol and n-propanol solvents[13] and to investigations performed in cyclohexane and hexadecane solvents.[12] The results are then discussed in the context of transition state theory and of Kramers' theory for condensed phase reaction dynamics.

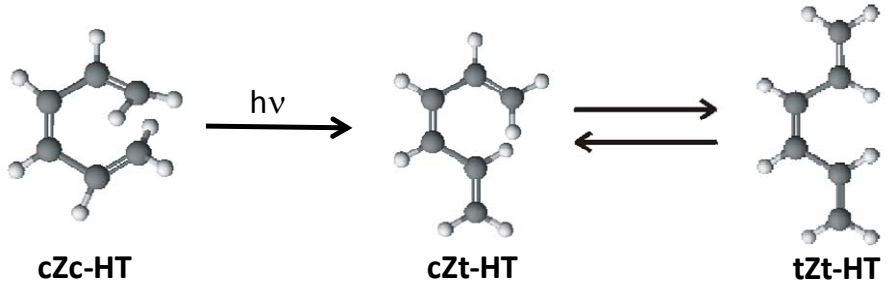

Figure 1.1: Outline of isomerization of cZt-HT to tZt-HT following direct excitation of cZc-HT (Z-HT)

In the field of biology, photochemical isomerization reactions of simple polyene chromophores have been shown to play a key role in the function of many important systems.[14,15] Typical examples include the *cis-trans* isomerization reactions of retinal in rhodopsins and of the chromophore in photoactive yellow protein[14-16] as well as the electrocyclic ring-opening reaction of 7 -dehydrocholesterol (provitamin D_3, DHC).[17-20]

In Chapter 3 the results of temperature-dependent measurements performed on 7-dehydrocholesterol (DHC) in methanol, ethanol, 1-propanol, 1-butanol, 2-butanol, n-heptane and n-hexadecane are presented. The experiments measured the decay of the excited state absorption of DHC and the influence of the solvent environment on the excited state dynamics. The results of the investigations suggest that the ESA relaxes thorough a biexponential decay with a fast component of *ca*. 0.4 – 0.65 ps and a slow component 1.0 - 1.8 ps, depending on the solvent. The relative amplitudes of the fast and slow components were likewise found to be influenced by the solvent. These results were supported by broadband UV-visible femtosecond transient absorption spectroscopy and steady-state integrated fluorescence measurements performed by K.C. Tang and A. Rury, respectively.[21]

As previously mentioned, transient absorption spectroscopy has proven useful in studies of atmospheric chemistry and in measuring solvent effect on photofragment recombination. Bromoiodomethane has proven equally useful for studies in both those fields of study.[6,22,23]

In Chapter 4 measurements of the decay of the metastable-species, iso-CH_2Br—I (Figure 1.2) are presented. Iso-CH_2Br--I is produced through the recombination of CH_2Br and I photofragments resulting from A-Band excitation of CH_2BrI at 271nm. Temperature-dependent transient absorption measurements using narrow band detection at 460 nm (near the peak of the iso-CH_2Br--I absorption) were performed in methanol, 1-butanol, 2-butanol and acetonitrile to determine the influence of solvent on the decay of the iso species. Broadband spectral measurements are also presented for samples of various concentrations at room temperature. The results are interpreted in terms of a model that includes both bimolecular reaction of iso-CH_2Br--I with ground state CH_2BrI and solvent-assisted unimolecular decay of the iso-CH_2Br--I.

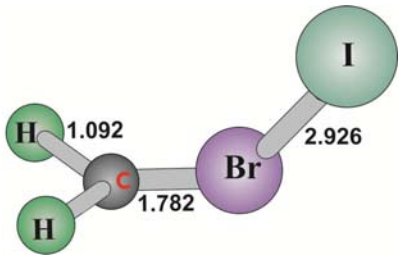

Figure 1.2: Optimized geometry of iso-CH_2Br—I calculated (DFT) by Wang et al.[24]

The date collected for each of the systems explored here provides valuable insight in to the nature of both intrinsic and extrinsic barriers as well as the

corresponding potential energy surfaces. Through comparison of the results the effects of solvent on the reaction surfaces has been explored. In these studies the effects viscosity and friction on the potential surface have observed as well as how solvent polarity may raise or lower barrier heights. In addition to providing information about the potential energy surfaces, these studies provide valuable insight into the nature of reaction rates through the examination of three types of reactions.

One of these reactions types is intramolecular, which we explored through the single-bond isomerization of *cis*-1,3,5-hexatriene and the excited state decay of 7-dehydrocholesterol. A second is photo-fragment recombination which led to the formation of iso-bromoiodomethane following UV excitation of bromoiodomethane. The third reaction type, intermolecular, occurs between at least two molecules and was observed in the decay of the iso- species. In each case, the results of the measurements could be used to compare the accuracy and limitations of various solvent models. And, in the case of bromoiodomethane, to compare three methods of modeling solvation.

Chapter 2. **CIS-1,3,5-HEXATRIENE: SYNTHESIS, ISOLATION AND INVESTIGATION**[1]

BACKGROUND

Solvent-solute interactions play a vital role in chemical reactions by influencing the reactivity of, and energy flow within, the species involved. The ring-opening reaction of 1,3-cyclohexadiene (CHD) and subsequent relaxation of hot 1,3,5-*cis*-hexatriene (Z-HT) provides an interesting paradigm for the detailed investigation of energy flow in a chemical system. Several groups have investigated both the electrocyclic ring-opening reaction of CHD,[25-50] and of the related 7-dehydrocholesterol chromophore responsible for the photoreaction that results in vitamin D formation.[51-55] Initial UV excitation of CHD produces a population in the 1^1B state which decays by internal conversion to an optically forbidden 2^1A state on a time scale of ca. 10 fs.[28,55] The electrocyclic ring opening reaction of CHD occurs on the 2^1A state and produces vibrationally hot *cis*-1,3,5-hexatriene with a quantum yield of 0.40.[25] A cartoon illustrating this process is sketched in Figure 2.1.

[1] Extracted from: Harris, D.A, Orozco, M.B. and Sension, R.J.,"*Solvent dependent conformation dynamics of cis-1,3,5-hexatriene*", Journal of Physical Chemistry A **110**(30):9325-9333, **2006**; With the exception of synthetic methods and solvent enhanced structural calculations.

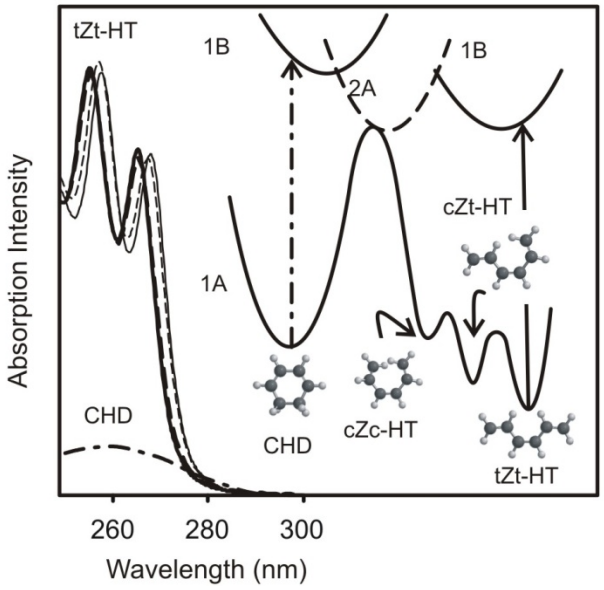

Figure 2.1: (left) Ground state absorption spectra of CHD in cyclohexane (dot dashed line) and Z-HT in cyclohexane (thin dashed line), hexadecane (thin solid line), methanol (thicker solid line) and 1-propanol (thicker dashed line). The spectrum of CHD does not change significantly with solvent. (right) Cartoon of relevant potential energy surfaces for the CHD ring opening reaction

Upon ground state recovery following photo-initiation of the ring-opening reaction, rapid interconversion among the three conformers of HT produces a dynamic equilibrium mixture of cZc-HT, cZt-HT, and tZt-HT (where the labels c and t designate *cis* (or more precisely *gauche*) and *trans* configurations about the single bonds). As the molecules relax, the mixture evolves in composition and deposits energy into the surrounding solvent. Thermal equilibration with the solvent occurs on a time scale of 0-20 picoseconds, leaving a small population of cZt-HT molecules trapped for a period >100 ps by the barrier for single bond isomerization to tZt-HT[56,57].

The ground state relaxation of hot Z-HT was analyzed by Anderson *et. al.* [56] using a time dependent molecular temperature in the context of Kramers' theory for barrier crossing processes.[41,58] These studies demonstrated that the rate of relaxation is

essentially independent of the macroscopic solvent shear viscosity (η), with little difference in the rate measured in cyclohexane (η = 0.894 mPa s, 25°C)[59] and hexadecane (η= 3.032 mPa s, 25°C) solvents. In contrast the relaxation observed by Lochbrunner et al. in ethanol (η = 1.074 mPa s, 25°C) is approximately four times faster than in the alkanes.[41,44] In addition, the absolute magnitude of the trapped cZt-HT population is lower in ethanol than in the alkanes. These results posed a conundrum as solvent polarity is expected to have little influence on the barrier for single bond isomerization and the typical mode of interaction in a barrier crossing process is correlated with the solvent friction and thus the solvent viscosity.

The influence of solvent on the conformational relaxation of Z-HT is discussed herein. These studies used temperature as a tool to explore the influence of solvent on the ground state barrier for the cZt-HT $\rightarrow$ tZt-HT conformational isomerization in methanol, cyclohexane, propanol and hexadecane.

EXPERIMENTAL PARAMETERS

Pump-probe transient absorption experiments were performed using 0.3 mJ laser pulses from a homebuilt 1 kHz titanium-sapphire laser system. 1,3,5-hexatriene samples were prepared in solution to have an optical density of approximately 1 at 267 nm for a 1 mm sample thickness. A pump and flow cell were used to refresh the sample volume between laser shots. The sample was excited at 267 nm with the output of a 3rd

harmonic generation setup consisting [60-62]of two cascaded nonlinear stages: second harmonic generation, followed by sum frequency generation.

In order to study the temperature dependence of the cZt-HT -> tZt-HT isomerization barrier it was necessary to have a significant population of the cZt-HT isomer. Direct excitation of Z-HT resulted in an excited population of purely hot HT opposed to experiments where CHD was excited to produce hot HT with only a 40% yield.[63] The increased yield effectively reduces background contributions to the transient absorption signal. In previous experiments, HT was commercially available as a mixture of isomers and the isomers separated[34]. At the time of these studies HT was no longer commercially available and so a method of synthesis was sought out. The ideal synthetic method would have a high yield and be stereo-specific - eliminating the need for a lossy separation step to isolate pure Z-HT. With those two requirements in mind three methods of synthesis were assembled and attempted.[60-62]

SYNTHESIS AND SEPARATION OF *CIS*-1,3,5-HEXATRIENE

The first of the two experimental synthetic methods was the irradiation of CHD with UV light. As previously mentioned, the closed-ring CHD molecule opens with a quantum yield of 0.40 to produce Z-HT. It is reasonable to assume that given a long enough irradiation all CHD molecules would be converted to HT. In designing this method it was clear that the end product would be a mixture of isomers and necessitate separation. While the requirement of a separation step is not in keeping with the

previously mentioned requirements the simplicity of the method overshadowed the shortcoming. As such, a separation method outlined by Hwa et. al.[62] was appended and the proposed method implemented.

CHD was purchased from Sigma-Aldrich, transferred to a sealed, quartz EPR tube and placed in a UV reactor for ~48hrs (Figure 2.2). After irradiation the tube was removed from the reactor and it was observed that the starting material had been converted to a polymer mass. The mass was examined for traces of hexatriene, but to no avail. Clearly a more involved synthetic method was required.

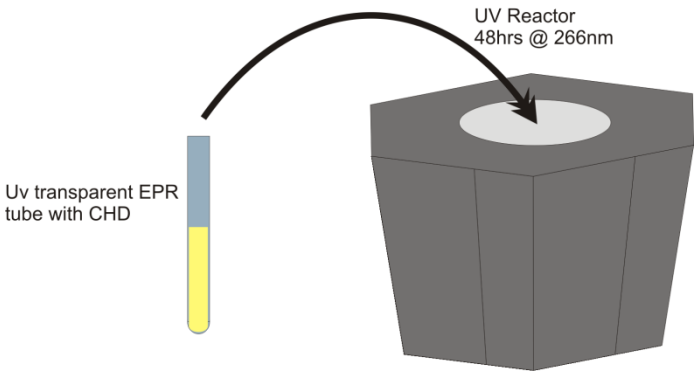

Figure 2.2: Diagram of first experimental synthesis wherein 1,3-cycohexadiene was placed in a UV transparent EPR tube irradiated in a UV reactor (centered at 266nm) for 48hrs.

The next method focused on minimizing losses that occur during transfers between reaction vessels and biasing the ratio of products in favor of the Z-HT. A literature review yielded two methods outlined by Chandrasekhar *et. al.*[64] and Danishefsky *et. al.*[61] which when combined would yield pure Z-HT through the hydrogenation of 1,6-Bis(trimethylsilyl)Hex-3-ene-1,5-dyne (TMS). The structure of 1,6-Bis(trimethylsilyl)Hex-3-ene-1,5-dyne (TMS) is such that the triple-bonds restrict the

molecule from isomerizing to the E- configuration during the removal of the trimethylsilyl groups. As outlined in Figure 2.3, TMS (Oakwood Products Inc.) was taken directly and treated with LiOH in a solution of THF and water according to the method outlined by Danishefsky *et. al.*[61]. In the vessel, LiOH stripped the trimethylsilyl groups from the molecule and replaced them with hydroxides. Anhydrous ether was then used to extract the resulting *cis*-Hex-3-ene-1,5-dyne and the solution placed in a Rotovapor® to remove the ether. The pure *cis*-Hex-3-ene-1,5-dyne left behind was then transferred to a reaction vessel containing PEG(400), Quinoline, $Pd/CaCO_3$ (Lindlar catalyst) and placed under a hydrogen atmosphere as outlined by Chandrasekhar *et. al.*[64] The Lindlar catalyst, in conjunction with the hydrogen atmosphere, specifically hydrogenated the triple-bonds to double-bonds without affecting the central double-bond. The transformation of *cis*-hex-3-ene-1,5-dyne into *cis*-1,3,5-hexatriene was successful.

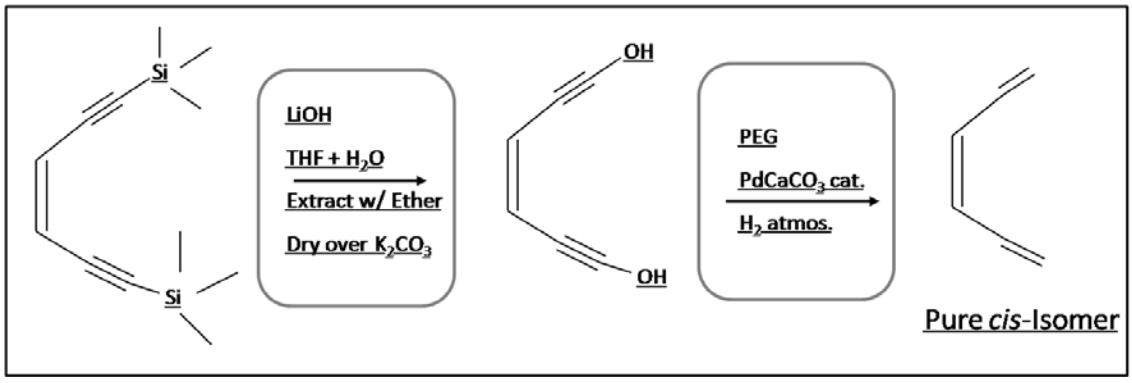

Figure 2.3: Outline of the 2nd experimental synthesis wherein 1,6-Bis(trimethylsilyl)Hex-3-ene-1,5-dyne is converted to Hexa-3-ene-1,5-dyne[61]which is then hydrogenated[60] to Z-1,3,5-hexatrienes.

This second synthetic method, having been successful, should have been the high yield, stereo-specific reaction desired. Unfortunately, TMS is a highly specialized

reagent, expensive, and only available in small quantities (TMS being sold by milligram). Even with HT having a high extinction coefficient, the amount of Z-HT required to complete the planned experiments was on the gram scale. In order to obtain the necessary yields a third, larger scale, means of the production of Z-HT was sought out. The third, and most complex, method was a revision of that outlined by Hwa *et. al.*[62]

Previously examined, the method outlined by Hwa *et. al.* had been rejected due to the number of steps, the lack of stereo-specificity and the large amounts of reagents involved. However, the method was now the most viable means of obtaining HT and so it was attempted with some modifications. In revising the procedure, the reagent amounts were reduced and a portion of the synthesis was omitted. Part A of the synthesis called for a Grignard reaction between allyl bromide and Acrolein to produce 1,5-Hexadiene-3-ol for use in Part B. At the time of synthesis, 1,5-Hexadien-3-ol was commercially available from Sigma-Aldrich and could be purchased in sufficient quantities to justify the exclusion of Part A. With those two modifications the synthesis and separation of Z-HT were successfully performed as outlined by Hwa *et. al.* [62] (Figure 2.4)

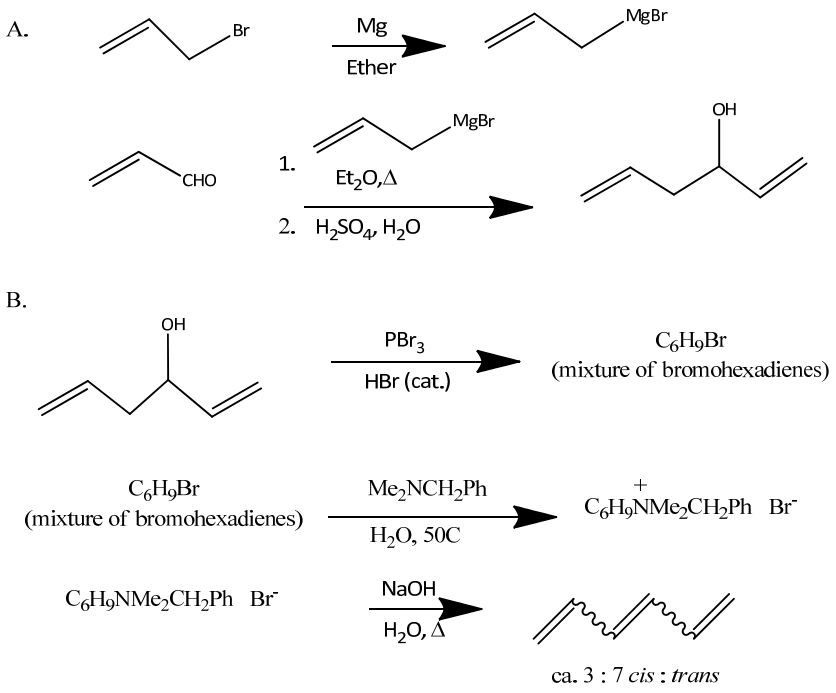

Figure 2.4: Synthesis of 1,3,5-hexatriene from allyl bromide as outlined by Hwa et al.[62]

TRANSIENT ABSORPTION MEASUREMENTS

One color ($\lambda_{pump} = \lambda_{probe} = 266$ nm) transient absorption kinetics traces were obtained for Z-HT as a function of temperature. The pump pulse was produced as described above. The probe pulse was obtained by sending a portion of the 800 nm fundamental laser beam onto a 1.5 m computer controlled delay stage. This delay stage permits accurate measurements spanning six decades in time from 10 fs to 10 ns. The third harmonic was generated by using back-to-back BBO crystals after the stage. The first crystal is used for Second Harmonic Generation, and the second crystal produces the third harmonic through sum frequency generation. The 800 nm beam was carefully aligned on the delay stage to ensure that the pulse energy of the third harmonic probe

was the same when the retro-reflector was at the back of the stage and at the front of the stage. The pump and probe polarizations were oriented at magic angle (54.7˚) with respect to each other to eliminate the influence of rotational relaxation, allowing for the direct observation of the population relaxation.

Temperature control was achieved by immersing the sample reservoir in a bath with a 50/50 mixture of water and ethylene glycol. The temperature of the bath was controlled by a NesLab RTE-111 Refrigerated Bath/ Circulators, capable of maintaining temperatures from -25˚C to +150˚C. The sample was flowed with a peristaltic pump and the temperature was measured with a temperature probe inserted in a T-joint located immediately after the sample cell. The temperature of the solvents were varied from 15°C to 70°C in cyclohexane, 21°C to 80°C in hexadecane, 10°C to 56°C in methanol and 10°C to 76°C in n-propanol. The temperature was maintained with an accuracy of ± 0.5°C.

RESULTS

GROUND STATE BARRIER FOR CZT-HT → TZT-HT ISOMERIZATION[65]

Previous measurements observed a long time transient absorption signal following excitation of CHD. The signal was attributed to the trapping of the ground state cZt-HT population following formation of Z-HT. To get a better observation of the cZt-HT population dynamics the ground state recovery of initially excited Z-HT has been measured instead of initially excited CHD.

One color ($\lambda_{pump} = \lambda_{probe} = 266$ nm) transient absorption kinetics traces were obtained for Z-HT in cyclohexane, hexadecane, propanol and methanol as a function of temperature between 10°C and 80°C to observe the effect of solvent polarity on the ground state conformational relaxation of Z-HT. A typical trace is shown in Figure 2.5.

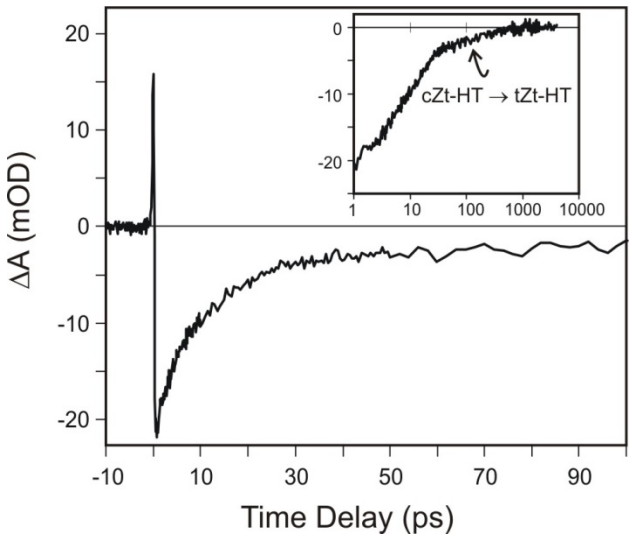

Figure 2.5: Transient absorption kinetics of Z-HT in methanol at 19˚C. The rapid (<50 ps) bleach recovery is independent of the solvent temperature over the temperature range studied, but the long time (>50 ps) residual recovery displays a notable temperature dependence. The data in the inset is plotted on a logarithmic time scale to highlight the temperature dependent component corresponding to the slow relaxation of trapped cZt-HT.

The ground state recovery shows two distinct temporal regions. The fast component (< 50 ps) corresponded to the thermalization of hot Z-HT following internal conversion from the excited electronic state. That component was essentially independent of the bulk solvent temperature. The slower component (> 50 ps) corresponded to the decay of the population of the trapped cZt-HT conformer after thermalization with the surrounding solvent. The rate of decay of this latter component is strongly dependent on the temperature of the bulk solution. The transient absorption

traces for times longer than 40 or 50 ps were well modeled by a single exponential decay. These data were analyzed using an Arrhenius type equation for the rate constant:

$$k = A_h e^{-E_a / RT} \tag{1}$$

An activation energy barrier height for the cZt-HT $\rightarrow$ tZt-HT transition was extracted from the slope of a plot of ln (k) vs. 1/T.

$$\ln(k) = \frac{E_a}{RT} + \ln\left(A_h\right) \tag{2}$$

These linear fits to the data are plotted in Figure 2.6. It is important to note, however, that the errors are not constant and a weighted least squares method must be used to extract accurate values and error estimates for E_a and A_h. Fits obtained for the two alkane solvents are indistinguishable within the scatter of the data (see the inset in Figure 2.5). The same is true of the alcohol solvents, although the data sets are smaller, and the scatter is larger, resulting in a greater uncertainty in the parameters of the fit. In the analysis that follows the data obtained in both alcohols will be grouped together as will the data obtained in both alkanes.

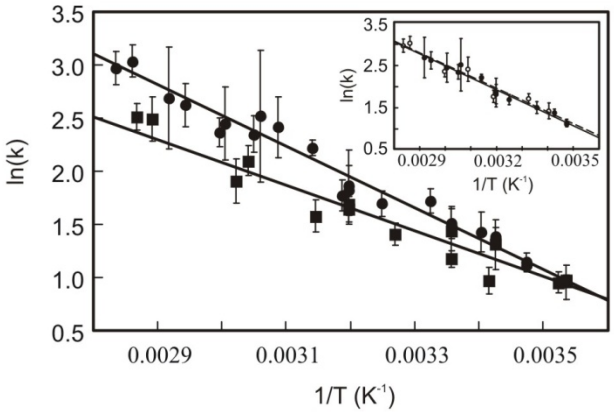

Figure 2.6: Weighted linear least squares fit of the rate constants (ns^{-1}) as a function of temperature to Equation 3. The best fit parameters are Alcohols (squares): $E_a = 17.2 \pm 2.4$ kJ/mol, $A_h = 3.8$ (-2.3, +6.2) $\times 10^{12}$ s^{-1}, and Alkanes (circles): $E_a = 23.5 \pm 2.5$ kJ/mol, $A_h = 6.0$ (-3.8, +10.1)$\times 10^{13}$ s^{-1}. The error ranges are calculated as the standard uncertainties in a weighted least-squares fit. The inset shows a comparison of the fits for hexadecane (open circles, dashed line) and cyclohexane (filled circles, solid line) separately.

An activation energy barrier height for the cZt-HT $\rightarrow$ tZt-HT transition was also extracted directly via a nonlinear fit directly to Equation 1. Fits to the data in both alkane and alcohol solvents are plotted in Figure 2.7. In both cases the reduced chi square for the best fit is near 1 (1.0815 in alcohols and 0.8343 in alkanes). The range of values for the parameters A_h and E_a consistent with the data are highly correlated. These ranges are illustrated in the form of contour plots of $\chi_r^2(A_h, E_a)$ in Figure 2.8.

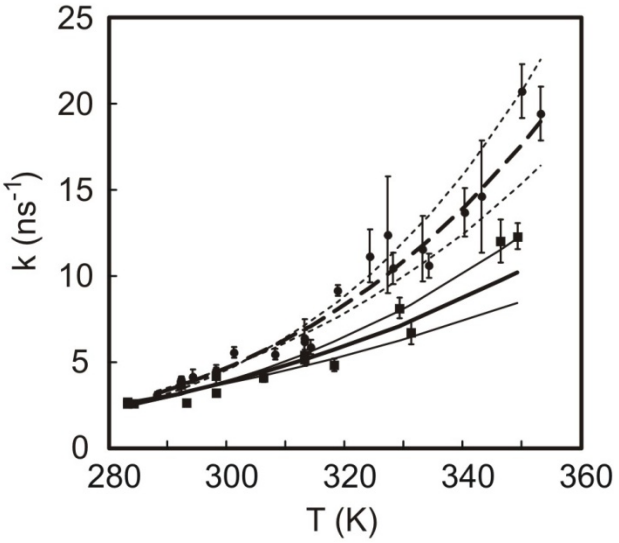

Figure 2.7: Fits of the rate constants obtained for the cZt→tZt isomerization to an Arrhenius expression. Circles and dashed curves are the rates in alkanes, while the squares and solid curves are the rated in alcohols. The thin lines represent the ranges calculated using parameters for Ah and Ea for which $\chi_r^2 \leq \chi_r^2$ (min) + 0.2. The best fit parameters are Alcohols: E_a = 17.4 kJ/mol, $A_h = 4.1 \times 10^{12}$ s^{-1}, and Alkanes: E_a = 23.2 kJ/mol, $A_h = 5.2 \times 10^{13}$ s^{-1}.

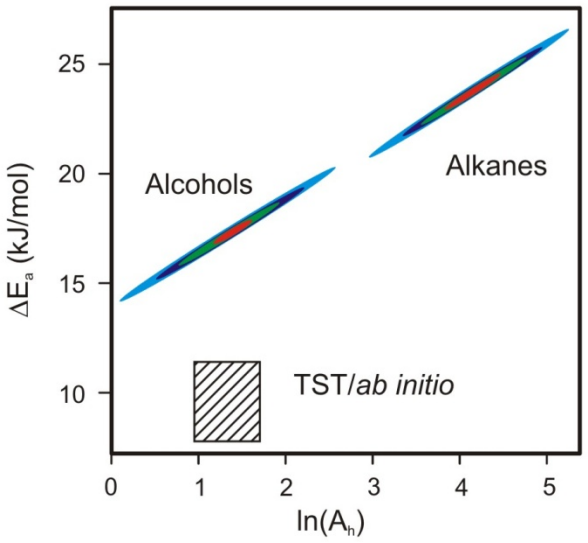

Figure 2.8: Contour plot of χ_r^2 as a function of the fit parameters Ah and Ea for the data obtained in alcohols and alkanes. The contours are red: χ_r^2 within 0.01 of the minimum, green: χ_r^2 within 0.05 of the minimum, dark blue: χ_r^2 within 0.1 of the minimum, light blue χ_r^2 within 0.2 of the minimum. The dashed box represents the range of barriers calculated as described in the text and the range for A_h calculated using transition state theory. The dark blue ellipses are essentially equivalent to the error ranges obtained in the weighted linear least squares fit.

From this data set it is clear that the relaxation of cZt-HT in thermal equilibrium with the solvent is consistently faster in the alkane solvents than in the alcohol solvents. This is in striking contrast to the observation for the hot HT initially formed following excitation of CHD where relaxation in alcohols is faster than in alkanes.[63] It is also noteworthy that within the scatter of the data set there is no significant dependence on the specific alcohol or alkane solvent. The effective barrier for the cZt-HT $\rightarrow$ tZt-HT single bond isomerization in the alkane solvents (23.5 $\pm$ 2.5 kJ/mol) is higher than the effective barrier in alcohol solvents (17.2 $\pm$ 2.4 kJ/mol). The Arrhenius prefactor is an order of magnitude smaller in alcohol solvents, $A_h = 4\times10^{12}$ s^{-1}, than in alkane solvents, $A_h = 6\times10^{13}$ s^{-1}.

DISCUSSION

COMPARISON OF THE cZT → tZT-HT BARRIER WITH OTHER CALCULATIONS AND EXPERIMENTS

The activation barriers reported above for the cZt→tZt isomerization are in reasonable agreement with similar measurements reported in the literature for other polyenes. The barrier for the cEtEt→tEtEt single bond isomerization of trans-octatetraene was determined by photoproduction of cEtEt and thermal recovery of the tEtEt ground state at low temperature in an alkane matrix.[66] In this experiment the disappearance of the cEtEt conformer was monitored at 6 temperatures between 49 and 53K. The data was fit to an Arrhenius expression, Equation 2, yielding a barrier of 16.4 ± 0.8 kJ/mol. A somewhat lower barrier has been deduced for butadiene from high resolution Raman spectra of overtone torsional vibrations in the gas phase (13 kJ/mol for g→t).[67] Finally, it should be noted that this barrier is similar to the barrier reported for the related cZc→cZt isomerization of previtamin D in ethanol (15.5 ± 1 kJ/mol).[52]

A few calculations of the cZt→tZt isomerization of hexatriene have been reported in the literature. Calculations performed with GAUSSIAN92 gave a barrier of 8.6 kJ/mol (720 cm^{-1}) from the RHF (6-31G*) calculation reported earlier,[50] while a slightly higher barrier of 13.6 (11.2 with zero point correction) kJ/mol was reported for a calculation using DFT(B3LYP/6-31G**) methods.[46] These calculated barriers were much smaller than the experimentally determined effective barriers for Z-HT and did not include solvation effects.

In addition to Gaussian 92 calculations, torsional potentials for single bond isomerization in 1,3-butadiene and cZt→tZt-HT were performed in Spartan 04 (Wavefunction, Inc. Irvine CA) and are plotted in Figure 2.9.[63] These potentials were calculated using the RHF 6-31G* *ab initio* method and the B3LYP/6-31G** density functional method with optimization of all other coordinates at each constrained value of the torsional angle. For all calculations the *trans* configuration is defined as 180° while the *cis* configuration is defined as 0°. The torsional potential for butadiene is in good agreement with the HF calculation reported by Fabiano and Della Sala[68], in qualitative agreement with the other calculations reported, and in excellent, although somewhat fortuitous, agreement with the experimental barrier. In contrast to the experimental observation on Z-HT however, this RHF 6-31G* calculation predicts a lower barrier for cZt→tZt-HT isomerization in hexatriene than for c→t isomerization in butadiene. The B3LYP density functional calculation predicts a higher barrier for the c→t isomerization for both butadiene and hexatriene, in good agreement with the results both of Fabiano and Della Sala for butadiene[68] and of Henseler *et al.* for hexatriene.[45,46].

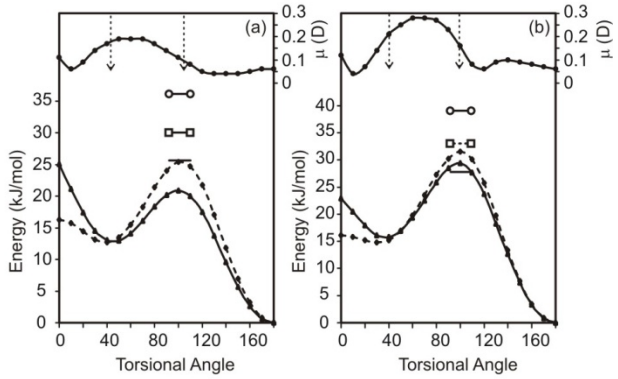

Figure 2.9: Calculated torsional potentials for the c→t isomerization of 1,3-butadiene (dashed line, diamonds) and the cZt→ tZt isomerization of 1,3,5-hexatriene (solid line, triangles) (a) RHF 6-31G*; (b) B3LYP/6-31G. The angle is defined as 0° in the cis configuration and 180° in the trans configuration. The horizontal lines represent the experimental barriers for c→t isomerization, butadiene vapor (no end caps), Z-HT in alcohols (square end caps), Z-HT in alkanes (circle end caps). The calculated dipole moment (circles) is plotted along the scale on the right axis for each method. The vertical dashed arrows indicate the approximate positions of the cZt minimum (ca. 40°) and the cZt→tZt transition state (ca. 100°).**

The dependence of torsional barriers on environment and on environmental friction has been the subject of many investigations. Most of these studies have dealt with the motion of groups much larger than the $C=CH_2$ group displaced in the single bond isomerizations reactions described here. In particular, the excited state isomerization of *trans*-stilbene has been the subject of exhaustive investigation.[69-87] The effective barrier obtained from Arrhenius plots of the *trans*-stilbene lifetime in a series of alkanes contains a contribution arising from the activation energy for viscous flow acting as a friction on the reaction coordinate. Sun and Saltiel have reported a careful comparison of the excited state *trans*→ p isomerization of stilbene and determined that the intrinsic barrier for isomerization in alkanes was independent of solvent, ΔH_t = 11.9 kJ/mol.[79] If a torsional frequency of ca. 100 cm^{-1} is assumed, the transition state barrier is 13.8 kJ/mole (*vide infra*),[80] in good agreement with the gas phase value of *ca*. 14

kJ/mol. Extensive investigations by Troe and co-workers have also identified minimal medium effects on excited state torsional barriers in low viscosity nonpolar solvents for a broad range of stilbene and diphenylbutadiene derivatives.[87]

While the excited state isomerization of *trans*-stilbene is in many respects similar to the cZt→tZt isomerization of hexatriene, there are distinct differences as well. The hexatriene molecule is smaller than *trans*-stilbene, and the reorientational diffusion is faster. The time scale for the reorientation of Z-HT is estimated to be ca. 4 ps in cyclohexane assuming slip boundary conditions, in good agreement with the 5 ps decay of the absorption anisotropy.[50] The reorientation should be as fast or faster in the two alcohol solvents. The reorientation may be somewhat slower in hexadecane, but is still fast compared with the time scale for single bond isomerization. In addition, the $=CH_2$ group displaced in the cZt→tZt isomerization of hexatriene is much smaller than the phenyl group displaced in the isomerization of *trans*-stilbene. The change in volume may be estimated from the reaction coordinate calculations described above, with the prediction of a volume change no larger than 0.35% along the reaction coordinate. Because the reorientational diffusion is fast with respect to the cZt→tZt isomerization, and the volume change is small, the molecule can easily reorient during the reaction. These observations are consistent with the insignificant viscosity dependence manifest in the data. It is unlikely that the frictional influence of viscous flow on this small volume change will have a substantial influence on the effective barrier height for this single bond isomerization reaction.

The excited state trans→ p isomerization of stilbene is substantially faster in polar than in nonpolar solvents of comparable viscosity.[88] This effect has been attributed to the influence of the medium on the intrinsic barrier for activation and on the influence of solvation dynamics on the isomerization coordinate.[82] The barrier in the S_1 state of *trans*-stilbene is generally attributed to an avoided crossing between electronic states and it is relatively easy to imagine a mechanism by which solvent polarity could influence the barrier height. In contrast, the cZt→tZt isomerization is a ground state single bond rotation, albeit within the π framework of a conjugated polyene. The dipole moment of the molecule will vary as a function of the torsional angle although the variation is expected to be small.

The magnitude of the dipole moment of Z-HT calculated for both the RHF 6-63G* and B3LYP/6-31G** DFT calculations is plotted in Figure 2.9. The change in dipole moment along the reaction coordinate may provide a mechanism to modify the torsional potential in polar solvents. However, the change in the magnitude of the dipole moment is modest in the DFT calculation, and even smaller in the RHF calculation. Although there is a change in direction as well as in magnitude of the dipole, fast solute reorientation will minimize the influence of the dipole direction on the activation energy. Rapid solvation by methanol (ca. 5 ps) and propanol (ca. 26 ps) will also serve to mitigate the influence of the change in dipole direction on the effective barrier for isomerization.[89]

The torsional potential calculations discussed above did not account for solvent effects upon the cZt→tZt-HT isomerization. In order to account for solvent effects upon the single bond isomerization Gaussian 03 was used. As above, torsional potentials were calculated using the RHF 6-31G* *ab initio* method and the B3LYP/6-31G** density functional method with the *trans* and *cis* configurations defined as 180° and 0° respectively. The structures were optimized at each constrained torsional angle, similar to the previously mentioned Spartan 04 calculation, and a continuum solvent model included in the calculation. Potentials calculated using Gaussian 03 are shown in Figure 2.10 both without solvent and with a continuum models representing cyclohexane and methanol.

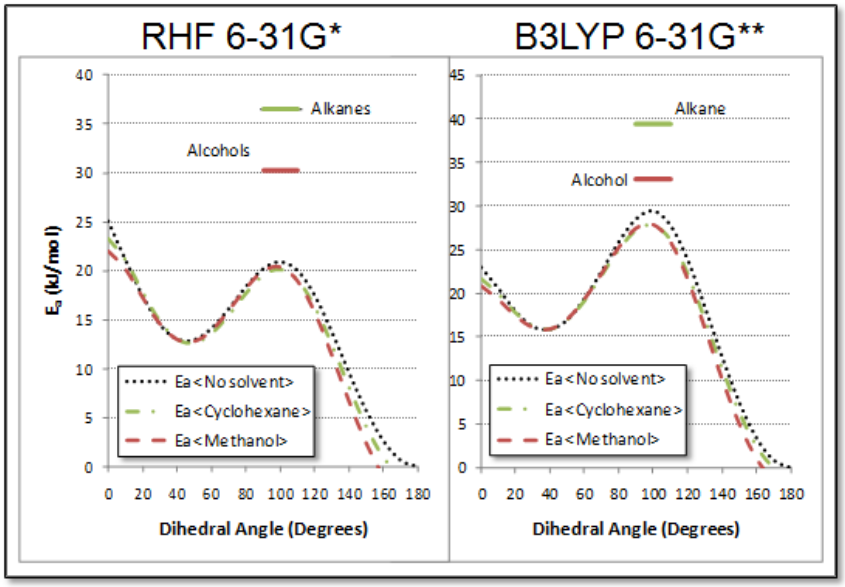

Figure 2.10: Calculated torsional potentials for cZt→ tZt isomerization of 1,3,5-hexatriene performed with (left) RHF 6-31G*; (Right) B3LYP/6-31G without solvent (black dotted), in cyclohexane (green dot-dash) and in methanol (red dashed). The angle is defined as 0° in the cis configuration and 180° in the trans configuration. The horizontal lines represent the experimental barriers Z-HT in alcohols (red), Z-HT in alkanes (green).**

Barrier heights in both cyclohexane and methanol were calculated using two continuum solvent models with both the RHF (6-31G*) and DFT (B3LYP 6-31G**) methods (Table 2.1). For cyclohexane the calculated barrier heights were 7.3 kJ/mol RHF (6-31G*), 11.8 kJ/mol DFT (B3LYP 6-31G**) using the IEFPCM solvent model and 7.4 kJ/mol RHF (6-31G*), 11.8 kJ/mol DFT (B3LYP 6-31G*) with the CPCM solvent model. For methanol the values were 7.5 kJ/mol RHF (6-31G*) and 11.8 kJ/mol DFT (B3LYP 6-31G**) in the IEFPCM solvent model 7.5 kJ/mol RHF (6-31G*) and 11.9 kJ/mol DFT (B3LYP 6-31G**) in the CPCM solvent model. The calculated barrier heights for cyclohexane fell below the alkane experimental value regardless of the solvent model used in either method. The discrepancy between calculated and experimental barrier heights made it apparent that the inclusion of a continuum model for the solvent was insufficient to replicate the dynamics occurring in cyclohexane. In methanol the calculations performed with the RHF (6-31G*) and DFT (B3LYP 6-31G**) methods and both solvent models resulted in calculated barrier heights which fell within the error bars of the alcohol experimental value.

Isomer and (solvent model)	RHF (6-31G*) Barrier Height (kJ/mol)	RHF (6-31G*) Difference b/n theory and experiment (kJ/mol)	DFT (B3LYP 6-31G**) Barrier Height (kJ/mol)	DFT (B3LYP 6-31G**) Difference b/n theory and experiment (kJ/mol)	Solvent
cZt					none
tZt					none
trans	7.279	---	11.850	---	none
cZtC(IEFPCM)					Cyclohexane
tZtC(IEFPCM)					Cyclohexane
transC(IEFPCM)	7.305	**-16.195**	11.787	**-11.713**	Cyclohexane
cZtM(IEFPCM)					Methanol
tZtM(IEFPCM)					Methanol
transM(IEFPCM)	7.526	**-9.874**	11.845	**-5.555**	Methanol
cZtC(CPCM)					Cyclohexane
tZtC(CPCM)					Cyclohexane
transC(CPCM)	7.389	**-16.111**	11.829	**-11.671**	Cyclohexane
cZtM(CPCM)					Methanol
tZtM(CPCM)					Methanol
transM(CPCM)	7.544	**-9.856**	11.858	**-5.542**	Methanol

Table 2.1: Calculated energies and barrier heights for cZt→tZt isomerization of 1,3,5-hexatriene performed with RHF (6-31G*) and DFT (B3LYP 6-31G*). Values were obtained with both methods and calculated using both IEFPCM and CPCM continuum solvent models. The differences between calculated and experimental results for the barrier height are also listed.

In addition to calculations in Spartan and Gaussian molecular dynamics simulations of the cZt→tZt-HT isomerization have been performed by the Geva group in both cyclohexane and methanol. The results were able to replicate the faster relaxation in methanol compared to cyclohexane and it was speculated that it was an entropic effect. In the model, cyclohexane molecules were shown to more easily envelop the cZt-HT molecule which had the effect of stabilizing the isomer and lowering the barrier to isomerization. However, in addition to stabilization the close packing between cyclohexane and cZt-HT molecules inhibited the bond rotation to form tZt-HT. With the motion inhibited the rate of isomerization in cyclohexane is reduced when compared to methanol.[90]

INTERPRETATION OF THE ARRHENIUS PREFACTOR

In the context of transition state theory the unimolecular rate constant for the cZt-HT $\rightarrow$ tZt-HT single bond isomerization is the canonical rate constant:

$$k_{TST}(T) = \frac{k_b T}{h} \frac{Q_{TS}(T)}{Q_r(T)} e^{-E_a / k_b T} \qquad (3)$$

where Q_{TS} and Q_r are the vibration/rotation partition functions for the transition state and the reactant respectively, k_b is the Boltzmann constant, T is the temperature, and E_a is the activation energy. Calculated vibrational frequencies for the cZt conformer and the transition state (RHF/6-31G**) may be used to estimate A_h directly from Equation 3 in the limit of harmonic potentials. These calculations yield values of A_h = 2.8 - 3.4 $\times 10^{12}$ s^{-1} for the temperature range investigated here. This is slightly lower than the value of A_h deduced from the measurements in alcohol solvents ($A_h = 4 \times 10^{12}$ s^{-1}), but well within the error, which permits values ranging from 1.5×10^{12} s^{-1} to 1×10^{13} s^{-1}. In the context of transition state theory a higher value for A_h requires a larger partition function for the transition state or a smaller partition function for the reactant minimum.

In the absence of precise knowledge of the transition state, the expression in Equation 3 is often used in a simplified form. Assuming that only the reactive coordinate differs between the ground state and the transition state, the expression for k_{TST} can be written as:

$$k_{TST}(T) = \frac{k_b T}{h}[1 - e^{-h\nu_a / k_b T}]e^{-E_a / k_b T} \quad (4)$$

where ν_a is the frequency of the effective reactive vibration. Under the assumption that the reactive coordinate will be a torsional vibration with a frequency of 100-500 cm^{-1} the pre-exponential factor in Equation 5 is estimated to be $2.3 - 6.6 \times 10^{12}$ s^{-1} over the temperature range from 283 K to 353 K. An effective frequency of 125 to 150 cm^{-1} for the torsional coordinate reproduces the values calculated using Equation 3. In the high temperature limit where $k_b T >> h\nu_a$, the polynomial expansion of $e^{-h\nu_a / k_b T}$ in Equation 4 leads to a simplified equation for the transition state rate constant where the exponential prefactor is independent of temperature:

$$k_{TST}(T) = \nu_a e^{-E_a / k_b T} \quad (5)$$

According to Kramers' theory for unimolecular reactions in liquids the frictional influence of the environment should result in a rate constant given by:

$$k = k_{TST}\kappa \quad (6)$$

where κ is the Kramers' transmission coefficient, which may be approximated as

$$\kappa = \left[1 + \left(\frac{\beta}{2\omega_a}\right)^2\right]^{1/2} - \frac{\beta}{2\omega_a} \quad (7)$$

In this equation ω_a is the (imaginary) frequency describing the curvature of the barrier and β describes the friction of the solvent on the reactive motion.[58,64,91] In the high friction limit ($\beta > 2\omega_a$) the Kramers' coefficient reduces to $\kappa = \omega_a / \beta$.

In the Smoluchowski-Stokes-Einstein limit the friction on the reaction coordinate is related to the macroscopic shear viscosity of the solvent with $\beta = \eta$.[58] However, sub-linear dependences of the rate constant for isomerization reactions on the solvent viscosity are commonly reported in the literature.[69,75,76,92] This sub-linear dependence on viscosity leads to an equation for the transmission coefficient:

$$\kappa = \frac{\omega_a}{\eta^{\gamma}} \qquad (8)$$

where $0 \leq \gamma \leq 1$.[71] The parameter γ can be interpreted as the fraction of the activation energy for viscous flow that acts as a friction on the reaction coordinate.[78]

In the limit of medium friction ($\beta << 2\omega_a$) the Kramers' coefficient in equation 8 will approach unity. Thus κ is always less than or equal to one in the presence of environmental friction. It is never predicted to be greater than one. A generalization of this equation with a frequency dependent friction was put forth by Grote and Hynes.[93-95] However, in Grote-Hynes theory the transmission coefficient will still be less than 1.

The range of values for A_h estimated by transition state theory for cZt→tZt single bond isomerization is an order of magnitude lower than the value of 6×10^{13} s^{-1} determined from the data obtained in alkane solvents. As transition state theory should

provide an upper limit for the reaction rate in the region of moderate to high friction, where rapid energy randomization is guaranteed, this result provides a significant puzzle. Interestingly, Schroeder et al. also report an order of magnitude deviation between the calculated and experimental rate constant of *trans*-stilbene in low viscosity polar solvents, with the experimental rate faster than predicted by transition state theory. This is not a universal phenomena however as *trans*-stilbene was the only system observed to exhibit this anomalous behavior, while good agreement between calculated and predicted rates was reported for several larger systems.[87] Sun *et al*. also comment on an observed "k_{tst}" for the *trans*$\rightarrow$ p isomerization of stilbene in alkane solvents larger than the k_{tst} calculated by Equation 6 with an anticipated torsional frequency of ν = 100 cm^{-1}. Although only the difference reported by Sun *et al*. is only a factor of 2.5, not the order of magnitude found here for Z-HT.[80]

The value of A_h in alcohol solvents is systematically lower than the value in simple alkanes, falling within the range of values consistent with transition state theory. The difference observed between the alkane and alcohol solvents may suggest an additional frictional dependence of A_h for the alcohol solvent, which is not present in simple alkanes. However, this friction is not simply related to the solvent shear viscosity, in fact the most striking feature of the data is the complete lack of dependence of the reaction rate on the solvent shear viscosity. Over the range of temperatures investigated the ratio of viscosities in like solvents range from 2 to 5 with no apparent effect on the reaction rate. This is apparent for the alkane data as

illustrated in the inset to Figure 2.6, and is also true of the two alcohol solvents. In one specific example the measured rate constants in methanol and propanol at 10°C are 2.6 ns^{-1} and 2.7 ns^{-1} respectively despite a four-fold increase in the solvent viscosity from 0.7 mPa s to 2.9 mPa s.

It seems likely that the correspondence between the transition state rate value for A_h and the observed value in alcohol solvents reflects the general validity of transition state theory and the discrepancy observed for alkane solvents identifies an additional contribution to the transition state partition function not yet accounted for. It is interesting to speculate that this difference is related to intermolecular packing of the solvent. One potential source is a close packing interaction between Z-HT and the alkane solvents resulting in a solvent induced confinement term at the cZt minimum correlated with a corresponding increase in entropy of the transition state. This is not observed in alcohols where the hydrogen bonding interactions between solvent molecules decrease the confinement.

SUMMARY AND CONCLUSIONS

A careful comparison of the conformational relaxation dynamics of Z-HT in alkane and alcohol solvents is presented. These data confirm the earlier observation that the relaxation and thermalization of hot Z-HT is much faster in alcohol solvents than in alkane solvents. The solvent influence is related to the nature of the alcohol versus alkane solvent, but is not related in any simple fashion to the macroscopic

solvent shear viscosity. A measurement of the temperature dependent cZt→tZt isomerization highlights two aspects of the solvent dependence. First, the barrier for the cZt→tZt conformational isomerization is influenced by the solvent, and is 25% lower in alcohols (ca. 1450 cm^{-1}, 17.4 kJ/mol) than in alkanes (ca. 1950 cm^{-1}, 23.5 kJ/mol). In addition, the equilibrium Arrhenius prefactor, A_h, is an order of magnitude smaller for alcohols (ca. 4×10^{12} s^{-1}) than alkanes (ca. 6×10^{13} s^{-1}) and is independent of the solvent viscosity. These values for A_h provide something of a conundrum as the value in alkane solvents is an order of magnitude larger than that predicted by simple transition state theory. The difference cannot be easily attributed to an activated viscous friction on the reactive motion as the data is independent of solvent viscosity. A similar, as yet unexplained, phenomenon was reported for *trans*-stilbene in the low viscosity solvent liquid ethane.[87]

Chapter 3. **7-DEHYDROCHOLESTEROL: DECAY OF AN EXCITED-STATE ABSORPTION**[2]

BACKGROUND

In chapter 2, the results of studies of the relaxation of hot Z-hexatriene on the ground state manifold were presented. Temperature-dependent transient absorption spectroscopy was used to determine the barrier height for the cZt→ tZt isomerization in various solvents. Through a comparison of the measured barriers in alkanes and alcohols we were able to ascertain the influences of solvent polarity and viscosity upon the relaxation dynamics of Z-HT. In those experiments the isomerization of cis-1,3,5-hexatriene was studied following direct excitation of pure Z-HT, while in previous studies[13] CHD had been excited to create the hexatriene population. Through this direct excitation we were able to determine that it was neither solvent polarity nor viscosity that was affecting the ground-state potential and thus relaxation. In fact, the key solvent property affecting the isomerization rate was the inherent nature of the solvent and its' ability to coordinate around the solute.

[2] Extracted from K.C. Tang, A. Rury, M.B. Orozco, J. Egendorf, K.G. Spears, and R.J. Sension, "*Ultrafast electrocyclic ring-opening of 7-dehydrocholesterol in solution: The influence of solvent on excited state dynamics",*(Submitted)

In this chapter we increase the complexity of the studies by turning to the CHD chromophore embedded in provitamin D. With this added complexity, the dynamics and potential energy surfaces become more complex and may display more sensitivity to the solvent environment. To determine the extent of this sensitivity we have performed similar temperature dependent experiments designed to explore the excited electronic state of DHC and the influence of the solvent environment on the decay of the excited state.

In the body, DHC plays an important role as precursor to the natural production of vitamin D_3.[96,97] As mentioned in the previous chapter, at the core of DHC is a CHD chromophore which, when excited with UV light, initiates the reaction leading to formation of vitamin D_3. Once excited, the cyclohexadiene chromophore proceeds through an electrocyclic ring-opening reaction to form a conjugated triene species which undergoes a thermal hydrogen migration to form vitamin D_3. (Figure 3.1) The photochemistry of DHC and production of vitamin D_3 is complicated by a web of photochemical pathways and byproducts.[98,99] Most of these byproducts are conjugated dienes or trienes that absorb in the UV between 300 nm and 250 nm, resulting in the desired yields and photostationary states being wavelength dependent.[19,100-103] In addition the solvent environment has been shown to play a significant role in the conformational equilibrium of previtamin D_3 and on the various photochemical pathways.[98,99]

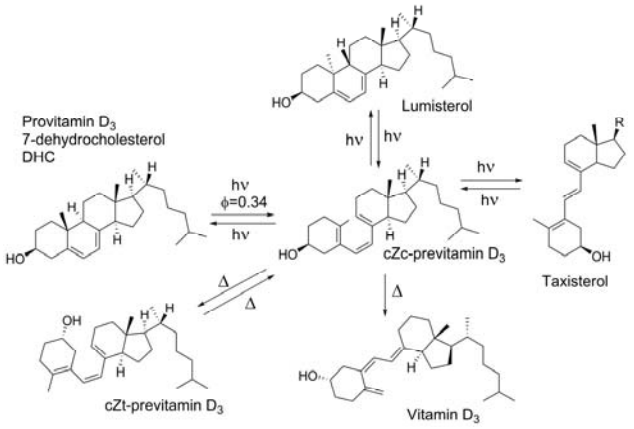

Figure 3.1: The provitamin D_3 7-dehydrocholesterol (DHC) molecule undergoes a photochemical ring-opening reaction to form cZc-previtamin D_3 which undergoes conformational relaxation producing an equilibrium mixture of the cZc and cZt conformers. The cZc-previtamin D_3 undergoes a hydrogen transfer and electronic rearrangement to form vitamin D_3. Photochemical side reactions compete with formation of vitamin D_3. The hydrocarbon tail, R, on taxisterol is the same as for the other compounds.

The electronic absorption spectrum of DHC is located in the UV, with the lowest allowed transition peaking at 282 nm (see Figure 3.2). The DHC spectrum exhibits a vibrational progression of *ca*. 1350 cm^{-1} with at least four and as many as six bands visible in the progression. This mode is consistent with a displacement along delocalized C=C stretching coordinates in the excited state, typical of $\pi \rightarrow \pi^*$ transitions in conjugated polyenes. The DHC spectrum measured in alcohols (methanol, ethanol, n-propanol, 2-butanol) and alkanes (heptane, dodecane, hexadecane) is weakly dependent on the solvent, with peak shifts of under 0.4 nm and slight differences in band width. The maximum extinction coefficient (ε_{max}) is *ca*. 1×10^4 M^{-1} cm^{-1}.

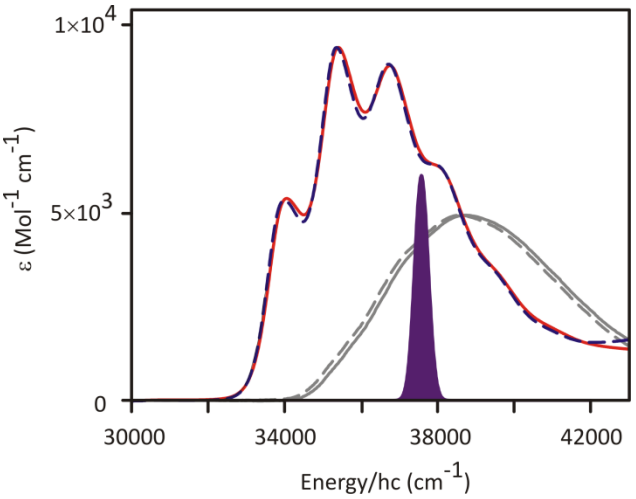

Figure 3.2: Absorption spectrum of 7-dehydrocholesterol (DHC) in hexadecane (blue dashed line) and methanol (red line). The absorption spectra of 1,3-cyclohexadiene in methanol and hexadecane are indicated in gray for comparison. The excitation pulse is 3 nm wide, centered at 266.3 nm. This is also indicated in the figure. The extinction coefficient is accurate to 2 significant figures.

Early UV transient absorption measurements of DHC concentrated on the photoproduct formation and conformational relaxation.[17-20] Studies of DHC in methanol, ethanol, and heptane solvents demonstrated the rapid internal conversion from the excited state manifold to form vibrationally and conformationally excited molecules on a picosecond time scale.[17-20] Product formation is followed by vibrational relaxation on a time scale of 2 - 9 picoseconds in heptane and 2 - 5 ps in methanol.[17,18] Conformational relaxation leading to an equilibrium mixture of cZt and cZc conformers occurs on a time scale > 100 ps in heptane and *ca*. 100 ps in methanol. Temperature dependent measurements by Fuss *et al*. determined the ground state barrier for conformational relaxation for the cZc $\rightarrow$ cZt-previtamin D transition to be *ca*. 15.5 $\pm$ 1 kJ/mol in methanol and ethanol solvents.[20]

In recent work we have studied the excited state ring-opening reaction in greater detail. DHC is known to possess a CHD chromophore which undergoes a similar ring-opening mechanism on the excited state manifold. It was proposed that the decay of the DHC excited state may provide insight into the nature of the species present on the excited state, the dynamics occurring there and how they may be affected by the solvent environment. This chapter reports on the temperature and solvent dependence of the excited state of DHC following excitation at 266nm recently measured by narrow-band transient absorption spectroscopy. The focus of these experiments was determining: 1) if there was a barrier for the decay of the DHC ESA, 2) the height of the barrier (if any) and 3) how solvent may affects that barrier and subsequent dynamics. The results of the these studies necessitated fitting the population with a biexponential decay which was subsequently verified by Tang et al.[21]

EXPERIMENTAL PARAMETERS

The temperature dependence of the excited state dynamics was measured using a home-built 1 kHz multi-pass ultrafast amplifier seeded by a Ti:Sapphire oscillator generated femtosecond laser pulses with central wavelength of 805 nm, pulse duration of ~60 fs and pulse energy of ~450 μJ. The pump was generated from the third harmonic of the laser and used without additional compression. The probe pulse was generated using a home-built non-collinear optical parametric amplifier tunable from 470 nm to 700 nm. Measurements were performed with the relative polarizations of the pump and

probe pulses set at the magic angle of 54.7°. Temperature control was achieved by immersing the sample reservoir in a bath consisting of a 50/50 mixture of water and ethylene glycol. The temperature of the bath was controlled by a NesLab RTE-111 Refrigerated Bath/Circulator, capable of maintaining temperatures from -25 °C to +150 °C. The samples were flowed through a 1 mm path length cell to refresh the sample volume between laser pulses, and the temperature was measured with a temperature probe inserted in a Y-joint located immediately after the sample cell. The temperature of the sample was varied from 1 °C to 97 °C and was maintained within ±0.5 °C. The exact temperature range used for the experiment varied depending on the melting and boiling points of the solvent.

The 7-dehydrocholesterol sample was purchased from Aldrich and used without further purification. Sample concentrations were *ca.* 2.7 mM.

RESULTS

TEMPERATURE DEPENDENCE OF THE EXCITED STATE DECAY

The studies of the excited state(s) properties of DHC were performed by measuring the lifetime as a function of temperature in a number of solvents – the two alkanes, heptane and hexadecane, and the range of alcohols: methanol, ethanol, 1-propanol, 1-butanol, and 2-butanol. The temperature was varied from 1°C to 97°C with the limits for any given sample determined by the solvent properties. Traces at the extreme temperatures in heptane, hexadecane, ethanol, and 2-butanol are shown in

Figure 3.3. These data illustrate a clear temperature dependence to the excited state lifetime. The transient absorption traces were fit to a bi-exponential decay of the excited state absorption to analyze the change in decay rate as a function of temperature. None of the solvents exhibit any significant temperature dependence to the ratio of the amplitudes of the fast and slow components.

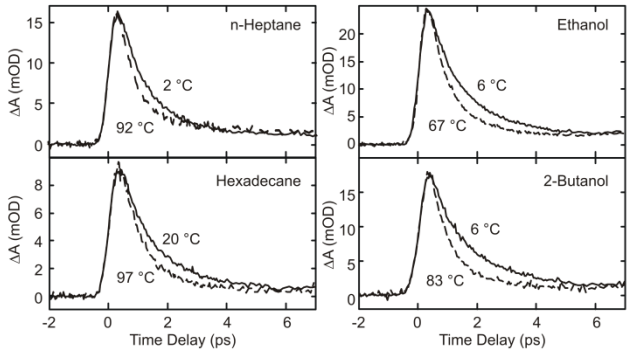

Figure 3.3: Typical decay traces at the extremes of the temperature range in each solvent. The probe wavelength is 480 nm in 2-butanol and 500 nm in the other solvents.

Interpretation of the temperature dependence of a condensed phase reaction is often complicated by the temperature dependence of solvent properties. When a unimolecular reaction involves a significant conformational change the friction on the reaction coordinate often correlates with the solvent viscosity. As the viscosity is a temperature dependent property, the observed influence of temperature on the reaction rate will include contributions from the intrinsic intramolecular barrier for the reaction and from the change in solvent viscosity. This has been discussed in great detail in the context of the excited state trans→cis isomerization of trans-stilbene.[104,105]

The solvent polarity can also influence the intrinsic potential energy surface and the reaction rate. This is particularly evident when a charge redistribution occurs in the excited state.[106] In many polyenes the reaction coordinate involves conical intersections or avoided crossings between states with different internal charge distributions. In these systems the solvent polarity can influence the intrinsic barrier for reaction even if there is no explicit charge transfer. Again, the isomerization of cis and trans-stilbene provides a well studied example with the effective barrier for isomerization much lower in polar than nonpolar solvents.[75,76,82,107,108] Solvent polarity is also a function of temperature, decreasing as the temperature increases. Thus the observed influence of temperature on the reaction rate may include contributions from the intrinsic barrier for the reaction and from the change in solvent polarity with temperature.

The excited state lifetime in all solvents investigated here depends weakly on specific solvent properties. This is particularly evident in the alkane solvents. At 25 °C the viscosity ranges from 0.387 mPa·s in heptane, 1.383 mPa·s in dodecane, to 3.032 mPa·s in hexadecane, yet the observed excited state lifetimes are nearly identical. This observation is consistent with a model where conformational changes in the initial ring-opening process are small. The solvent dependence of the rate constant in alcohols is more pronounced and the temperature dependence of the rate constants may include factors arising from the temperature dependence of solvent properties. These are factors that must be taken into account when interpreting the data.

Analysis of the temperature dependence using the Arrhenius expression for excited state decay constant provides an estimate for the excited state barrier including both intrinsic and solvent dependent contributions. The rate constant is given by:

$$k_{obs}(T) = A_h e^{-E_a / k_B T} \qquad ((1)$$

where E_a is the activation energy for internal conversion to the ground state and A_h is the frequency prefactor. The relationship between $\ln(k_{obs})$ and 1/T is linear and both a barrier and prefactor can be determined for each solvent as illustrated in Figure 3.4.

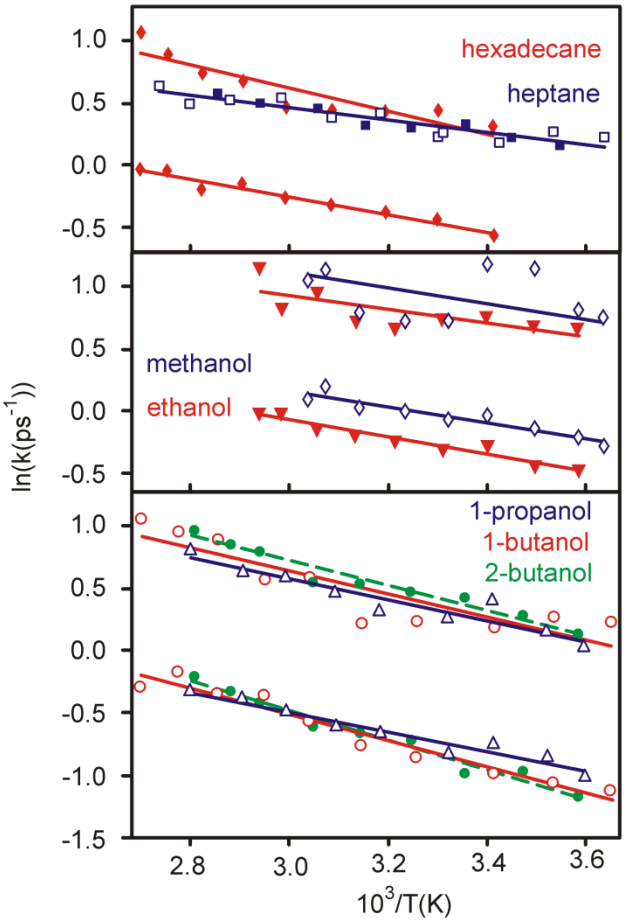

Figure 3.4: Arrhenius plot of temperature dependent rate constants for the decay of the DHC ESA. Lowest Panel: 2-butanol (green filled circles, 480 nm), 1-butanol (red open circles), 1-propanol (blue open triangles). Middle Panel: ethanol (red filled triangles), methanol (blue open diamonds). Top Panel: n-heptane (blue squares, open 500 nm, filled 620 nm), hexadecane (red filled diamonds). For n-heptane only the fast component is plotted. The linear fits to the data are also shown.

The fast and slow components in each solvent are approximately parallel. The barriers and Arrhenius prefactors obtained from the fits are given in Table 3.1. The major difference is in the prefactor, not the barrier. The effective barriers and prefactors, in the longer alcohols, especially in 2-butanol, are comparable to those measured for ergosterol in a low temperature 1:1 methylcyclohexane-isopropane matrix (11.1 ± 0.15 kJ/mol and 40 ± 20 ps^{-1}).[109] Separating solvent induced from intrinsic

intramolecular barriers is difficult. The full discussion in a later section suggests the existence of a barrier intrinsic to the molecule.

Solvent	Fast Component		Slow Component		Sequential Model[(c)]	
	E_a (kJ/mol)	A_h (ps^{-1})	E_a (kJ/mol)	A_h (ps^{-1})	E_a (kJ/mol)	A_h (ps^{-1})
Methanol[(a)]			5.4 ± 0.7	8 ± 3		
Ethanol	4.5 ± 1.6	12 ± 8	5.8 ± 0.5	8 ± 2		
1-Propanol	7.0 ± 1.0	22 ± 8	6.6 ± 0.6	7 ± 2	6.5 ± 1.0	8.5 ± 3
1-Butanol	7.7 ± 1.5	30 ± 18	8.8 ± 0.7	14 ± 4	9.3 ± 1.0	26 ± 10
2-Butanol	8.3 ± 0.6	42 ± 10	9.9 ± 0.6	22 ± 5	10.3 ± 0.8	37 ± 10
n-Heptane[(a)]	4.2 ± 0.4	7 ± 1				
n-Hexadecane	7.7 ± 1.3	30 ± 15	5.9 ± 0.5[(b)]	7 ± 1	5.5 ± 0.8	7 ± 2

Table 3.1: Effective activation energy and Arrhenius prefactor for the excited state decay of DHC as a function of solvent. (a) The small relative amplitude of the slow component in n-heptane and the fast component in methanol leads to large error bars in the rate constant as a function of temperature. These do not yield reliable results and are not included in the table as separate fits. (b) The error bar given for this barrier is from the least squares fit to the data, however there is a decay component arising from the solvent only signal on roughly the same time scale and this will decrease the overall accuracy of the fit and increase the effective error bar for the barrier. (c) Barrier for internal conversion to product assuming a sequential model, E $\rightarrow$ (E $\leftrightarrows$ I) $\rightarrow$ P. See the discussion section for details.

The transient absorption measurements suggest that the relative amplitudes of the fast and slow components depend on the solvent but do exhibit any temperature dependence within the error of the fits to the data. In addition, the temperature dependence of the excited state lifetime provides barriers for internal conversion of *ca*. 4-10 kJ/mol. The barriers arise from the intramolecular potential energy surface and the external influence of the surroundings on the molecule. The magnitude of the barriers and the amplitude of the prefactors are consistent with the values deduced for ergosterol at low temperature.[98,99]

DISCUSSION

MODELS FOR EXCITED STATE DECAY

The temperature-dependent measurements were fit to a biexponential decay, which was corroborated the results of Tang et al.[21] Two potential explanations for a biexponential decay of the ESA originating from excited state relaxation (Figure 3.5) are: (i) The excited state population undergoes a sequential internal conversion $E \rightarrow I \rightarrow P$ or $E \rightarrow (E \leftrightarrows I) \rightarrow P$ with an intermediate state "I" between the initially excited state "E" and the photoproduct "P". (ii) Dynamics on the initial excited state result in parallel decay pathways for an effectively homogeneous initial population of DHC: $P \leftarrow I \leftarrow E \rightarrow I' \rightarrow P'$ (or P). In this model, the initially excited state, E, branches between two excited state populations (I and I') before formation of one or more photoproducts transparent in the visible region of the spectrum.

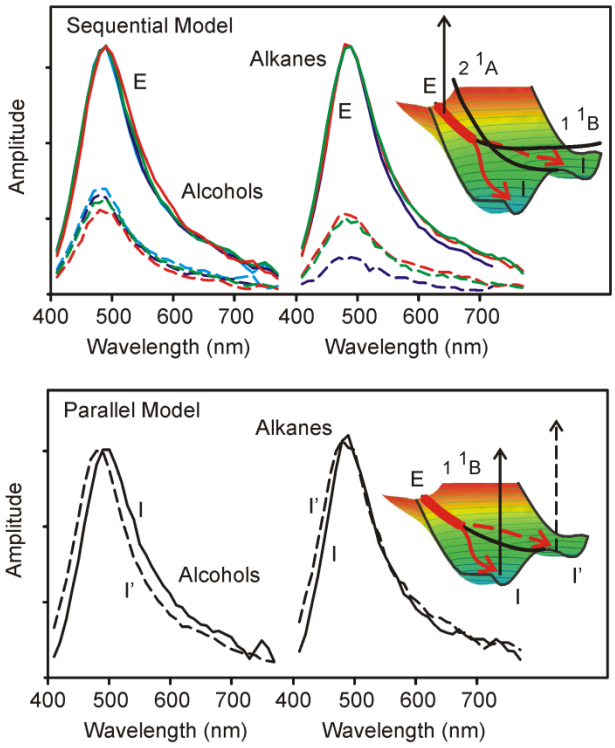

Figure 3.5: Top: In a model consisting of sequential internal conversion between two excited state species, E and I, the amplitudes of the decay components are used to construct excited state spectra for the two species. These are plotted for the various solvents. Alcohols: Methanol, lt. blue; ethanol, dk. blue; propanol, green; butanol, red. Alkanes: heptane, dk. blue; dodecane, red; hexadecane, green. Bottom: In a model consisting of parallel excited state pathways the decay associated spectra are the spectra of the two intermediates I and I'. The average spectra are plotted for alcohols and alkanes (solid lines, fast components; dashed lines, slow components). The schematic potential energy surface indicates one possible model with parallel paths based on analogy with CHD. The two intermediates could also correspond to excitation of distinct conformations of the ground state molecules.

The fluorescence and anisotropy data both supported assignment of the transient absorption signal to the initially excited state. This assignment is consistent with a sequential model where the S_2 1 ^{1}B state and S_1 2 ^{1}A states are nearly isoenergetic in DHC. In this case the fast component corresponds approximately to the rapid equilibration of the two populations E $\rightarrow$ (E $\leftrightarrows$ I) and the slow component corresponds approximately to the decay of this equilibrated population, (E $\leftrightarrows$ I) $\rightarrow$ P. A dipole-allowed S_2 1^{1}B $\rightarrow$ S_n transition from the initially populated S_2 1^{1}B state (E) along

with a dipole-forbidden transition $S_1\,2^1A \rightarrow S_n$ will account for both the constant anisotropy and the biexponential decay of the amplitude of the ESA[21]. While the observed rate constants can be assigned qualitatively to equilibration and product formation, they are actually complex functions of the intrinsic rate constants for the equilibration of E and I and the rate constant for the formation of product from the intermediate state I. The sequential model can be considered quantitatively to estimate molecular parameters using a simple model for the dynamics:

$$E \rightarrow I \qquad k_1$$

$$I \rightarrow E \qquad k_2 = k_1/g$$

$$I \rightarrow P \qquad k_{3'} = k_3 - k_2 = k_3 - k_1/g$$

where g is the ratio of the effective degeneracy or density of states of the intermediate state I to the initially excited state E under the assumption that these two states are essentially isoenergetic. The master equations describing the time dependent populations of the three states are

$$\dot{n}_E(t) = -k_1 n_E(t) + k_2 n_I(t) \tag{2a}$$

$$\dot{n}_I(t) = k_1 n_E(t) - k_3 n_I(t) \tag{2b}$$

$$\dot{n}_P(t) = k_{3'}\, n_I(t) \tag{2c}$$

These can be solved numerically or analytically yielding an expression for the population of the E, I, and P. The analytical solution for the population of the initially excited state, E, leads to:

$$n_E(t) = A_- e^{\lambda_- t} + A_+ e^{\lambda_+ t} \tag{3}$$

where

$$\lambda_\pm = \tfrac{1}{2}\left(-k_1 - k_3 \pm \sqrt{k_1^2 - 2k_1k_3 + 4k_2k_1 + k_3^2}\right) \tag{4}$$

$$A_- = \frac{(k_1 - k_3) + \sqrt{k_1^2 - 2k_1k_3 + 4k_2k_1 + k_3^2}}{2\sqrt{k_1^2 - 2k_1k_3 + 4k_2k_1 + k_3^2}} \tag{5}$$

$$A_+ = \frac{(k_3 - k_1) + \sqrt{k_1^2 - 2k_1k_3 + 4k_2k_1 + k_3^2}}{2\sqrt{k_1^2 - 2k_1k_3 + 4k_2k_1 + k_3^2}} \tag{6}$$

The three quantities extracted from the data are the two observed decay constants -λ_-, -λ_+, and the relative amplitudes of the two components $A_-/(A_- + A_+)$. These quantities can be used to obtain best estimates for the three intrinsic quantities k_1, g, and $k_{3'}$ as a function of solvent and as a function of temperature. We discuss this further below.

In the sequential model, E $\rightarrow$ (E $\leftrightarrows$ I) $\rightarrow$ P, the temperature dependence of the observed rate constants reflects a combination of the influence of temperature on the equilibration process and on the decay of the intermediate state I. The experimental decay constants are not defined sufficiently well by the data in methanol, ethanol, or n-

heptane to permit such an analysis. However, the data in the longer alcohols and hexadecane can be analyzed to extract estimates for the intrinsic rate constants for the I $\rightarrow$ P reaction and the E $\rightarrow$ I equilibration as a function of temperature using equations 4 - 6. The effective barrier for the transition from I $\rightarrow$ P is strongly dependent on the solvent, 10.3 ± 0.8 kJ/mol in 2-butanol, 9.3 ± 1.0 kJ/mol in 1-butanol, 6.5 ± 1.0 kJ/mol in 1-propanol, and 5.5 ± 0.8 kJ/mol in hexadecane.

The equilibration reaction E $\rightarrow$ I is also temperature dependent with an effective barrier for of 7.9 ± 1.0 kJ/mol in 2-butanol, 7.3 ± 2.0 kJ/mol in 1-butanol, 7.1 ± 1.4 kJ/mol in 1-propanol, and 8.0 ± 1.6 kJ/mol in hexadecane obtained from an Arrhenius plot of the intrinsic rate constants as a function of temperature. Within the error of the analysis this effective barrier is independent of the solvent. The existence of any barrier for E $\rightarrow$ I implies that a fluorescence yield approaching unity would be expected at cryogenic temperature, while a quantum yield of ca. 0.19 is reported at *ca.* 77 K.[109] Although the data quality and assumption of degeneracy make these barrier estimates for the equilibration reaction uncertain, this is additional support for choosing the parallel model. Further work might refine the outcome for this type of analysis.

In summary, both parallel and sequential models are consistent with the transient absorption data and the previous fluorescence measurement[21]. Several factors lead to a preference for the parallel model but, future studies, both theoretical and experimental, will be required to fully elucidate the excited state dynamics.

INFLUENCE OF SOLVENT ON THE BARRIERS FOR DECAY OF THE EXCITED STATE.

The solvent dependence of the effective barrier reported in Table 3.1 points to a contribution from the environment. The influence of solvent on the isomerization barrier in stilbene has been studied extensively.[104,105,107] The temperature dependence of the solvent friction on the reaction coordinate provides an extrinsic barrier for the isomerization reaction in addition to the intrinsic intramolecular barrier observed for the gas phase molecule. Saltiel and coworkers used the solvent shear viscosity and the temperature dependence of the viscosity to gain insight into the combined effects of the intrinsic and extrinsic activation barriers.[104,105] In contrast, the ground state single-bond isomerization of cZt-hexatriene $\rightarrow$ tZt-hexatriene does not exhibit any significant evidence for a viscosity dependent extrinsic barrier for isomerization.[13] Nonetheless the solvent still influences the reaction rate and the barrier in ways that depend, not on macroscopic solvent properties such as the solvent shear viscosity, but on the molecular details of the solvent. As noted in the previous chapter, preliminary molecular dynamics simulations suggested that the barrier for the cZt$\rightarrow$tZt isomerization is higher in the alkanes studied by Harris *et al*. because the molecules pack tightly around the hexatriene molecule and hinder the barrier crossing. This is not observed for the more open structure of the alcohol solvents.[90]

The molecular distortion coupled to the ring-opening coordinate in DHC to form the cZc conformer of previtamin D_3 does not involve a large amplitude change in the shape of the molecule. Thus the mechanism for the influence of the solvent on the

reaction coordinate must involve an indirect coupling with the solvent which affects the overall flexibility of the molecule in the excited state. Assuming that there is no static change in the intrinsic intramolecular barrier as a function of solvent, the intrinsic barrier for decay of the fast component is $\leq 4.2 \pm 0.4$ kJ/mol, with the upper limit set by the effective barriers in low viscosity ethanol and heptane solvents (Table 3.1). The intrinsic barrier for the slow component is $\leq 5.4 \pm 0.4$ kJ/mol with the upper limit set by the effective barriers in methanol and ethanol.

The model developed by Saltiel and coworkers provides a simple way to separate the intrinsic intramolecular and extrinsic solvent barriers for a reaction.[104,105] The effective activation barrier is the sum of the intrinsic barrier E_o and the barrier E_v introduced by the solvent. The solvent induced barrier can be approximated as $E_v = \alpha E_\eta$ where α is generally between 0 and 1, accounting for the fact that the relationship between reaction rate and $1/\eta$ is generally sublinear. Using the effective activation barriers in Table 3.1 and values for E_η determined from the temperature dependence of the solvent viscosity over the range from 1°C to 97°C,[110,111] the parameters α and E_o can be estimated from the slope and intercept of a plot of E_{eff} as a function of E_η. A linear least squares fit to the data provides values of $E_o = 1.8 \pm 0.9$ kJ/mol and $\alpha = 0.30 \pm 0.05$. There may be a difference in the intrinsic barrier for the fast and slow components, but the difference is within the error estimate on E_o. These values are also consistent with the solvent dependence of the $I \rightarrow P$ transition if the data is analyzed using the sequential model for excited state decay.

While the parameters obtained from the simple model described above are reasonable, it is not clear that they accurately capture the dynamical influence of solvent on the reaction coordinate in DHC. Nakashima *et al*. reported that the fluorescence intensity for ergosterol in a methylcyclohexane:isopropanol glass was approximately constant between 77 K and 89 K and decreased with increasing temperature between 89 K and 150 K.[109] The temperature dependence was used to calculate the effective barrier for the excited state decay (11.1 kJ/mol). This barrier is only slightly larger than the effective barriers for the decay of the DHC excited state absorption in 2-butanol at room temperature[21] (8.3 ± 0.6 kJ/mol and 9.9 ± 0.6 kJ/mol; or 10.3 ± 0.8 kJ/mole in the sequential model), although the effective viscosity is much larger. The low temperature measurement suggests that the magnitude of the solvent induced barrier saturates at *ca*. 9 kJ/mol. That is, the environment can hinder, but not prevent the ring-opening reaction. This is consistent with a mechanism where the solvent response allows molecular relaxation, lowering an intrinsic barrier for reaction within the molecule.

More detailed analysis of the excited state dynamics will require both an accurate excited state potential energy surface and a more extensive data set designed to address separately the various factors that may influence the behavior.

SUMMARY AND CONCLUSIONS

This study used temperature-dependant femtosecond transient absorption spectroscopy to probe the excited state dynamics of DHC. The temperature dependence of the excited state decay as a function of solvent suggests that there is an intrinsic intramolecular barrier to ring-opening as well as a solvent dependent barrier arising from the friction of the environment on the reaction coordinate. The effective barrier in the low viscosity solvents sets an upper limit for the intrinsic barrier of *ca*. 4 kJ/mol. A simple model for the influence of the solvent provides an estimate for the intrinsic barrier of 1.8 ± 0.9 kJ/mol.

Chapter 4. ISO-BROMOIODOMETHANE: DECAY OF A METASTABLE SPECIES

BACKGROUND

Bromoiodomethane (CH_2BrI), shown in Figure 4.1, has proven useful in numerous experiments across a wide range of fields of investigation. CH_2BrI has been shown to participate in atmospheric chemistry,[6,23] a subject for coherent control experiments[10,112] and used to investigate the effects of solvent on photofragment recombination[22]. In the investigations reported here it serves as a probe of the effects of solvent on photo-fragment recombination and the subsequent reaction dynamics.

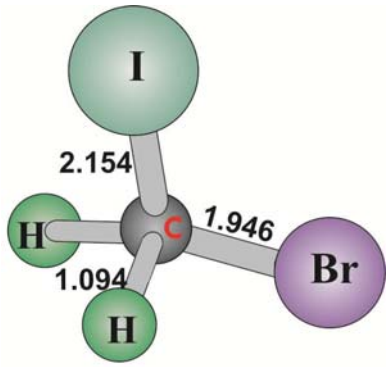

Figure 4.1: Optimized geometry of CH_2BrI as calculated using density functional theory by Wang et al.[24]

The composition and structure of CH_2BrI is similar to other polyhalomethanes studied in the field of atmospheric chemistry.[6] It has been observed alongside CH_2Br_2, CH_2I_2, and CH_2Cl_2 serving as an important source of reactive halogens found in the

troposphere and marine boundary layer. CH_2BrI and similar dihalomethanes are also considered to be important contributors of organoiodine and organobromine compounds to the atmosphere.[2-6,113] In addition to investigations in atmospheric chemistry CH_2BrI possesses qualities which make it a candidate for coherent control experiments. [9]

CH_2BrI possesses two distinct chromophores[112]. Each chromophore has a large absorptive cross-section and can be excited independently. The two absorption bands, centered at 274 nm and 231nm, are referred to as the A-band and B-band absorptions respectively (Figure 4.2). It has been well documented that excitation in either band promotes an electron from a bonding orbital to an anti-bonding orbital on (Br, I) → σ^*(C-Br, C-I) which results in cleavage of either the carbon-bromine or carbon-iodine bond.[112,114] In the A-Band, excitation promotes an electron on the iodine atom - severing the carbon-iodine bond. Excitation in the B-Band severs the carbon-bromine bond by promoting an electron on the bromine atom.[10] The specificity with which each excited chromophore cleaves a bond has made CH_2BrI a prototype for bond selective electronic excitation and photochemistry.[10,112,115-117]

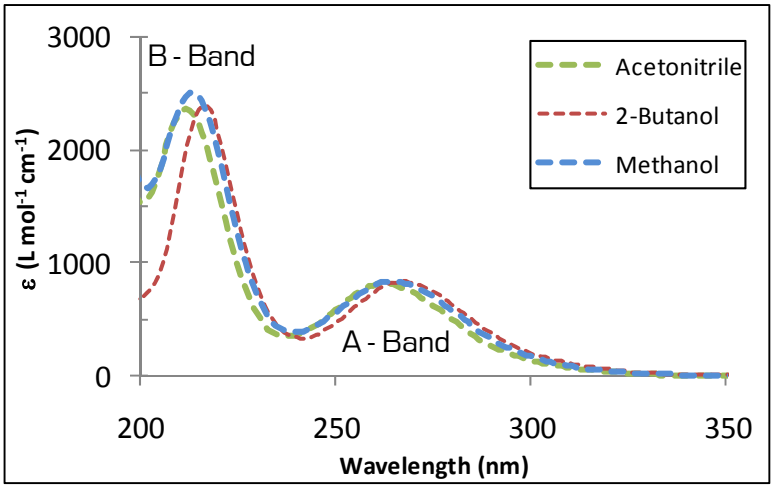

Figure 4.2: Ultraviolet absorption spectra of CH_2BrI in acetonitrile (dashed green), methanol (dashed blue) and 2-butanol (dashed red). Excitation at 266 nm falls near the peak of the A band corresponding to n→σ* transition localized on the C–I bond [5].

The photochemistry of bromoiodomethane has been studied following UV photoexcitation in the gas phase and condensed phase on timescales ranging from femtosecond out to delay times of 6ns. In an experiment conducted by Tarnovsky et al. ultrafast pump-probe spectroscopy was performed on CH_2BrI in acetonitrile following excitation in the A-Band (266nm).[114] After excitation, the photofragments underwent ultrafast reorganization reactions within the solvent cage. The proposed reactions for the photofragments were the formation of the iso-CH_2Br--I isomer, recombination to the parent molecule or cage escape resulting in solvated CH_2Br and I(or I*) as shown in Figure 4.3. Analysis of the results led them to conclude that vibrationally excited "hot" ground state iso-CH_2Br—I is formed from excited CH_2BrI within ~1ps. The iso compound then undergoes vibrational relaxation on two timescales: a few (~7.5ps) and tens of picoseconds. The absorption signal corresponding to iso-CH_2Br--I began to decay at sub-ns delays, leading them to an estimated lifetime of ~2.5ns for the ground-state of the

isomer. Lastly, they found no spectral absorption which would support the formation of the iso-CH_2I-Br isomer within their experimental window (0-700ps)[114].

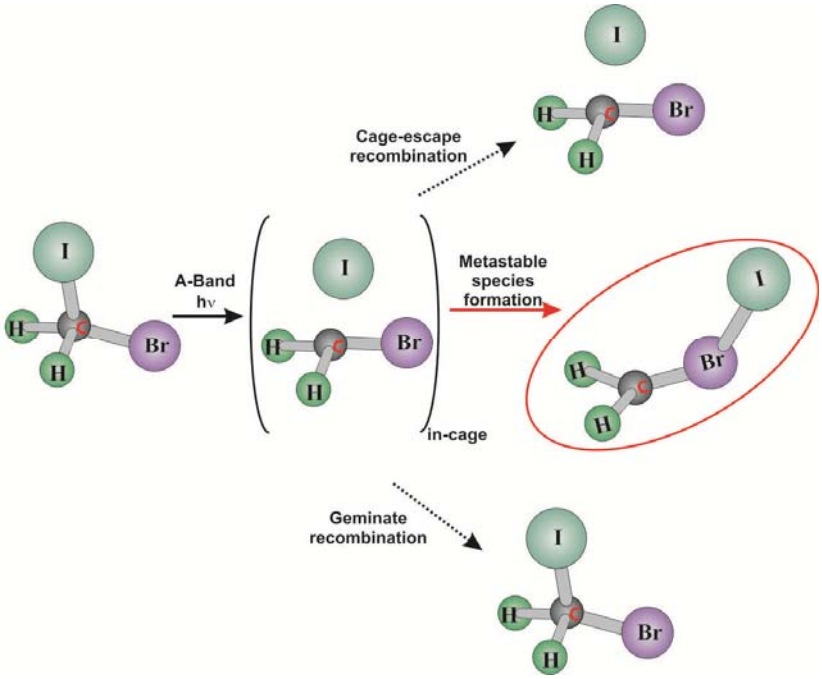

Figure 4.3: Proposed photofragment recombination reactions following A-Band excitation of CH_2BrI. The optimized geometry of the observed iso-CH_2Br--I species was calculated using DFT by Wang et al.[24] and circled in red.

While Tarnovsky et al. found no evidence of iso-CH_2I--Br on sub-nanosecond time scales in acetonitrile, nanosecond transient resonance Raman experiments gave a different result. Performed in cyclohexane by Zheng et al. the nanosecond transient resonance Raman experiments confirmed the presence of the iso-CH_2I-Br isomer on the 10 ns time scale.[23] Density functional theory and spin-orbit ab initio calculations were also reported. The calculations predicted that the iso-CH_2I-Br isomer is more stable than the iso-CH_2Br--I isomer (0.4 - 4.1 kcal mol^{-1}) with a much longer expected lifetime.[11,24,118] Kwok et al. suggested iso-CH_2I-Br may arise through isomerization of iso-CH_2Br--I along a

similar pathway as they concluded for iso-CH_2I-Cl arising from iso-CH_2I-Cl in picosecond time-resolved resonance Raman experiments.[119] The pathway they propose includes a transition state with a concerted mechanism where a C-I bond is formed concurrently with a strengthening of the I-Cl (Br) bond and ultimately results in C- Cl (Br) cleavage.[120] This mechanism is further supported by the results of picosecond time-resolved resonance Raman experiments performed on CH_2BrI in cyclohexane in which they observed the iso-CH_2Br--I species and assigned it a lifetime of 2-3 ns.[120]

In the investigations reported here the effects of solvent on reaction dynamics of iso-CH_2Br—I were studied. Solvent polarity was chosen as one of the parameters to vary due to the stabilizing effect that a polar solvent may have. If solvent polarity stabilizes the photoproduct we would expect decay times of the excited species to be slower in more polar solvents. To determine how solvent polarity factors in the decay of iso-CH_2Br--I experiments were performed in alcohols of various lengths; the length of the alcohol allowing systematic variation of the solvent polarity. The observed dynamics, e.g. relaxation times, were then compared to changes in the alcohol length to determine if solvent polarity is a controlling factor in the relaxation of iso-bromoiodomethane and to what extent. Although polarity is an important solvent property capable of influencing reaction dynamics another key property must be taken in to consideration.

Solvent viscosity can have as strong an influence on the dynamics of a reactive species as solvent polarity. As a result, it was necessary to select polar solvents

spanning a range of viscosities. At room temperature (25°C) the viscosity of methanol is 0.544 mPa·s while the viscosities of 1- and 2-butanol are 2.54 and 3.1 mPa·s, respectively. This range in viscosities allows for the investigation of the effects of viscosity on the reaction dynamics in polar solvents. Our discussion can then focus on how changes in viscosity can affect the movement of excited species through the solvent and ultimately what affect that has upon the decay pathways available to iso-CH_2Br--I. An example of how the solvent can restrict reaction pathways is through the formation of a sphere of solvent molecules around a reactive species. This "solvent cage" can hinder the diffusion of reactive species or even prevent reaction. Much of our discussion below will focus on the temperature dependence of the viscosity.

In the work reported here CH_2BrI was excited in the A-Band at 271nm resulting in the cleavage of the carbon-iodine bond. The subsequent recombination of the photofragments was found to lead to a population of the iso-CH_2Br--I isomer (Figure 4.3). Transient absorption spectroscopy was then used to determine the influence of solvent on the decay of iso-CH_2Br--I. Experiments were performed in 1-butanol, 2-butanol, methanol, and acetonitrile. Broadband spectral measurements were also conducted at room temperature in each of the solvents. The temperature dependence of the iso-CH_2Br--I decay was measured using narrow band detection, near the peak of the iso-CH_2Br--I absorption, at 460 nm. The results have been interpreted in terms of a model including both bimolecular reaction of iso-CH_2Br--I with ground state CH_2BrI and solvent-assisted unimolecular decay of the iso-CH_2Br--I.

EXPERIMENTAL PARAMETERS

Pump-probe transient absorption experiments were performed with 400 μJ laser pulses from a home-built 1 kHz Ti: Sapphire laser system. Bromoiodomethane was purchased from Sigma-Aldrich and used without further purification. Samples were prepared by diluting 3mL of pure CH_2BrI with solvent in a 100mL volumetric flask, resulting in a ~400mM solution. A peristaltic pump was employed to flow through a 1mm path length quartz flow cell rapidly enough to refresh the volume between laser pulses and avoid measuring the same volume. The samples were excited using 271nm UV pulses obtained from a third harmonic generation setup consisting of two cascaded linear stages: second harmonic generation followed by sum frequency generation as described previously.[63] Following the second generation crystal, the fundamental beam and the second harmonic were separated using a dichroic mirror and the second harmonic directed towards a delay stage. The two beams were then recombined using another dichroic mirror such that they travelled collinearly for sum frequency mixing in a 1mm β-BaB_2O_4 (BBO) crystal. The output of the third harmonic setup was then collimated, passed through two consecutive dichroic mirrors (T800/R400, T400/R266) and a 1cm Ni_2SO_4 filled quartz cell before being measured on a chopped power meter. While monitoring the power the relative timing of the fundamental and second harmonic beams were adjusted to ensure optimal temporal overlap and then the grating separation of the laser compressor was adjusted to optimize 3rd harmonic generation.

Transient absorption kinetics measurements were performed as a function of time-delay by sending a portion of the 800nm fundamental laser beam onto a computer-controlled delay stage. The 1.5 m delay stage allowed for accurate measurements from 10 fs to 10 ns. Use of the delay stage required painstaking alignment to ensure the 800 nm fundamental beam was well collimated and the pulse energy equivalent at either. The fundamental was beam was then tightly focused into a 1 cm cell filled with flowing ethylene glycol. In the cell, self-phase modulation broadened the spectrum into a while light continuum which was subsequently collimated and an interference filter inserted to obtain the desired probe wavelength. The pump beam, 271 nm, was generated as described above. The polarization of the pump beam was then adjusted using a half-wave plate such that it was oriented at magic angle with respect to the probe. To ensure optimal overlap the two beams were aligned through a 100μm pinhole which represented the position of the flow cell. At the sample, the incoming probe was split into reference and signal beams which were focused onto matching diodes to adjust for laser fluctuations.

The transient absorption measurements were performed as a function of temperature. Temperature control of the sample was achieved by flowing it through insulated tubing attached to a glass coil and reservoir which were immersed in a bath of 50/50 water/ethylene glycol. The bath temperature was controlled with a NesLab RTE-111 refrigerated bath/circulator, capable of maintaining temperatures from -25 to +150°C. A peristaltic pump flowed the sample from the reservoir to the coil and then to

the flow cell through insulated tubing. An accurate temperature measurement was ensured by incorporating a T-joint in the loop immediately following the sample cell with a temperature probe inserted. Solvent temperatures were varied from 2°C to 88°C in the butanols, 2°C to 54°C in methanol and from 3°C to 69°C in acetonitrile. For all solvents the temperature was maintained with an accuracy of ±0.5°C.

Time delayed absorption spectra were obtained of ~135mM solutions of CH_2BrI in 1-butanol, 2-butanol, methanol and acetonitrile at a delay of 20ps before time-zero, and at 4 or 5 set time delays after excitation ranging from 50ps to 6ns. The sample was pumped using a 271 nm UV excitation pump and probed with a white light continuum generated by focusing 800nm fundamental into an ethylene glycol filled cell. The signal was focused into a fiber optic cable fitted to an Ocean Optics spectrometer and averaged for ~2 minutes at each delay.

RESULTS

Transient absorption measurements were used to determine the rate constants for the decay of iso-CH_2Br--I. More detailed measurements as a function of temperature were then performed at specific characteristic wavelengths to determine any barrier(s) of the iso species. Broadband spectral measurements were also performed, at room temperature, to allow for characterization of the spectral response. The sections that follow will first present the results from spectral measurements and then the results from the temperature-dependent transient absorption measurements.

ABSORPTION SPECTRA

Time-dependent spectral measurements were performed on CH_2BrI in 1-butanol, methanol, and acetonitrile at room temperature and a concentration of ~135mM. (Figure 4.4) For 2-butanol, two sets of measurements were performed - the first at a concentration of ~135mM (Figure 4.5) and the second at 15mM (not shown[121]). All spectral measurements were conducted using a white-light continuum to probe the visible transient from 350 nm to 750 nm following excitation in the A-Band (271nm). The resulting spectra contained two strong absorptions; with the stronger of the two centered at ~443nm and decaying within the temporal range of the measurements. The weaker absorption was centered at ~380nm and increased in strength at longer delays. The wavelength and lifetime of the stronger absorption are distinct characteristics of the iso-CH_2Br--I species as determined by Tarnovsky et al[114].

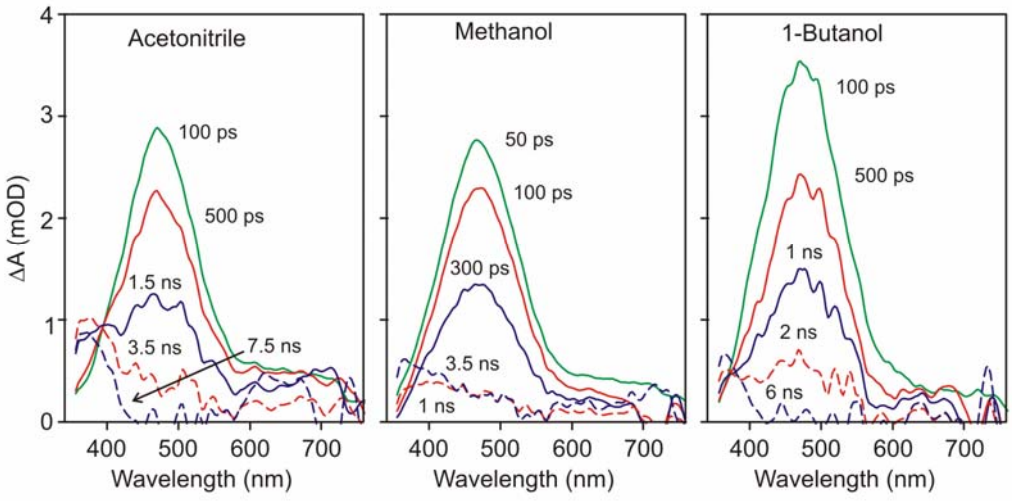

Figure 4.4: Fit Transient spectra obtained after excitation of CH_2BrI at 271 nm in acetonitrile, methanol and 1-butanol. Time delays are indicated in the figure. Temperature was 23-24°C.

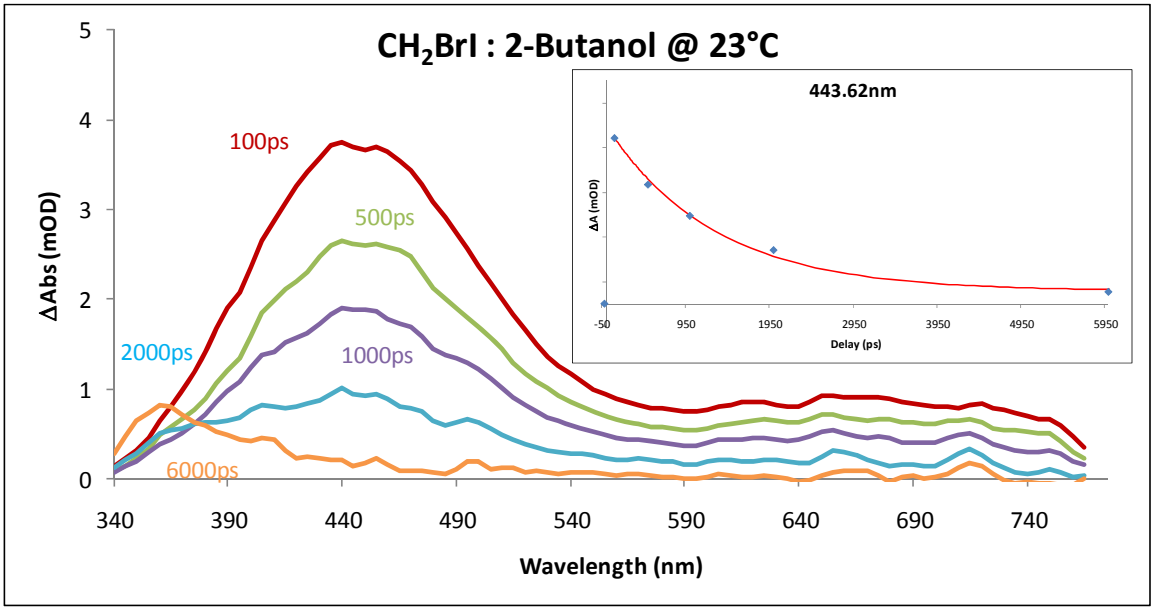

Figure 4.5: Time-dependent absorption spectra of CH_2BrI in 2-butanol (~130mM, 23°C) taken following 271nm excitation pulse at delays of -20ps (dark blue), 100ps (red), 500ps (green), 1000ps (purple), 2000ps (light blue), 6000ps (orange). Inset: fit to absorption values at 443nm as extracted from absorption spectra using two exponentials with R^2 = 0.9935.

A wavelength range was chosen from the peak absorption of the spectrum in each solvent and the rate of the decay extracted. The absorbance values for this wavelength range were plotted at each delay and fit to a decay component and a plateau. A typical example is shown for 2-butanol in Figure 4.5. The resulting fits provide an average rate constant, $k_{Spectral}$, for the decay of the iso-CH_2Br--I excited state species at room temperature. In 1-butanol, $k_{Spectral}$ was fit to a rate constant of 1.0×10^{-3} ps^{-1}, in 2-butanol (135mM) it was fit to 7.8×10^{-4} ps^{-1}, in methanol 2.7×10^{-3} ps^{-1} and in acetonitrile to a value of 7.2×10^{-4} ps^{-1}.(Table 4.1) More recent measurements were performed in 2-butanol at concentrations of 8, 15, and 33mM for which rate constants of 6×10^{-4}, 5×10^{-4} and 7×10^{-4} ps^{-1} were found.[121]

Solvent	$k_{Spectral}$ (ps^{-1})
1-Butanol	10 E-04
2-Butanol	7.8E-04
Methanol	2.7E-04
Acetonitrile	7.2E-04

Table 4.1: $k_{Spectral}$ values determined from time-delayed absorption spectral measurements performed in 1-butanol, 2-butanol, methanol and acetonitrile at room temperature with a concentration of ~135mM.

The decay rate constants, $k_{Spectral}$, obtained in all four solvents are of comparable magnitude and do not appear to be strongly influenced by the solvent type or concentration.

TEMPERATURE-DEPENDENT TRANSIENT ABSORPTION MEASUREMENTS

In order to investigate how the decay rate constant changed as a function of temperature narrow band transient absorption measurements were performed in 1-butanol, 2-butanol, methanol, and acetonitrile. All samples were prepared at a concentration of ~400mM and the sample was flowed to promote the excitation of a new volume with each laser pulse. Each volume was excited with a ~550nJ pulse centered at 271nm and probed with a time delayed pulse centered at 460nm. Accurate results were ensured by maintaining the temperature within ± 0.5°C as it was varied over the liquid phase range of the solvent.

1-BUTANOL

Measurements in 1-butanol were performed at temperatures ranging from 2 - 88°C with delay times extending from -35ps out to 8.6ns Figure 4.6). At approximately every 12 degrees the temperature was locked (±0.5C) and a series of scans performed then averaged. The averaged scans for each temperature were then fit to a series of three exponentials and a plateau using MRQ v.1.8 as developed by Ken Spears et al.[122] A typical fit result for CH_2BrI in 1-butanol is shown in Figure 4.7 at 2°C along with the residual difference between the scan and fit. The first exponential was assigned to a large, fast growth with a rate constant that increased from $2.1x10^{-01}$ ($\pm$ $0.3x10^{-01}$) ps^{-1} to $5.2x10^{-01}$ ($\pm$ $0.8x10^{-01}$) ps^{-1} as the temperature was increased from 2 to 88°C. A smaller growth was fit with rate constants ranging from $7.1x10^{-02}$ ($\pm$ $2x10^{-02}$) ps^{-1} to $6.9x10^{-02}$ ($\pm$ $0.5x10^{-02}$) ps^{-1}. The third exponential in the fit was a decay component with a rate constant that increased from $1.1x10^{-03}$ ($\pm$ $0.008x10^{-03}$) ps^{-1} to $4.3x10^{-03}$ ($\pm$ $0.08x10^{-03}$) ps^{-1} as the sample temperature was increased from 2.0 to 88.0°C. Lastly, a plateau was included in each fit to account for the signal that persisted through the observation window and increased in magnitude as the sample temperature was raised as shown in Figure 4.6. Fit values for each of the components in 1-butanol are listed in Table 4.2 at each temperature explored.

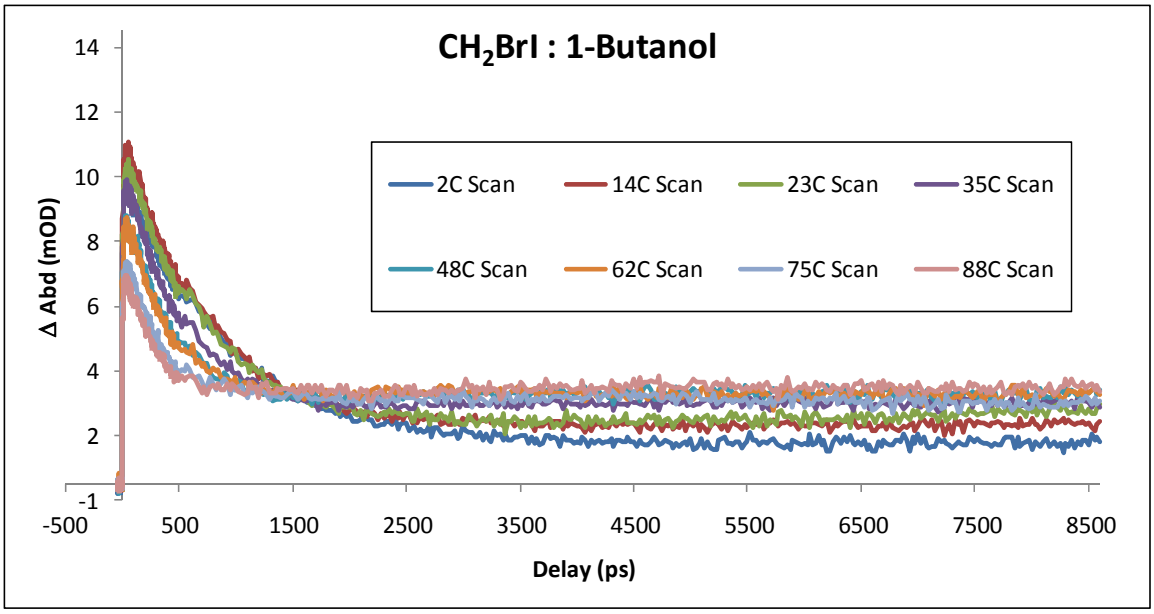

Figure 4.6: Temperature-dependent transient absorption scans of CH_2BrI dissolved in 1-butanol with delays spanning from -35ps to 8.6ns

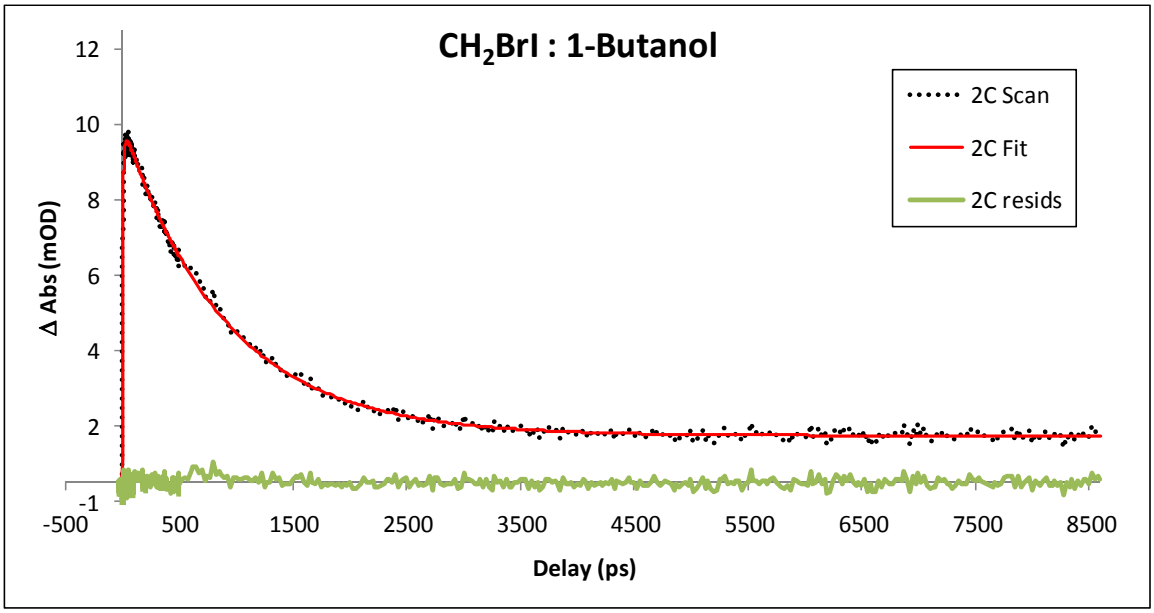

Figure 4.7: Transient absorption scan of CH_2BrI in 1-butanol (dotted black) with fit (solid red) and residuals (solid green) taken at 2°C.

	Temp °C	A_1	k_1 (ps^{-1})	*k_1 error*	A_2	k_2 (ps^{-1})	*k_2 error*	A_3	k_3 (ps^{-1})	*k_3 error*	A_4	k_4 (ps^{-1})
1-Butanol	2.0	-6.753	2.115E-01	*2.892E-02*	-2.466	7.098E-02	*1.668E-02*	9.432	1.112E-03	*8.019E-06*	1.421	0.00
	14.0	-9.005	2.784E-01	*2.290E-02*	-4.566	6.923E-02	*6.273E-03*	10.533	1.389E-03	*9.602E-06*	2.079	0.00
	23.0	-10.827	1.973E-01	*9.156E-03*	-2.207	3.435E-02	*4.630E-03*	9.805	1.495E-03	*1.566E-05*	2.192	0.00
	35.0	-7.760	3.335E-01	*2.878E-02*	-4.341	6.385E-02	*5.052E-03*	8.556	2.064E-03	*1.907E-05*	2.785	0.00
	48.0	-9.986	1.954E-01	*6.694E-03*	-3.300	1.087E-02	*1.522E-03*	9.008	3.189E-03	*1.264E-04*	3.129	0.00
	62.0	-7.228	3.188E-01	*2.607E-02*	-3.447	5.245E-02	*4.869E-03*	6.992	2.793E-03	*3.519E-05*	3.148	0.00
	75.0	-6.237	3.736E-01	*3.727E-02*	-3.244	5.697E-02	*5.344E-03*	5.604	3.131E-03	*4.724E-05*	2.935	0.00
	88.0	-4.903	5.205E-01	*7.557E-02*	-4.079	6.853E-02	*5.209E-03*	4.790	4.317E-03	*8.189E-05*	3.330	0.00

Table 4.2: Fit parameters to temperature-dependent transient absorption measurements as determined using MRQ v.1.8 for Bromoiodomethane in 1-butanol.

2-BUTANOL

Scans in 2-butanol were obtained with delays ranging from -35ps to 8.6ns (Figure 4.8) and temperatures spanning from 3°C to 88°C. A typical scan for CH_2BrI in 2-butanol is shown in Figure 4.9 alongside the fit result and residual difference between the two. As with 1-butanol, the best fit required three exponentials and a plateau. The first exponential represented a fast growth with a rate constant of 0.31(± 0.03) ps^{-1} at 3°C which shrank to 0.12(± 0.01) ps^{-1} at 88°C. The second component was also fit as a growth at 3°C with a value $7.9x10^{-02}$ (± $0.7x10^{-02}$). At 88°C the second component was fit with a smaller rate constant of 1.6×10^{-03} (± $3x10^{-03}$) which coincided with larger values being determined for the third the rate constant. The third exponential represented a decay component which was initially fit to a rate constant of $1.1x10^{-03}$ (± $0.007x10^{-03}$) ps^{-1} at 3°C and at 88°C to an artificially high value of 2.3×10^{-03} (±$2.2x10^{-03}$) ps^{-1}. The discrepancy can be attributed to the fitting algorithm inaccurately entangling the rate constants for the second and third components at the higher temperature. As observed for 1-butanol, the final component was a persistent plateau at all

temperatures and had a magnitude which increased with temperature as shown in Figure 4.8. For each of the scanned temperatures the fit values for each component are tabulated in Table 4.3.

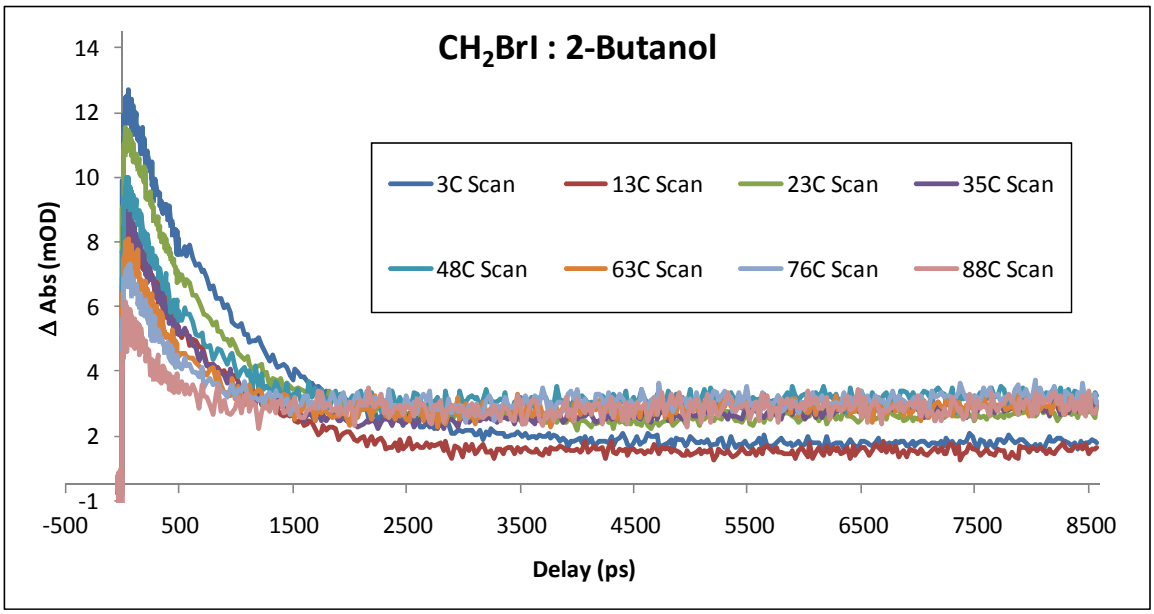

Figure 4.8: Temperature-dependent transient absorption scans of CH_2BrI in 2-butanol over delay range -36 ps to 8.6 ns.

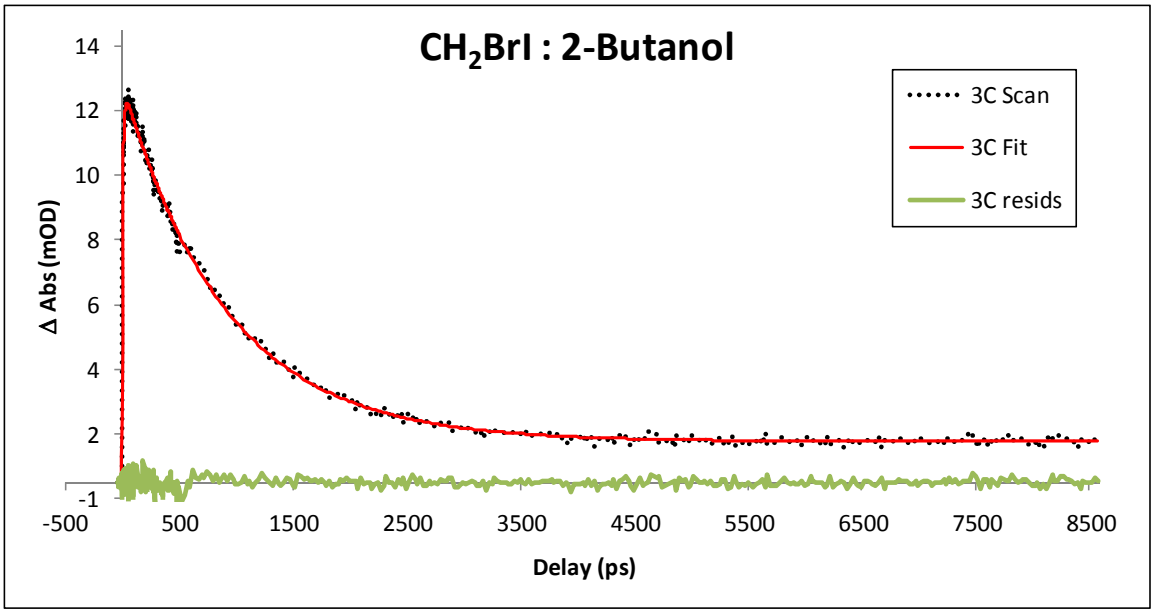

Figure 4.9: Typical transient absorption scan of CH_2BrI in 2-butanol (dotted black) along with the fit result (solid red) and the residuals (solid green).

	Temp °C	A_1	k_1 (ps^{-1})	*k_1 error*	A_2	k_2 (ps^{-1})	*k_2 error*	A_3	k_3 (ps^{-1})	*k_3 error*	A_4	k_4 (ps^{-1})
2-Butanol	3.0	-9.381	3.100E-01	*3.259E-02*	-6.214	7.910E-02	*6.873E-03*	13.088	1.097E-03	*7.259E-06*	1.494	0.00
	13.0	-6.286	1.628E-01	*1.054E-02*	-1.278	1.819E-02	*3.168E-03*	8.528	1.312E-03	*1.716E-05*	1.138	0.00
	23.0	-9.149	1.623E-01	*7.447E-03*	-1.832	2.527E-02	*3.678E-03*	11.152	1.558E-03	*1.516E-05*	2.360	0.00
	35.0	-7.143	1.205E-01	*3.709E-03*	-3.218	3.978E-03	*1.744E-03*	10.928	2.156E-03	*2.520E-04*	2.256	0.00
	48.0	-6.919	2.595E-01	*4.048E-02*	-3.960	5.164E-02	*6.936E-03*	9.032	2.025E-03	*2.825E-05*	3.168	0.00
	63.0	-5.592	1.050E-01	*6.903E-03*	-2.046	6.103E-03	*3.578E-03*	8.115	2.647E-03	*3.074E-04*	2.650	0.00
	76.0	-5.007	2.267E-01	*3.995E-02*	-2.461	3.489E-02	*7.234E-03*	5.787	2.751E-03	*8.240E-05*	3.098	0.00
	88.0	-4.892	1.189E-01	*1.061E-02*	-3.167	1.626E-03	*3.201E-03*	6.857	2.284E-03	*2.240E-03*	2.873	0.00

Table 4.3: Fit parameters to temperature-dependent transient absorption measurements determined for CH_2BrI in 2-butanol.

In addition to 1- and 2-butanol, measurements were performed on CH_2BrI dissolved in methanol. As with the previous alcohols, methanol also required three components for an accurate fit. However, in contrast to the butanols where a plateau of increasing magnitude was required, the plateau in methanol was of a consistent magnitude that did not vary with temperature. (Figure 4.10)

Methanol

For the experiments performed in methanol the temperature was varied from 2°C to 54°C; a much narrower temperature range due to the decreased boiling point of the solvent. In addition, the extent of the time delays was decreased as all the dynamics occurred within the first 3ns. Figure 4.11 shows a typical transient absorption scan of CH_2BrI in methanol along with the fit to the scan and the residual. As stated above, fitting of the scans was accomplished using three components: a fast growth, a slow growth and a decay. The fast growth was fit to rate constants of $1.1x10^{-01}$ ($\pm$ $0.02x10^{-01}$) ps^{-1} at 2°C and $1.2x10^{-01}$ ($\pm$ $0.01x10^{-01}$) ps^{-1} at 54°C. For the second, slow, growth component the rate constants extracted increased from $8.3x10^{-04}$ ($\pm$ $0.8x10^{-04}$) ps^{-1} to $1.9x10^{-02}$ ($\pm$ $0.9x10^{-02}$) ps^{-1} as the temperature was raised from 2°C to 54°C. Rate constants for the final component increased from $2.5x10^{-03}$($\pm$ $0.03x10^{-03}$) ps^{-1} to $4.5x10^{-03}$ ($\pm$ $0.2x10^{-03}$) ps^{-1} between 2 and 54°C, suggesting an increasingly fast decay. Lastly, the small, temperature independent plateau included had an approximately constant magnitude (Figure 4.10). Table 4.4 lists the values obtained for each component across the temperature range explored.

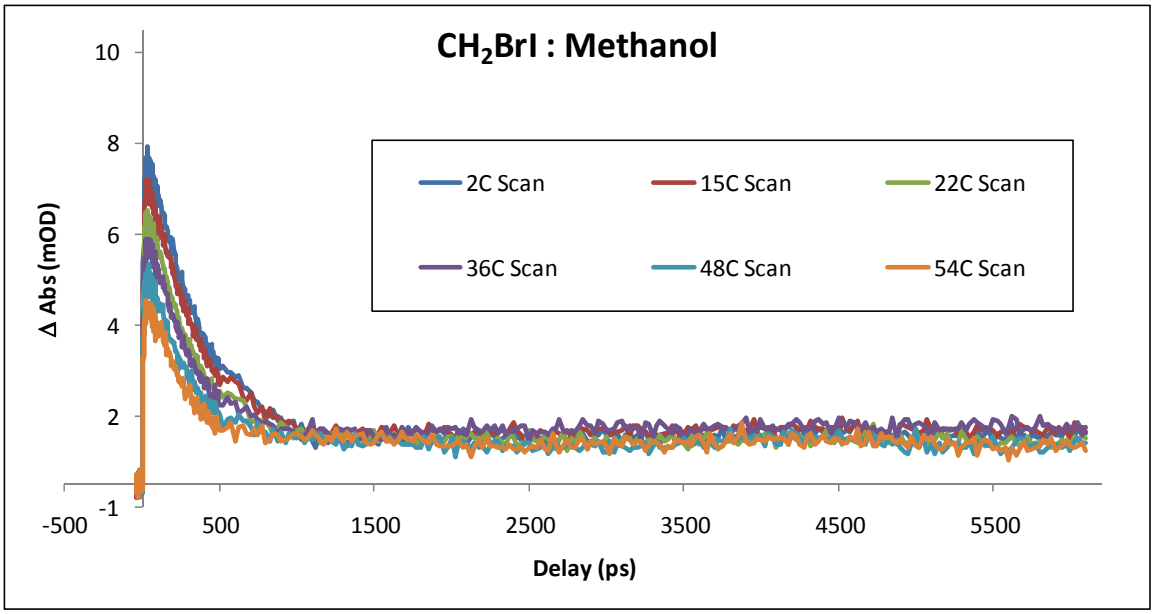

Figure 4.10: Temperature-dependent transient absorption scans of bromoiodomethane dissolved in methanol with delays ranging from -35ps to 6.1 ns.

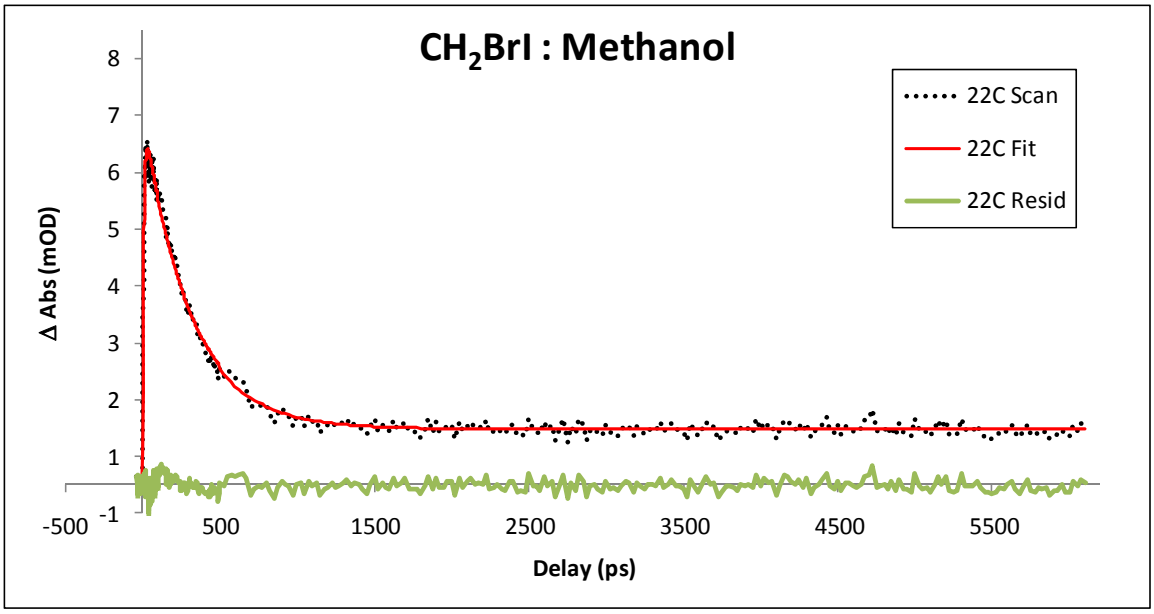

Figure 4.11: Typical scan of bromoiodomethane in methanol (dotted black) alongside the fit (solid red) and the residuals (solid green) at 22°C.

	Temp °C	A_1	k_1 (ps^{-1})	*k_1 error*	A_2	k_2 (ps^{-1})	*k_2 error*	A_3	k_3 (ps^{-1})	*k_3 error*	A_4	k_4 (ps^{-1})
Methanol	2.0	-8.499	1.140E-01	*2.189E-03*	-1.260	8.313E-04	*7.801E-05*	9.386	2.496E-03	*2.932E-05*	1.345	0.00
	15.0	-7.075	1.141E-01	*2.475E-03*	-1.360	1.013E-03	*6.205E-05*	8.209	2.616E-03	*2.601E-05*	1.376	0.00
	22.0	-7.001	1.144E-01	*3.031E-03*	-1.180	1.711E-03	*2.412E-04*	7.951	2.959E-03	*6.438E-05*	1.182	0.00
	36.0	-6.354	1.054E-01	*2.794E-03*	-1.500	1.125E-03	*1.265E-04*	7.256	2.981E-03	*7.274E-05*	1.541	0.00
	48.0	-5.214	1.036E-01	*3.589E-03*	-1.030	1.946E-03	*3.423E-04*	6.175	3.254E-03	*1.071E-04*	1.075	0.00
	54.0	-3.840	1.231E-01	*1.196E-02*	-1.030	1.868E-02	*9.359E-03*	4.654	4.471E-03	*2.159E-04*	1.031	0.00

Table 4.4: Fit parameters to temperature-dependent transient absorption measurements as determined for bromoiodomethane in methanol.

Acetonitrile

Acetonitrile was the final solvent chosen to investigate the temperature-dependent dynamics of iso-bromoiodomethane for multiple reasons. First, it was the solvent used by Tarnovsky et al. and allows for comparison with their studies.[114] Second, while acetonitrile and methanol are both short polar solvents, acetonitrile does not contain hydrogen bonding. This key difference affords investigation into the effects of polarity on reaction dynamics without the complication of a hydrogen bonded solvent.

Scans at select temperatures of CH_2BrI in acetonitrile are shown in Figure 4.12. Qualitatively the dynamics in acetonitrile appear to differ quite a bit from other solvents explored. This assessment is supported quantitatively with three exponentials corresponding to fast and slow growth components and a decay component with rate constants differing by at least one order of magnitude from one another. The fast growth component fit to rate constants of 10×10^{-02} ($\pm 0.4\times10^{-02}$) ps^{-1} and 12×10^{-02}($\pm2\times10^{-02}$) ps^{-1} at 3°C and 69°C, respectively. The second component was fit to rate constants of 2.2×10^{-03}($\pm 1\times10^{-03}$) ps^{-1} at 3°C and 1.9×10^{-02}($\pm0.4\times10^{-02}$) ps^{-1} at 69°C. The final

component, the decay, was the most surprising as it was fit with rate constants of $8.8x10^{-04}(\pm 0.6x10^{-04})$ ps^{-1} at 3°C and $9.5x10^{-04}(\pm 0.4x10^{-04})$ ps^{-1} at 69°C. The two rate constants are essentially the same within the error bars, suggesting that the decay is temperature independent in acetonitrile. The temperature independence of this decay is in direct contradiction to the results measured in the alcohols. Lastly, a small plateau was included in the fit with a magnitude that was essentially constant.

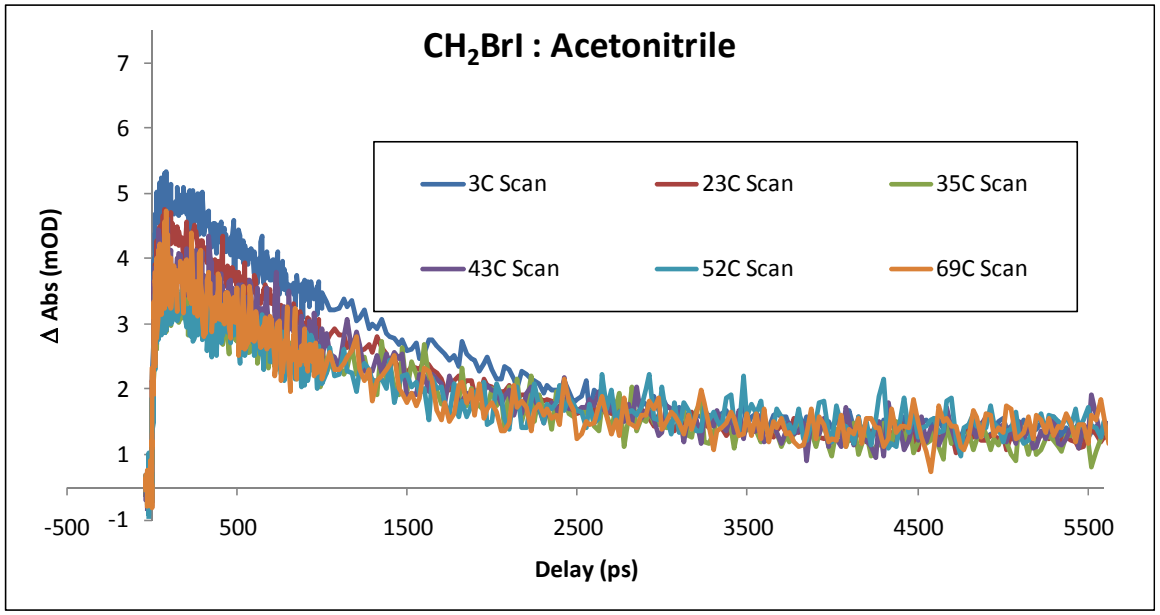

Figure 4.12: Temperature-dependent transient absorption scans of Bromoiodomethane in Acetonitrile.

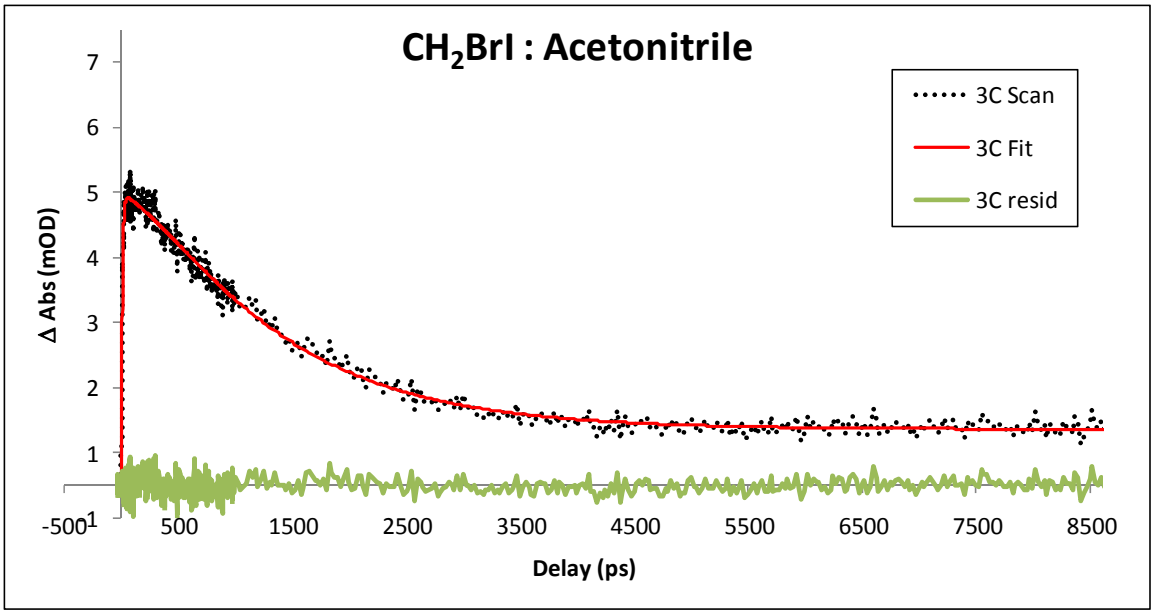

Figure 4.13: Typical transient absorption scan of CH_2BrI in Acetonitrile (dotted black) with the fit result (solid red) and residuals (solid green).

	Temp °C	A_1	k_1 (ps^{-1})	*k_1 error*	A_2	k_2 (ps^{-1})	*k_2 error*	A_3	k_3 (ps^{-1})	*k_3 error*	A_4	k_4 (ps^{-1})
Acetonitrile	3.0	-5.385	1.047E-01	*3.958E-03*	-1.822	2.243E-03	*5.662E-04*	5.915	8.841E-04	*6.097E-05*	0.975	0.00
	23.0	-3.601	1.177E-01	*8.319E-03*	-1.160	1.440E-02	*1.922E-03*	4.172	8.085E-04	*1.294E-05*	0.821	0.00
	35.0	-2.604	6.798E-02	*5.013E-03*	-1.123	1.184E-03	*1.758E-03*	3.563	6.994E-04	*3.339E-04*	0.720	0.00
	43.0	-3.148	8.816E-02	*9.134E-03*	-1.093	3.632E-03	*1.494E-03*	3.916	9.335E-04	*8.485E-05*	0.971	0.00
	52.0	-2.600	7.704E-02	*8.909E-03*	-0.854	4.186E-03	*2.188E-03*	2.822	1.087E-03	*1.301E-04*	1.132	0.00
	69.0	-2.268	1.183E-01	*2.407E-02*	-1.192	1.831E-02	*4.419E-03*	3.172	9.541E-04	*3.888E-05*	0.949	0.00
	6.0	-6.131	1.251E-01	*7.615E-03*	-1.427	1.085E-02	*2.027E-03*	6.596	7.842E-04	*1.724E-05*	0.935	0.00
	22.0	-5.538	1.110E-01	*7.617E-03*	-1.591	1.039E-02	*1.929E-03*	6.009	7.478E-04	*1.923E-05*	0.906	0.00
	42.0	-4.235	8.145E-02	*3.206E-03*	-2.501	2.147E-03	*5.680E-04*	5.893	9.768E-04	*9.669E-05*	0.839	0.00
	61.0	-3.366	9.496E-02	*5.821E-03*	-1.151	6.975E-03	*1.297E-03*	3.352	9.572E-04	*3.595E-05*	0.742	0.00

Table 4.5: Fit parameters to temperature-dependent transient absorption measurements as determined using MRQ v.1.8 for Bromoiodomethane in Acetonitrile.

DISCUSSION

Kwok et al. performed picosecond time-resolved resonance Raman experiments in cyclohexane following A-band excitation at 266nm and concluded that iso-CH_2Br--I was the primary product following A-band excitation of CH_2BrI. [120] They proposed that

iso-CH_2Br--I is produced within several picoseconds through geminate recombination and decays within ~2-3ns. Their DFT calculations also predict that the iso-CH_2I--Br isomer is more stable than iso-CH_2Br--I (4.1 kcal·mol^{-1}) and should have a lifetime on the order of >10ns. This predicted lifetime suggest that iso-CH_2I--Br was likely the species observed in ns- resonance Raman experiments performed by Zheng et al. which resulted from isomerization of iso-CH_2Br--I to iso-CH_2I--Br.[120]

In our analysis, rate constants measured in all four solvents from time-delayed absorption spectra ($k_{Spectral}$) and room temperature transient absorption spectroscopy ($k_{Experimental}$) are compared. The rate constants for $k_{Experimental}$ are significantly larger than the values obtained for $k_{Spectral}$. The lifetimes corresponding to these rate constants (Table 4.6) are all shorter than the decay lifetimes proposed by Kwok et al in cyclohexane. As a result, the hypothesis presented here is that iso-CH_2Br--I decays through a solvent-assisted isomerization, as Kwok et al suggested[120], and a diffusion-controlled reaction between iso-CH_2Br--I and CH_2BrI as shown below in Figure 4.14.

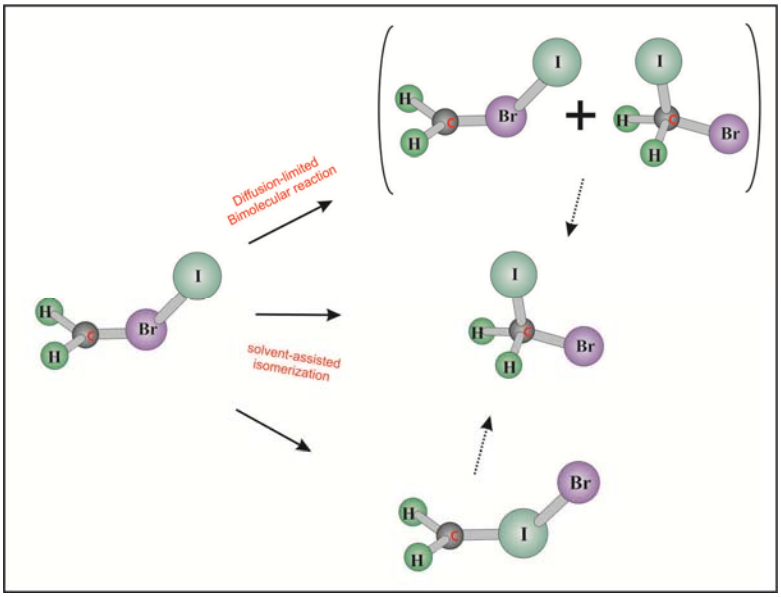

Figure 4.14: Suggested decay pathways for iso-CH_2Br—I through solvent assisted isomerization and diffusion-limited bimolecular reaction with CH_2BrI

In order to support the assignment of a diffusion-controlled reaction, rate constants were calculated for the possible reactions of iso-CH_2Br--I with CH_2BrI in each solvent using several approximations. The resulting diffusion-controlled rate constants were then compared to the experimentally measured values from temperature-dependent transient absorption and time-delayed spectral measurements.

Iso-CH_2I-Br Lifetimes

Temp(°C)	Methanol	1-Butanol	2-Butanol	Acetonitrile
2.0	400 (± 5)	900 (± 6)		
3.0			911 (± 6)	1131 (± 73)
4.0				
6.0				1275 (± 27)
12.0				
13.0			762 (± 10)	
14		720 (± 5)		
15.0	382 (± 4)			
16.0				
20.0				
22.0	338 (± 7)			1337 (± 34)
23		669 (± 7)	642 (± 6)	1237 (± 20)
25				
34.0				
35.0		485 (± 4)	464 (± 49)	1430 (± 462)
36.0	335 (± 8)			
42.0				1024 (± 92)
43.0				1071 (± 90)
47.0				
48.0	307 (± 10)	314 (± 12)	494 (± 7)	
50.0				
52.0				920 (± 98)
54.00	224 (± 10)			
61.0				1045 (± 38)
62		358 (± 5)		
63.0			378 (±39)	
69.0				1048 (± 41)
75		319 (± 5)		
76.0			364 (± 11)	
88.0		232 (± 4)	438 (± 217)	

Table 4.6: Tabulated values for iso-CH_2Br--I lifetimes expressed in picoseconds (with error bars) as determined from fits using MRQ v.1.8 of temperature-dependent transient absorption measurements.

As a first approximation, the reaction between iso-CH_2Br--I and CH_2BrI was performed using the simplest model for a diffusion-controlled bimolecular reaction in solution. In this model each species is represented as an uncharged, spherical isotropic

particle, each “encounter”, or collision, between solute molecules results in reaction and the solvent is represented as a continuum.[123,124] The diffusion coefficient of each particle is related to the viscosity via the Einstein-Stokes relationship,

$$D(T) := \frac{k_B \cdot T}{6 \cdot \pi \cdot r \cdot \eta(T)} \tag{1}$$

where $\eta(T)$ is the temperature-dependent viscosity of the solvent, r is the particle radius, k_B is the Boltzmann constant and T is temperature in Kelvin. The diffusion-limited rate constant, k_D, for the reaction between iso-CH_2Br--I and CH_2BrI is equal to the sum of the diffusion coefficient for each species interacting at a critical radius R.

$$k_D(T) := 4\pi \, R \cdot \left(\frac{k_B \cdot T}{6\pi \, \eta(T) \cdot r_{isoCH2BrI}} + \frac{k_B \cdot T}{6\pi \, \eta(T) \cdot r_{MeBrI}} \right) \tag{2}$$

The critical radius is then assumed to be equal to the sum of the radii for both molecules. Substituting R with (r_{iso} + r_{MeIBr}), equation 2 simplifies to:

$$k_D(T) := N_A \cdot \left[\frac{2 \cdot k_B \cdot T \cdot \left(r_{iso} + r_{MeIBr} \right)^2}{3 \cdot \eta(T) \cdot r_{iso} \cdot r_{MeIBr}} \right] \tag{3}$$

Equation 3 is then multiplied by the concentration, C_{MeIBr}, giving the rate constant:

$$k_{Diffusion}(T) := \frac{k_D(T) \cdot C_{MeIBr}}{10^{12}} \quad (4)$$

for the decay of iso-CH_2Br--I through interaction with CH_2BrI.[123,124] All calculations used radii lengths of 5.4Å and 3.93Å for iso-CH_2Br--I and CH_2BrI, respectively. These radii lengths were calculated using optimized geometries from DFT calculations performed by Wang et al.[24] Rate constants for the diffusion-limited reaction between iso-CH_2Br--I and CH_2BrI were calculated in1-butanol, 2-butanol, methanol and acetonitrile assuming a concentration of ~398mM. Due to the high concentration of the sample it is presumed that iso-CH_2Br--I reacts primarily with CH_2BrI through a diffusion-controlled bimolecular reaction. The diffusion-limited rate constants were then compared to the decay rate constants measured in temperature-dependent transient absorption measurements "$k_{Experimental}$" and from the time-delayed absorption spectra "$k_{Spectral}$".

The natural log of the experimental rate constants were plotted against inverse temperature and fit with a linear regression such that:

$$\ln k = \ln A - \frac{Ea}{RT} \quad (5)$$

where, A is the Arrhenius pre-factor, Ea is the effective activation energy, T is the temperature(K) and R is the universal gas constant. Rate constants were then calculated using Equation 4 for the first approximation of the diffusion-controlled reaction between iso-CH_2Br--I and CH_2BrI. The natural log of the rate constants from calculations

(ln $k_{Diffusion}$), experiments (ln $k_{Experimental}$), and the Arrhenius fit to experimental values were then plotted against T^{-1} for comparison.

1-BUTANOL

The natural log of the rates constants, $k_{Diffusion}$ and $k_{Experimental}$, determined in 1-butanol are plotted in Figure 4.14. First, it is clear from the figure and values in Table 4.7 that the Arrhenius fit is a good approximation to the experimental data. Figure 4.14 also shows how the diffusion-controlled rate constants ($k_{Diffusion}$, dash-dotted green) do a good job of estimating the experimentally measured rate constants at high temperatures but underestimate it at low temperatures. A linear fit of the diffusion-controlled rate constants has a steeper slope than the Arrhenius fit to the experimental results. The steeper slope suggests that the diffusion-controlled model assigns a more significant temperature dependence to the rate constant than is measured experimentally.

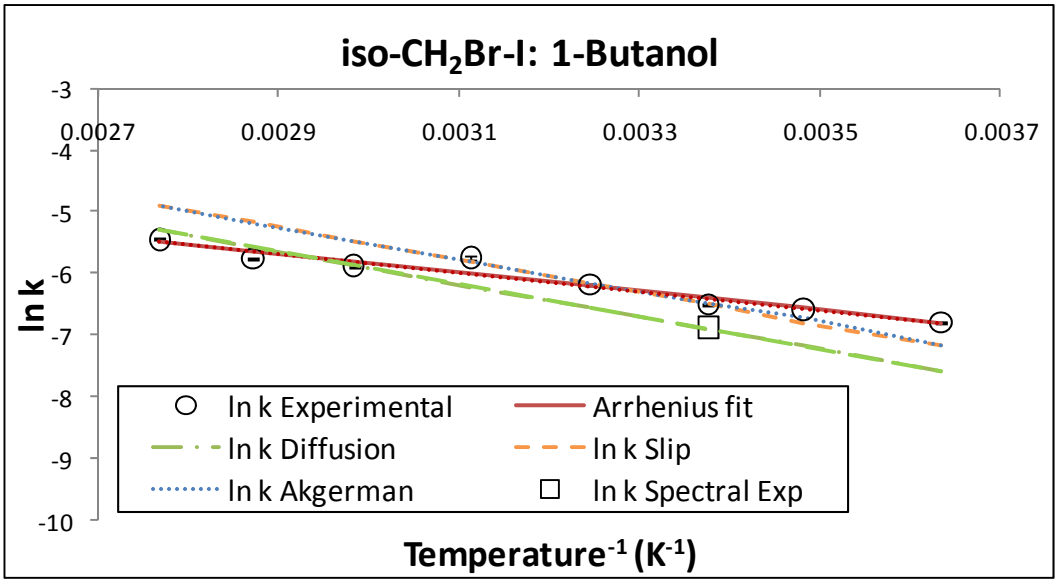

Figure 4.15: ln k vs T^{-1} plot of iso-CH_2Br--I decay rate constants in 1-butanol determined experimentally ($k_{Experimental}$, open circles), from an Arrhenius fit to the experimental values (solid red), and calculated values $k_{Diffusion}$ (dash-dot green), k_{Slip} (orange dashed) and $k_{Akgerman}$ (dotted blue), and the experimental value of $k_{Spectral}$ (black box).

In addition to differences in the expected temperature-dependence of the decay rate constant, the diffusion-controlled model predicts rate constants lower than were measured in temperature-dependent transient absorption measurements at low temperatures (Table 4.7). The significant underestimation of the rate constant for low temperatures suggests that iso-CH_2Br--I likely decays through an additional mechanism at the higher concentration. At a concentration of ~135mM, the similarity of the room temperature rate constant values for $k_{Spectral}$ and $k_{Diffusion}$ seems to support a diffusion-controlled reaction for the decay of iso-CH_2Br—I. It would seem that the discrepancy between $k_{Spectral}$ and $k_{Experimental}$ become significant only for the higher concentration (~398mM) used in temperature-dependent transient-absorption measurements. As a

result, it seems that a better model is needed to calculate the decay rate constants for iso-CH_2Br—I at the higher concentrations.

Rate Constants - 1-Butanol

Temp (°C)	$k_{Experimental}$ ±(error) (ps^{-1})	$k_{Arrhenius}$ (ps^{-1})	$k_{Diffusion}$ (ps^{-1})	k_{Slip} (ps^{-1})	$k_{Akgerman}$ (ps^{-1})	$k_{Spectral}$ (ps^{-1})
2.0	1.1E-03 *±(8.0E-06)*	1.115E-03	0.5E-03	0.8E-03	0.8E-03	
14.0	1.4E-03 *±(9.6E-06)*	1.405E-03	0.8E-03	1.1E-03	1.2E-03	
23.0	1.5E-03 *±(1.6E-05)*	1.651E-03	1.0E-03	1.5E-03	1.5E-03	1.0E-03
35.0	2.1E-03 *±(1.9E-05)*	2.017E-03	1.4E-03	2.1E-03	2.1E-03	
48.0	3.2E-03 *±(1.3E-04)*	2.464E-03	2.0E-03	3.0E-03	3.0E-03	
62.0	2.8E-03 *±(3.5E-05)*	3.005E-03	2.8E-03	4.2E-03	4.2E-03	
75.0	3.1E-03 *±(4.7E-05)*	3.561E-03	3.8E-03	5.7E-03	5.6E-03	
88.0	4.3E-03 *±(8.2E-05)*	4.169E-03	5.0E-03	7.5E-03	7.4E-03	

Table 4.7: Tabulated values of the experimental rate constant ($k_{Experimental}$), calculated values using the Arrhenius fit ($k_{Arrhenius}$), and calculations, of increasing complexity, ($k_{Diffusion}$, k_{Slip}, $k_{Akgerman}$) for the diffusion-controlled reaction model between iso-CH_2Br--I and CH_2BrI in 1-butanol. Also included is the value for $k_{Spectral}$ determined from time-delayed spectral measurements.

The discrepancies in the iso-CH_2Br--I decay rate constants measured at room temperature are likely due to approximations in the model used for calculating the diffusion-controlled rate constants. To test this theory, more rigorous methods were employed to calculate the diffusion coefficients of iso-CH_2Br--I and CH_2BrI.

The second method used for calculating the diffusion coefficients for the diffusion-controlled bimolecular collision between iso-CH_2Br--I and CH_2BrI included a key improvement in how the solvent was modeled. Rather than representing the solvent as a continuum the solvent was now comprised of nonpolar, isotropic spherical

particles. This adjustment now allowed for some portion of solute particles to "slip" by solvent molecules rather than diffusing through a continuum representing its properties.[123-126] In this model, the diffusion coefficient for each solute particle is related to the viscosity in the same way as Equation 1 with the number of solvent molecules around each solute particle, or correlation number, changed from 6 to 4 in Equation 6:

$$D_{slip}(T) := \frac{k_B \cdot T}{4\pi \ \eta(T) \cdot r} \tag{6}$$

The diffusion coefficient is again the sum of the diffusion coefficients for each molecule and the critical radius $R = (r_{iso} + r_{MeIBr})$, giving Equation 7.

$$k_{Dslip}(T) := \frac{N_A \cdot k_B \cdot T \cdot \left(r_{iso} + r_{MeIBr}\right)^2}{\eta(T) \cdot r_{iso} \cdot r_{MeIBr}} \tag{7}$$

Once again, we multiple the diffusion coefficient by the concentration to get:

$$k_{Slip}(T) := \frac{k_{Dslip}(T) \cdot C_{MeIBr}}{10^{12}} \tag{8}$$

k_{Slip} was then used to calculate rate constants for the decay of iso-CH_2Br--I through a diffusion-controlled bimolecular reaction with CH_2BrI. As with the previous calculation, CH_2BrI was chosen as the most likely candidate for iso-CH_2Br--I to react with due to the

high concentration of the sample. The results of the calculations are listed in Table 4.7 and the natural log of the rate constants plotted as "ln k_{Slip}" in Figure 4.15 (orange-dashed).

Rate constants calculated using Equation 8 are an improvement over those calculated with the previous diffusion coefficient. While previous calculations did a good job predicting the decay rate constant at high temperatures they did poorly at low temperatures. With the change in the correlation number the values of the calculated rate constants were increased across the entire temperature range. The net effect being a "translation" of the ln k line such that it overlapped the experimental values at the intermediate temperatures. As a result of the translation, the rate constants calculated using K_{Slip} are in better agreement with the experimental values at all temperatures. Although the new results are a better representation of the experimental values, the discrepancies at both high and low temperatures are still considered unfavorable and imply that the calculations be further improved.

The implication of the new results is that the decay of iso-CH_2Br--I is better represented by a diffusion-controlled bimolecular reaction in which the solvent does not affect every solute particle equally. However, the differences also suggest that k_{Slip} may overcompensate and/or underestimate the extent to which the solvent affects the decay dynamics. The agreement between the new approximation and the experimental values can be further improved through an empirical determination of the correlation

number in Equation 6[124]. When this strategy is employed a correlation number of 1.15 gives the best fit but does not seem to suggest a physical explanation.

Finally, the most rigorous method used to calculate diffusion-controlled rate constants involved diffusion coefficients which account for the mass and volume of each particle. In order to accomplish this, an additional term is incorporated which accounts for the energy necessary for a solute molecule to diffuse or "jump" away from the solvent molecules with which it is correlated. The net effect of which is to create a "hole" which is subsequently filled by a solvent molecule. In this formalism, developed by Akgerman and Gainer[127-129], the diffusion coefficients are:

$$D_{Akgerman\_CH2BrI}(T) := \frac{k_B \cdot T}{\xi_C \cdot \eta(T)} \cdot \left(\frac{N_A}{V_{Butanol}} \right)^{\frac{1}{3}} \cdot \left(\frac{M_{Butanol}}{M_{MeIBr}} \right)^{\frac{1}{2}} \cdot e^{\left(\frac{\Delta E}{RT} \right)} \quad (9)$$

$$D_{Akgerman\_isoCHBrI}(T) := \frac{k_B \cdot T}{\xi_A \cdot \eta(T)} \cdot \left(\frac{N_A}{V_{Butanol}} \right)^{\frac{1}{3}} \cdot \left(\frac{M_{Butanol}}{M_{iso}} \right)^{\frac{1}{2}} \cdot e^{\left(\frac{\Delta E}{RT} \right)} \quad (10)$$

where k_B is the Boltzmann constant, $\eta(T)$ is the temperature dependent viscosity, N_A is Avogadro's number, $V_{Butanol}$ and $M_{Butanol}$ represent the molar volume and molecular weight of 1-butanol, respectively. ζ is the correlation number for the particle as determined from Equations 11 and 12 and ΔE is the activation energy difference

between jumping energies associated with different molecules calculated with Equation 13.[128]

$$\xi_A := 6\left(\frac{V_{iso}}{V_{Butanol}}\right)^{\frac{1}{6}} \qquad \xi_C := 6\left(\frac{V_{MeIBr}}{V_{Butanol}}\right)^{\frac{1}{6}} \tag{11 \& 12}$$

$$\Delta E := E_{BB} - E_{AB} \tag{13}$$

Where E_{BB}, E_{AB} and E_{AA} are calculated according to equations put forth by Akgerman and Gainer[128]:

$$E_{BB} := \frac{-R\cdot\ln\left(\frac{\eta(T_2)}{\eta(T_1)}\right) + \frac{R}{2}\cdot\ln\left(\frac{T_1}{T_2}\right)}{\frac{1}{T_1} - \frac{1}{T_2}} \qquad E_{AB} := \left(E_{BB}\right)^{\frac{\xi_A}{\xi_{A+1}}}\cdot E_{AA}^{\frac{1}{\xi_{A+1}}} \tag{12 \& 13}$$

$$E_{AA} := 5875.3\cdot\left(M_{MeIBr}\right)^{-0.186} \tag{14}$$

With, T_1 and T_2 covering the range for which $\eta(T)$ is most accurate. As with previous calculations the diffusion coefficient for the diffusion-controlled bimolecular collision is the sum of the individual diffusion coefficients

$$k_{D\_Akgerman}(T) := \left[4\cdot\pi\cdot N_A\left(r_{iso} + r_{MeIBr}\right)\cdot\left(D_{Akgerman\_CH2BrI}(T) + D_{Akgerman\_CH2BrI}(T)\right)\right] \tag{15}$$

Where the radius, R, has already been replace as the sum of r_{iso} and r_{MeIBr} and the final rate constants are calculated according to:

$$k_{Akgerman}(T) := \frac{k_{D\_Akgerman}(T) \cdot C_{MeIBr}}{10^{12}} \tag{16}$$

The rate constants calculated using this approach are listed in Table 4.6, plotted in Figure 4.14 (blue dotted) and are quite similar to those calculated using Equation 9. At high temperatures the two vary only slightly while $k_{Akgerman}$ gives slightly better correlation with the experimental results at low temperatures. Overall, $k_{Akgerman}$ does the best job of replicating the temperature-dependence observed experimentally. $k_{Diffusion}$ accurately predicts $k_{Spectral}$ - implying that at room temperature and lower concentration (~135mM) it is the best representation of the dynamics occurring.

The hypothesis put forth above suggested that iso-CH_2Br--I undergoes similar dynamics in all four solvents. If this assumption is true then the same analysis can be applied to analyze the temperature-dependent rate constant in each of the additional three solvents. The results of those analyses are presented below.

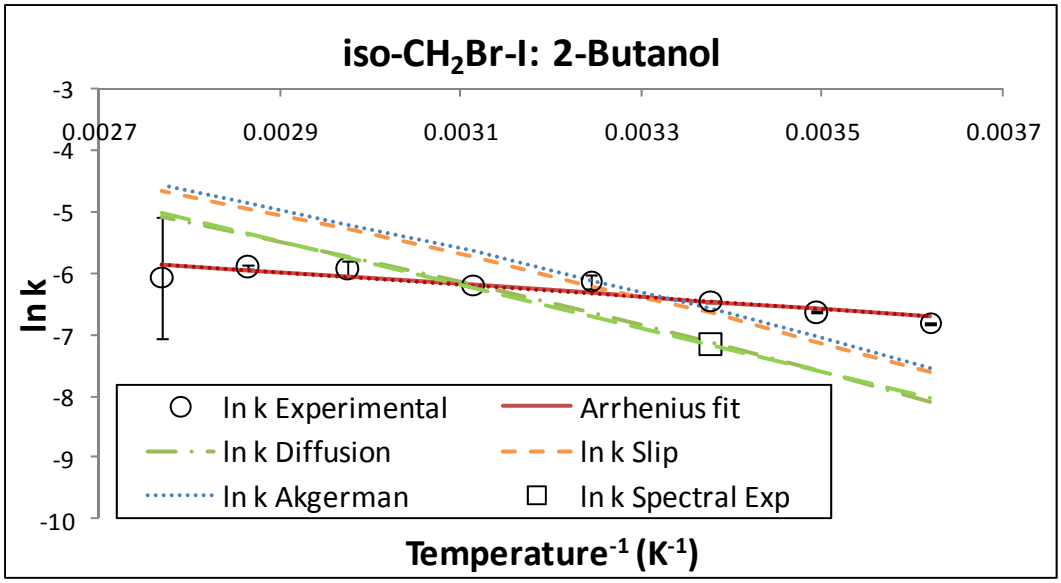

Figure 4.16: ln k vs T^{-1} plot of iso-CH_2Br--I decay rate constants in 2-butanol determined experimentally ($k_{Experimental}$, open circles), from an Arrhenius fit to the experimental values (solid red), and calculated values $k_{Diffusion}$ (dash-dot green), k_{Slip} (orange dashed) and $k_{Akgerman}$ (dotted blue), and the experimental value of $k_{Spectral}$ (black box).

2-BUTANOL

As with 1-butanol, rate constants were calculated using all three approaches – $k_{Diffusion}$, k_{Slip} and $k_{Akgerman}$ for the diffusion-controlled bimolecular reaction between iso-CH_2Br--I and CH_2BrI. In 2-butanol all three diffusion coefficients produced similar results. Each approximation predicted a much larger temperature dependence to the decay of iso-CH_2Br--I as well as overestimating (underestimating) the rate constants at high(low) temperatures respectively.(Figure 4.15) $k_{Diffusion}$, has the best correlation with values for $k_{Spectral}$ as measured by time-delayed spectral measurement[121]. However, the calculated values are still ~0.5 the rate constant measured in the temperature-dependent transient absorption measurements. We propose that the differences are the result of the decay of iso-CH_2Br--I proceeding primarily through a solvent-assisted

isomerization at room temperature and concentrations up to 135mM. Once the concentration and temperature are increased the experimentally measured rate constants are dominated by the diffusion-controlled reaction with CH_2BrI in 2-butanol and possibly the other solvents.

Rate Constants - 2-Butanol

Temp (°C)	$k_{Experimental}$ ±(error) (ps^{-1})	$k_{Arrhenius}$ (ps^{-1})	$k_{Diffusion}$ (ps^{-1})	k_{Slip} (ps^{-1})	$k_{Akgerman}$ (ps^{-1})	$k_{Spectral}$ (ps^{-1})
3.0	1.1E-03 *±(7.3E-06)*	1.217E-03	0.3E-03	0.5E-03	0.5E-03	
13.0	1.3E-03 *±(1.7E-05)*	1.381E-03	0.5E-03	0.8E-03	0.9E-03	
23.0	1.6E-03 *±(1.5E-05)*	1.555E-03	0.8E-03	1.3E-03	1.4E-03	0.8E-03
35.0	2.2E-03 *±(2.5E-04)*	1.775E-03	1.3E-03	2.0E-03	2.2E-03	
48.0	2.0E-03 *±(2.8E-05)*	2.025E-03	2.1E-03	3.2E-03	3.5E-03	
63.0	2.6E-03 *±(3.1E-04)*	2.328E-03	3.3E-03	5.0E-03	5.4E-03	
76.0	2.8E-03 *±(8.2E-05)*	2.601E-03	4.6E-03	7.0E-03	7.7E-03	
88.0	2.3E-03 *±(2.2E-03)*	2.862E-03	6.2E-03	9.4E-03	10.0E-03	

Table 4.8: Tabulated values of the experimental rate constant ($k_{Experimental}$), calculated values using the Arrhenius fit ($k_{Arrhenius}$), and calculations, of increasing complexity, ($k_{Diffusion}$, k_{Slip}, $k_{Akgerman}$) for the diffusion-controlled reaction model between iso-CH_2Br--I and CH_2BrI in 2-butanol. Also included is the value for $k_{Spectral}$ determined from time-delayed spectral measurements.

METHANOL

In methanol, all three approximations overestimated the values for the diffusion-controlled rate constant at all temperatures (Table 4.9). In fact, it is clear from Figure 4.17 that the decay of iso-CH_2Br--I in methanol has no significant temperature dependence. A possible explanation is complexation of the solute species made possible by the smaller solvent molecules. The complexes formed would result in contact pairs which would react almost instantaneously with no need to diffuse. If this

is the case, then the decay of iso-CH_2Br--I is not diffusion controlled, but rather an intrinsic bimolecular reaction. This theory would explain why all three approximations for the diffusion-controlled rate constant did not succeed in replicating the experimental results. The value for $k_{Spectral}$ lying well beneath all calculated values provides further evidence that the primary mechanism for decay at room temperature and lower concentration is not a diffusion-controlled reaction.

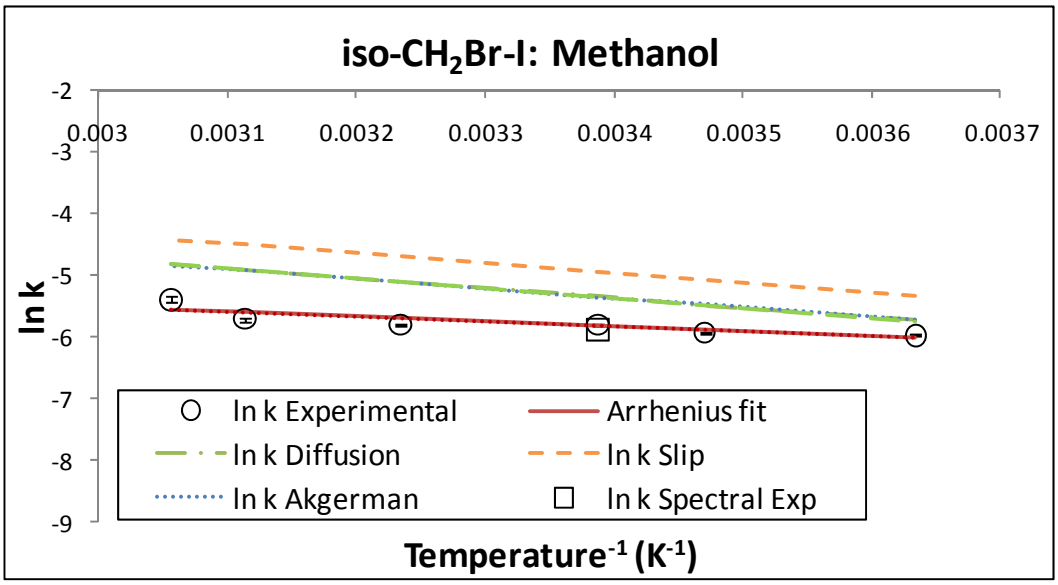

Figure 4.17: ln k vs T^{-1} plot of iso-CH_2Br--I decay rate constants in methanol determined experimentally ($k_{Experimental}$, open circles), from an Arrhenius fit to the experimental values (solid red), and calculated values $k_{Diffusion}$ (dash-dot green), k_{Slip} (orange dashed) and $k_{Akgerman}$ (dotted blue), and the experimental value of $k_{Spectral}$ (black box).

Rate Constants - Methanol

Temp (°C)	$k_{Experimental}$ ±(error) (ps^{-1})	$k_{Arrhenius}$ (ps^{-1})	$k_{Diffusion}$ (ps^{-1})	k_{Slip} (ps^{-1})	$k_{Akgerman}$ (ps^{-1})	$k_{Spectral}$ (ps^{-1})
2.0	2.5E-03 *±(2.9E-05)*	2.368E-03	3.2E-03	4.8E-03	3.2E-03	
15.0	2.6E-03 *±(2.6E-05)*	2.708E-03	4.0E-03	6.2E-03	4.1E-03	
22.0	3.0E-03 *±(6.4E-05)*	2.896E-03	4.7E-03	7.0E-03	4.6E-03	2.7E-03
36.0	3.0E-03 *±(7.3E-05)*	3.282E-03	5.9E-03	8.9E-03	5.9E-03	
48.0	3.3E-03 *±(1.1E-04)*	3.622E-03	7.2E-03	11.0E-03	7.2E-03	
54.0	4.5E-03 *±(2.2E-04)*	3.795E-03	7.9E-03	12.0E-03	7.8E-03	

Table 4.9: Tabulated values of the experimental rate constant ($k_{Experimental}$), calculated values using the Arrhenius fit ($k_{Arrhenius}$), and calculations, of increasing complexity, ($k_{Diffusion}$, k_{Slip}, $k_{Akgerman}$) for the diffusion-controlled reaction model between iso-CH_2Br--I and CH_2BrI in methanol. Also included is the value for $k_{Spectral}$ determined from time-delayed spectral measurements.

ACETONITRILE

In acetonitrile, the results are quite similar to those observed for methanol. All three approximations for the diffusion coefficient lead to rate constants which overestimate the experimental rate constants across the temperature range (Table 4.10). In addition, the approximations suggest a temperature dependence to the decay of iso-CH_2Br--I (Figure 4.18) in acetonitrile. However, as was the case in methanol, there does not seem to be a temperature dependence to the experimentally determined rate constants. We propose that all three approximations overestimate the temperature dependence because, like in methanol, iso-CH_2Br--I is complexed with CH_2BrI and decays without need to diffuse.

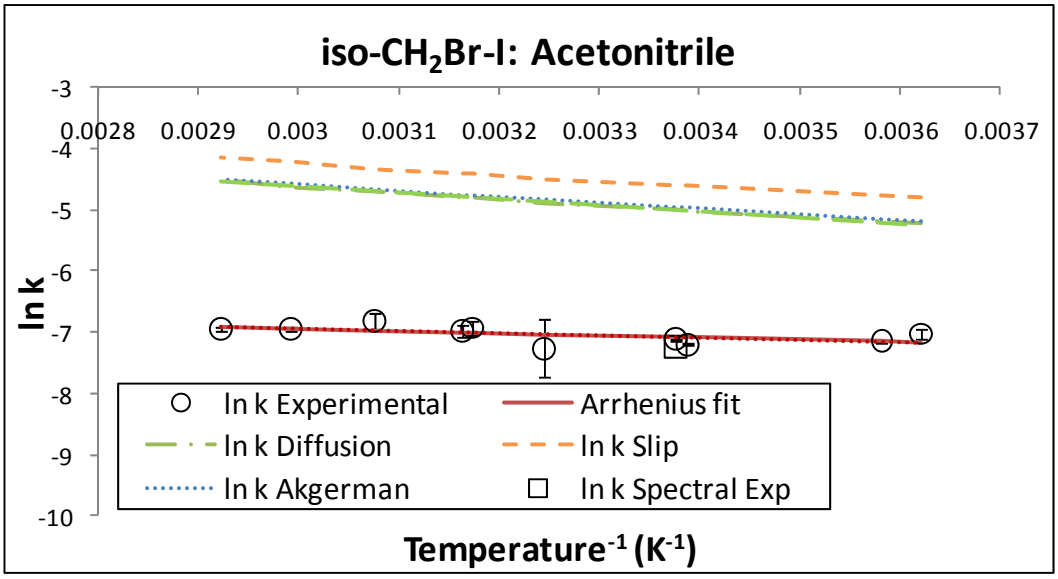

Figure 4.18: ln k vs T-1 plot of iso-CH_2Br--I decay rate constants in acetonitrile determined experimentally ($k_{Experimental}$, open circles), from an Arrhenius fit to the experimental values (solid red), and calculated values $k_{Diffusion}$ (dash-dot green), k_{Slip} (orange dashed) and $k_{Akgerman}$ (dotted blue), and the experimental value of $k_{Spectral}$ (black box).

Rate Constants - Acetonitrile

Temp (°C)	$k_{Experimental}$ ±(error) (ps^{-1})	$k_{Arrhenius}$ (ps^{-1})	$k_{Diffusion}$ (ps^{-1})	k_{Slip} (ps^{-1})	$k_{Akgerman}$ (ps^{-1})	$k_{Spectral}$ (ps^{-1})
3.0	0.88E-03 *±(6.1E-05)*	0.77E-03	5.4E-03	8.1E-03	5.6E-03	
6.0	0.78E-03 *±(1.7E-05)*	0.78E-03	5.6E-03	8.4E-03	5.8E-03	
22.0	0.75E-03 *±(1.9E-05)*	0.84E-03	6.6E-03	9.9E-03	6.9E-03	0.7E-03
23.0	0.81E-03 *±(1.3E-05)*	0.84E-03	6.7E-03	10.0E-03	6.9E-03	
35.0	0.69E-03 *±(3.3E-04)*	0.88E-03	7.5E-03	11.0E-03	7.9E-03	
42.0	0.97E-03 *±(9.7E-05)*	0.90E-03	8.1E-03	12.0E-03	8.4E-03	
43.0	0.93E-03 *±(8.5E-05)*	0.90E-03	8.2E-03	12.0E-03	8.5E-03	
52.0	1.09E-03 *±(1.3E-04)*	0.93E-03	9.0E-03	13.0E-03	9.4E-03	
61.0	0.96E-03 *±(3.6E-05)*	0.96E-03	9.8E-03	15.0E-03	10.0E-03	
69.0	0.95E-03 *±(3.9E-05)*	0.98E-03	11.0E-03	16.0E-03	11.0E-03	

Table 4.10: Tabulated values of the experimental rate constant ($k_{Experimental}$), calculated values using the Arrhenius fit ($k_{Arrhenius}$), and calculations, of increasing complexity, ($k_{Diffusion}$, k_{Slip}, $k_{Akgerman}$) for the diffusion-controlled reaction model between iso-CH_2Br--I and CH_2BrI in methanol. Also included is the value for $k_{Spectral}$ determined from time-delayed spectral measurements.

SUMMARY AND CONCLUSIONS

The calculations performed to estimate the diffusion-controlled rate constants took in to account temperature, concentration, solvent polarity, the temperature dependence of the viscosity and the sizes of the molecules involved. Rate constants calculated for a diffusion-controlled bimolecular reaction between iso-CH_2Br--I and CH_2BrI were performed using three different approximations for the diffusion coefficient of the solute particles. Comparison of the rate constants measured by temperature-dependent transient absorption scan and time-delayed spectral measurements suggest that at concentrations ≤135mM iso-CH_2Br--I decays primarily through a solvent-assisted isomerization in 2-butanol at room temperature. For concentrations >135mM the decay of iso-CH_2Br--I is dominated by a diffusion-limited bimolecular collision with another species in 1-and 2-butanol.

In methanol and acetonitrile, the solvent molecules are substantially smaller than the butanols and comparable to the CH_2BrI solute. The smaller solvent molecules, in conjunction with the high solute concentrations, make it more likely that the main decay pathway is through bimolecular reaction between contact pairs formed through solute molecule complexes. Reaction between the contact pairs occurs rapidly, with little to no diffusion which would explain the temperature independence of the measured rate constants in both methanol and acetonitrile.

FUTURE WORK

As previously mentioned, spectral measurements taken at concentrations of 8, 15 and 33mM seemed to free of any diffusion-controlled reactions. This suggests that concentration-dependent measurements may be taken to determine at what concentration the diffusion-controlled reaction becomes the dominant decay mechanism for iso-CH_2Br--I. With the correct sample concentration, the intrinsic barrier (if any) for the decay of iso-CH_2Br--I can be measured using temperature-dependent transient absorption measurements. A comparison of barrier heights in various solvents may then be performed to determine if there are extrinsic barriers to the decay of the metastable species.

Chapter 5. SUMMARY AND FUTURE WORK

In the preceding chapters the results of temperature-dependent transient absorption spectroscopic studies were presented. Those studies set out to determine the presence of reaction barriers and determine the relative heights of these barriers in three different molecular systems. In addition, the solvent environment was varied to determine the extent to which the reaction surfaces are affected by the surroundings. Each system was investigated in a range of solvents with different polarities and viscosities.

CIS-1,3,5-HEXATRIENE (Z-HT)

The influence of solvent on the cZt-HT → tZt-HT (Figure 5.1) isomerization barrier was investigated through measurements performed in methanol, propanol, cyclohexane and hexadecane. The measurements showed that the barrier for the cZt→tZt conformational isomerization is 25% lower in alcohols (ca. 1450 cm^{-1}, 17.4 kJ/mol) than in alkanes (ca. 1950 cm^{-1}, 23.5 kJ/mol). Fits to the data also yielded equilibrium Arrhenius prefactors which were an order of magnitude smaller for alcohols (ca. 4×10^{12} s^{-1}) than alkanes (ca. 6×10^{13} s^{-1}). The absolute rate of decay was faster in the

alkanes than in the alcohol solvents and was independent of the solvent viscosity. These results contrast with earlier observations where Z-HT was found to relax and thermalize more quickly in alcohol solvents than in alkane solvents.[39,56,63] Values for A_h in the alkane solvents were also found to be an order of magnitude larger than predicted by simple transition state theory. The data is independent of solvent viscosity and so the results cannot be attributed to an activated viscous friction on the reactive motion.

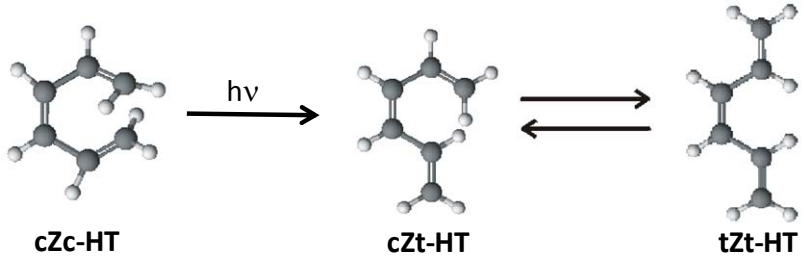

Figure 5.1: Outline of isomerization of cZt-HT to tZt-HT following direct excitation of cZc-HT (Z-HT)

Results of calculations performed using a continuum solvent model were then presented. These calculations failed to improve the agreement with the experiment data. As a result of the discrepancies, it was determined that calculations beyond the scope of Gaussian were necessary to explain the experimental results.

Molecular dynamic simulations of the cZt→tZt-HT isomerization in both cyclohexane and methanol were performed by the Geva group. The results were able to replicate a faster relaxation in methanol compared to cyclohexane and tentatively assigned it as an entropic effect. In the model, cyclohexane molecules were shown to more easily envelop the cZt-HT molecule, effectively stabilizing the isomer and lowering

the barrier to isomerization. However, in addition to stabilization, the close packing between cyclohexane and cZt-HT molecules inhibited the bond rotation to form tZt-HT. The inhibited motion caused a lower the rate of isomerization in cyclohexane compared to methanol as well determined that the reaction dynamics were affected by solvent type rather than viscosity or polarity [13,90].

7-DEHYDROCHOLESTEROL (DHC)

Measurements of the excited state dynamics of 7-dehydrocholetesterol (Figure 5.2) in methanol, ethanol, 1-propanol, 1-butanol, 2-butanol, n-heptane and n-hexadecane were reported in Chapter 3. The temperature dependence of the excited state decay in each solvent suggests an intrinsic intramolecular barrier to ring-opening as well as a solvent dependent barrier arising from the friction of the environment on the reaction coordinate. The effective barrier in the low viscosity solvents set an upper limit for the intrinsic barrier of *ca*. 4 kJ/mol. A simple model for the influence of the solvent provided an estimate for the intrinsic barrier of 1.8 ± 0.9 kJ/mol. When the results of these studies were then combined with additional [21] experimental work it was concluded that the excited state surface of 7-dehydrocholesterol is much more complicated than initially presumed. In fact, it is proposed that the excited state absorption decays through one of two models presented.

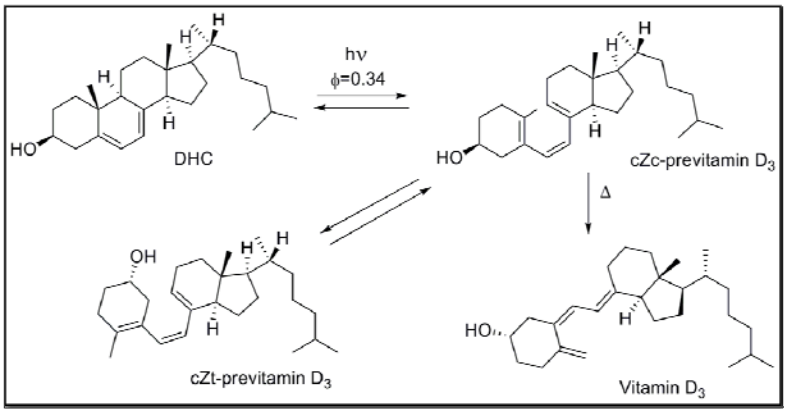

Figure 5.2: The provitamin D_3 7-dehydrocholesterol (DHC) molecule undergoes a photochemical ring-opening reaction to form cZc-previtamin D_3 which undergoes conformational relaxation producing an equilibrium mixture of the cZc and cZt conformers. The cZc-previtamin D_3 undergoes a hydrogen transfer and electronic rearrangement to form vitamin D_3.

ISO-BROMOIODOMETHANE (ISO-CH_2BR—I)

The effects of solvent on the decay of iso-CH_2Br—I were measured in 1-butanol, 2-butanol, methanol and acetonitrile (Figure 5.3). The measured rate constants were compared to calculations which assumed a diffusion-controlled bimolecular reaction between iso-CH_2Br-I and CH_2BrI. The estimated rate constants for the diffusion-controlled bimolecular reaction were performed using three different approximations for the diffusion coefficient of the solute particles. The estimated decay constants were also compared to broadband spectral measurements performed in each of the solvents.

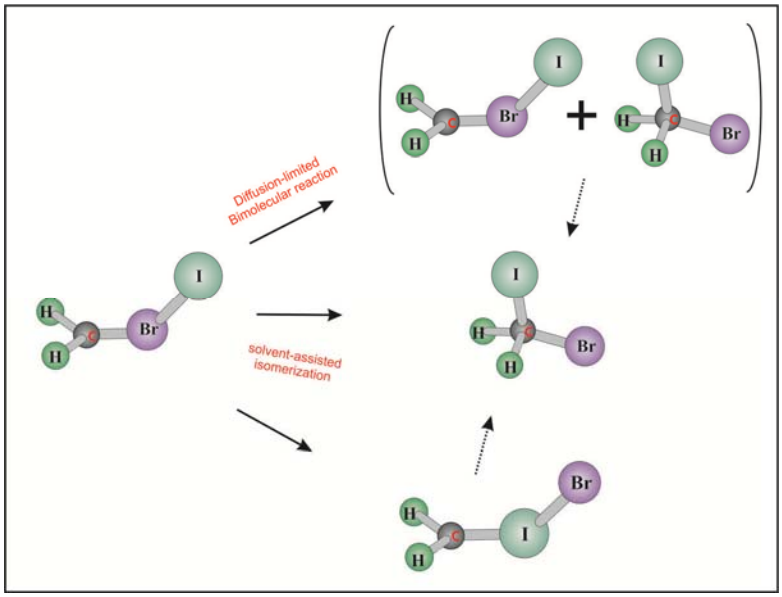

Figure 5.3: Suggested decay pathways for iso-CH_2Br—I through solvent assisted isomerization and diffusion-limited bimolecular reaction with CH_2BrI

The comparison of the calculated and experimental rate constants suggested that at concentrations <<135mM iso-CH_2Br--I decays primarily through a solvent-assisted 'unimolecular' isomerization in 2-butanol at room temperature. At concentrations ≥135mM the decay of iso-CH_2Br--I appears to occur predominately through a diffusion-limited bimolecular collision with another CH_2BrI molecule in 1-and 2-butanol. In methanol and acetonitrile, the measured rate constants displayed little to no temperature dependence and so the diffusion-limited mechanism was ruled out. It was replaced with a model where iso-CH_2Br—I decayed through the interaction of contact pairs formed when the iso and parent species complexed with one another. Spectral measurements taken at concentrations of 8, 15 and 33mM appear to be free of any diffusion-controlled reactions.

FUTURE WORK

The results and interpretations presented have provided some interesting insights but there is still more knowledge to be extracted from these systems. Thus far modeling of the hexatriene system has only replicated experimental results for cyclohexane. Further modeling is being conducted by the Geva group and compared to data obtained in methanol, propanol and hexadecane. In addition, measurements spanning a larger range of solvents may prove useful for comparison to future simulations. Some solvents that would be advantageous to pursue experiments in would be acetonitrile, 2-butanol and heptane. Such a study could help to explain the observed trends and assess the extent to which molecular packing affects the isomerization dynamics of the hexatriene molecule.

For 7-dehydrocholesterol calculations of the structure of the excited state surface and barriers on that surface need to be performed. This information can then be paired with molecular dynamics simulations to give a more detailed understanding of the extrinsic barrier we observed as well as the interactions which give rise to it. More specifically, a better understanding of the surface may explain whether the excited state absorption decays through the parallel or sequential models suggested and why.

The decay of iso-CH_2Br—I was measured at relatively high concentrations. In the high concentration regime it was determined that the diffusion-limited reaction between iso-CH_2Br—I and CH_2BrI is the dominant decay pathway in 1- and 2-butanol.

Preliminary concentration measurements by Anderson et al[121] has suggested that additional decay mechanisms for the iso species may exist and are only observable at much lower concentrations. Additional concentration dependent measurements should be performed and the concentration at which the diffusion-controlled reaction becomes less significant should be determined. Temperature-dependent measurements could then be performed at those concentrations to measure any barriers. It would be useful to perform these additional measurements in the solvents presented in this work for comparison. In addition, solvents of varying viscosity, polarity and molecular volume should be used, the effects on said barriers measured and the data gathered used to gain some insight into the reaction energy surface. Additional studies of the decay of iso-CH_2Br—I may also shed some light on why the decay is essentially barrierless in acetonitrile and methanol.

In addition to more experiments, the study of the decay of iso-CH_2Br—I may also benefit from additional theoretical work. The three methods implemented here overestimated the temperature dependence of the decay; particularly in methanol and acetonitrile. Molecular dynamics simulations might help to better explain the lack of temperature dependence in those solvents as well as the overestimations in the calculations presented here.

BIBLIOGRAPHY

(1) Roth, H. D.; Schilling, M. L. M.; Gassman, P. G.; Smith, J. L. *Journal of the American Chemical Society* **1984**, *106*, 2711.

(2) Carpenter, L. J.; Sturges, W. T.; Penkett, S. A.; Liss, P. S.; Alicke, B.; Hebestreit, K.; Platt, U. *Journal of Geophysical Research-Atmospheres* **1999**, *104*, 1679.

(3) Class, T. H.; Ballschmiter, K. *Journal of Atmospheric Chemistry* **1988**, *6*, 35.

(4) Klick, S.; Abrahamsson, K. *Journal of Geophysical Research-Oceans* **1992**, *97*, 12683.

(5) Moore, R. M.; Webb, M.; Tokarczyk, R.; Wever, R. *Journal of Geophysical Research-Oceans* **1996**, *101*, 20899.

(6) Mossinger, J. C.; Shallcross, D. E.; Cox, R. A. *Journal of the Chemical Society-Faraday Transactions* **1998**, *94*, 1391.

(7) Odelius, M.; Kadi, M.; Davidsson, J.; Tarnovsky, A. N. *Journal of Chemical Physics* **2004**, *121*, 2208.

(8) Scaiano, J. C.; Bucher, G.; Barra, M.; Weldon, D.; Sinta, R. *J. Photochem. Photobiol. A-Chem.* **1996**, *102*, 7.

(9) Abrashkevich, D. G.; Shapiro, M.; Brumer, P. *Journal of Chemical Physics* **2002**, *116*, 5584.

(10) Butler, L. J.; Hintsa, E. J.; Lee, Y. T. *Journal of Chemical Physics* **1986**, *84*, 4104.

(11) Liu, Y. J.; Ajitha, D.; Krogh, J. W.; Tarnovsky, A. N.; Lindh, R. *Chemphyschem* **2006**, *7*, 955.

(12) Anderson, N. A.; Pullen, S. H.; Walker, L. A.; Shiang, J. J.; Sension, R. J. *Journal of Physical Chemistry A* **1998**, *102*, 10588.

(13) Harris, D. A., Orozco, M. B.,Sension, R. J. *Journal of Physical Chemistry A* **2006**, *110*, 9325.

(14) Virshup, A. M.; Punwong, C.; Pogorelov, T. V.; Lindquist, B. A.; Ko, C.; Martinez, T. J. *Journal of Physical Chemistry B* **2009**, *113*, 3280.

(15) Sundstrom, V. *Annual Review of Physical Chemistry* **2008**, *59*, 53.

(16) Ritter, E.; Przybylski, P.; Brzezinski, B.; Bartl, F. *Current Organic Chemistry* **2009**, *13*, 241.

(17) Anderson, N. A.; Sension, R. J. In *Liquid Dynamics: Experiment, Simulation, and Theory*; Fourkas, J. T., Ed.; American Chemical Society: Washington, D.C., 2002; Vol. 820, p 148.

(18) Anderson, N. A.; Shiang, J. J.; Sension, R. J. *Journal of Physical Chemistry A* **1999**, *103*, 10730.

(19) Fuss, W.; Lochbrunner, S. *J. Photochem. Photobiol. A-Chem.* **1997**, *105*, 159.

(20) Fuss, W.; Hofer, T.; Hering, P.; Kompa, K. L.; Lochbrunner, S.; Schikarski, T.; Schmid, W. E. *Journal of Physical Chemistry* **1996**, *100*, 921.

(21) Tang, K.-C., Rury, Aaron, Orozco, Michael B., Egendorf, Joshua, Spears, Kenneth G., Sension, Roseane J. *Journal of Chemical Physics (submitted for publication)* **2010**.

(22) Tang, K. C.; Peng, J.; Spears, K. G.; Sension, R. J. *Journal of Chemical Physics* **2010**, *132*.

(23) Zheng, X. M.; Phillips, D. L. *Journal of Chemical Physics* **2000**, *113*, 3194.

(24) Wang, D. Q.; Phillips, D. L.; Fang, W. H. *Physical Chemistry Chemical Physics* **2002**, *4*, 5059.

(25) Minnaard, N. G., E. Havinga *Recueil Des Travaux Chimiques Des Pays-Bas-Journal Of The Royal Netherlands Chemical Society* **1973**, *92*, 1315.

(26) Trulson, M. O., G. D. Dollinger, R. A. Mathies *Journal of the American Chemical Society* **1987**, *109*, 586.

(27) Reid, P. J., S. J. Doig, R. A. Mathies *Chemical Physics Letters* **1989**, *156*, 163.

(28) Trulson, M. O., Dollinger, G. D., Mathies, R. A. *Journal of Chemical Physics* **1989**, *90*, 4274.

(29) Celani, P., S. Ottani, M. Olivucci, F. Bernardi, M. A. Robb *Journal of the American Chemical Society* **1994**, *116*, 10141.

(30) Reid, P. J., Lawless, M. K., Wickham, S. D., Mathies, R. A. *Journal of Physical Chemistry* **1994**, *98*, 5597.

(31) Hayden, C. C., D. W. Chandler *Journal of Physical Chemistry* **1995**, *99*, 7897.

(32) Pullen, S. H., Walker II, L. A., Donovan, B., Sension, R. J. *Chemical Physics Letters* **1995**, *242*, 415.

(33) Celani, P., Bernardi, F., Robb, M. A.,Olivucci, M. *Journal of Physical Chemistry* **1996**, *100*, 19364.

(34) Fuss, W., T. Schikarski, W. E. Schmid, S. Trushin, K. L. Kompa *Chemical Physics Letters* **1996**, *262*, 675.

(35) Ohta, K., Y. Naitoh, K. Saitow, K. Tominaga, N. Hirota, K. Yoshihara *Chemical Physics Letters* **1996**, *256*, 629.

(36) Fuss, W., Schikarski, T., Schmid, W. E., Trushin, S. A., Hering, P., Kompa, K. L. *Journal of Chemical Physics* **1997**, *106*, 2205.

(37) Garavelli, M., P. Celani, M. Fato, M. J. Bearpark, B. R. Smith, M. Olivucci, M. A. Robb *Journal of Physical Chemistry A* **1997**, *101*, 2023.

(38) Kauffmann, E., H. Frei, R. A. Mathies *Chemical Physics Letters* **1997**, *266*, 554.

(39) Lochbrunner, S., W. Fuss, K. L. Kompa, W. E. Schmid *Chemical Physics Letters* **1997**, *274*, 491.

(40) Trushin, S. A., Fuss, W., Schikarski, T., Schmid, W. E., Kompa, K. L. *Journal of Chemical Physics* **1997**, *106*, 9386.

(41) Anderson, N. A., S. H. Pullen, Walker II, L. A., Shiang, J. J., Sension, R. J. *Journal of Physical Chemistry A* **1998**, *102*, 10588.

(42) Pullen, S. H., Anderson, N. A., Walker II, L. A., Sension, R. J. *Journal of Chemical Physics* **1998**, *108*, 556.

(43) Ohta, K., Naitoh, Y., Tominaga, K., Hirota, N., Yoshihara, K. *Journal of Physical Chemistry A* **1998**, *102*, 35.

(44) Lochbrunner, S., Fuss, W., Schmid, W. E., Kompa, K. L. *Journal of Physical Chemistry A* **1998**, *102*, 9334.

(45) Henseler, D., Auer, A., Hohlneicher, G. *Journal of Information Recording* **1998**, *24*, 123.

(46) Henseler, D., R. Rebentisch, G. Hohlneicher *International Journal Of Quantum Chemistry* **1999**, *72*, 295.

(47) Anderson, N. A., C. G. Durfee, M. M. Murnane, H. C. Kapteyn, R. J. Sension *Chemical Physics Letters* **2000**, *232*, 365.

(48) Fuss, W., Schmid, W. E., Trushin, S. A., *Journal of Chemical Physics* **2000**, *112*, 8347.

(49) Garavelli, M., Page., C. S., Celani, P., Olivucci, M., Schmid, W. E., Trushin, S. A., Fuss, W. *Journal of Physical Chemistry A* **2001**, *105*, 4458.

(50) Pullen, S. H., Anderson, N. A., Walker II, L. A., Sension, R. J. *Journal of Chemical Physics* **1997**, *107*, 4985.

(51) Braun, M., Fuss, W., Kompa, K. L., Wolfrum, J. *J. Photochem. Photobiol. A-Chem.,* **1991**, *61.*, 15.

(52) Fuss, W., Hofer, T., Hering, P., Kompa, K. L., Lochbrunner, S., Schikarski, T., Schmid, W. E. *Journal of Physical Chemistry* **1996**, *100*, 921.

(53) Fuss, W., Lochbrunner, S. *J. Photochem. Photobiol. A-Chem.,* **1997**, *105*, 159.

(54) Anderson, N. A., Shiang, J. J., Sension, R. J. *Journal of Physical Chemistry A* **1999**, *103*, 10730.

(55) Anderson, N. A. a. S., R. J. In *Liquid Dynamics: Experiment, Simulation, and Theory.*; Fourkas, J., Ed.; ACS: 2002, p 148.

(56) Anderson, N. A., Pullen, S. H., Walker, L. A., Shiang, J. J., Sension, R. J. *Journal of Physical Chemistry A* **1998**, *102*, 10588.

(57) Pullen, S. H., Anderson, N. A., Walker, L. A., Sension, R. J. *Journal Of Chemical Physics* **1998**, *108*, 556.

(58) Hanggi, P., P. Talkner, M. Borkovec *Reviews Of Modern Physics* **1990**, *62*, 251.

(59) In *CRC Handbook of Chemistry & Physics, Internet Version*; 86 ed.; Lide, D. R., Ed.; Taylor and Francis: Boca Raton, FL, 2006.

(60) Chandrasekhar, S.; Narsihmulu, C.; Sultana, S. S.; Reddy, M. S. *Tetrahedron Lett.* **2004**, *45*, 9299.

(61) Danishefsky, S. J.; Yamashita, D. S.; Mantlo, N. B. *Tetrahedron Lett.* **1988**, *29*, 4681.

(62) Hwa, J. C. H.; Debenneville, P. L.; Sims, H. J. *Journal of the American Chemical Society* **1960**, *82*, 2537.

(63) Harris, D. A.; Orozco, M. B.; Sension, R. J. *Journal of Physical Chemistry A* **2006**, *110*, 9325.

(64) Chandrasekhar, S. *Reviews of Modern Physics* **1943**, *15*, 1.

(65) Lochbrunner, S.; Fuss, W.; Schmid, W. E.; Kompa, K. L. *Journal of Physical Chemistry A* **1998**, *102*, 9334.

(66) Kohler, J. R. A. a. B. E. *Journal of Chemical Physics* **1984**, *80*, 45.

(67) Engeln, R., Consalvo, D., Reuss, J. *Chemical Physics* **1992**, *160*, 427.

(68) Fabiano, E. a. D. S., F. *Chemical Physics Letters* **2006**, *418*, 496.

(69) Rothenberger, G., Negus, D. K., Hochstrasser, R. M. *Journal of Chemical Physics* **1983**, *79*, 5360.

(70) Sundstrom, V., T. Gillbro *Chemical Physics Letters* **1984**, *109*, 538.

(71) Courtney, S. H. a. F., G. R. *Journal of Chemical Physics* **1985**, *83*, 215.

(72) Lee, M. Y., Holtom, G. R., Hochstrasser, R. M. *Chemical Physics Letters* **1985**, *118*, 359.

(73) Balk, M. W., Fleming, G. R. *Journal of Physical Chemistry* **1986**, *90*, 3975.

(74) Courtney, S. H., Balk, M. W., Philips, L. A., Webb, S. P., Yang, D., Levy, D. H., Fleming, G. R. *Journal of Chemical Physics* **1988**, *89*, 6697.

(75) Kim, S. K.; Fleming, G. R. *Journal of Physical Chemistry* **1988**, *92*, 2168.

(76) Kim, S. K.; Courtney, S. H.; Fleming, G. R. *Chemical Physics Letters* **1989**, *159*, 543.

(77) Lee, M. Y., Haseltine, J. N., Smith, A. B., Hochstrasser, R. M. *Journal of the American Chemical Society* **1989**, *111*, 5044.

(78) Saltiel, J., Sun, Y. P. *Journal of Physical Chemistry* **1989**, *93*, 6246.

(79) Sun, Y. P., Saltiel, J. *Journal of Physical Chemistry* **1989**, *93*, 8310.

(80) Sun, Y. P., Saltiel, J., Park, N. S., Hoburg, E. A., Waldeck, D. H. *Journal of Physical Chemistry* **1991**, *95*, 10336.

(81) Schroeder, J., Troe, J., Vohringer, P. *Chemical Physics Letters* **1993**, *203*, 255.

(82) Waldeck, D. H. *Journal of Molecular Liquids* **1993**, *57*, 127.

(83) Schroeder, J., Schwarzer, D., Troe, J., Vohringer, P. *Chemical Physics Letters* **1994**, *218*, 43.

(84) Schroeder, J., Troe, J., Vohringer, P. *Zeitschrift Fur Physikalische Chemie-International Journal of Research in Physical Chemistry & Chemical Physics* **1995**, *188*, 287.

(85) Meyer, A., Schroeder, J., Troe, J., Votsmeier, M. *J. Photochem. Photobiol. A-Chem.* **1997**, *105*, 345.

(86) Meyer, A., Schroeder, J., Troe, J. *Journal of Physical Chemistry A* **1999**, *103*, 10528.

(87) Schroeder, J., Steinel, T., Troe, J. *Journal of Physical Chemistry A* **2002**, *106*, 5510.

(88) S. K. Kim, S. H. C., G. R. Fleming *Chemical Physics Letters* **1989**, *159*, 543.

(89) Maroncelli, M. *Journal of Chemical Physics* **1997**, *106*, 1545.

(90) Vazquez, F. X. Ph. D. Dissertation, University of Michigan, 2010.

(91) Kramers, H. A. *Physica* **1940**, *7*, 284.

(92) Akesson, E., Hakkarainen, A., Laitinen, E., Helenius, V., Gillbro, T., Korppi-Tommola, J., Sundstrom, V. *Journal of Chemical Physics* **1991**, *95*, 6508.

(93) Richard F. Grote, J. T. H. *Journal of Chemical Physics* **1981**, *74*, 4465.

(94) Grote, R. F., Vanderzwan, G., Hynes, J. T. *Journal of Physical Chemistry* **1984**, *88*, 4676.

(95) Grote, R. F., Hynes, James T. *Journal of Chemical Physics* **1980**, *73*, 2715.

(96) Dauben, W. G.; Share, P. E.; Ollmann, R. R. *Journal of the American Chemical Society* **1988**, *110*, 2548.

(97) Havinga, E.; Dekock, R. J.; Rappoldt, M. P. *Tetrahedron* **1960**, *11*, 276.

(98) Dmitrenko, O.; Reischl, W. *Theochem-Journal of Molecular Structure* **1998**, *431*, 229.

(99) Dmitrenko, O. G.; Terenetskaya, I. P.; Reischl, W. *J. Photochem. Photobiol. A-Chem.* **1997**, *104*, 113.

(100) Terenetskaya, I. P. *Theoretical and Experimental Chemistry* **2008**, *44*, 286.

(101) Dauben, W. G.; Zhou, B. L.; Lam, J. Y. L. *Journal of Organic Chemistry* **1997**, *62*, 9005.

(102) Braun, M.; Fuss, W.; Kompa, K. L.; Wolfrum, J. *J. Photochem. Photobiol. A-Chem.* **1991**, *61*, 15.

(103) Jacobs, H. J. C. *Pure and Applied Chemistry* **1995**, *67*, 63.

(104) Saltiel, J.; Sun, Y. P. *Journal of Physical Chemistry* **1989**, *93*, 6246.

(105) Saltiel, J.; D'Agostino, J. T. *Journal of the American Chemical Society* **1972**, *94*, 6445.

(106) Harris, D. A.; Stickrath, A. B.; Carroll, E. C.; Sension, R. J. *Journal of the American Chemical Society* **2007**, *129*, 7578.

(107) Saltiel, J.; Waller, A. S.; Sears, D. F.; Garrett, C. Z. *Journal of Physical Chemistry* **1993**, *97*, 2516.

(108) Schroeder, J.; Troe, J.; Vohringer, P. *Chemical Physics Letters* **1993**, *203*, 255.

(109) Nakashima, N.; Meech, S. R.; Auty, A. R.; Jones, A. C.; Phillips, D. *Journal of Photochemistry* **1985**, *30*, 207.

(110) Choi, Y. K.; Koo, Y. M.; Jung, K. W. *J. Photochem. Photobiol. A-Chem.* **1999**, *127*, 1.

(111) Yang, C.; Sun, Y.; He, Y.; Ma, P. *Journal of Chemical & Engineering Data* **2008**, *53*, 293.

(112) Lee, S. J.; Bersohn, R. *Journal of Physical Chemistry* **1982**, *86*, 728.

(113) Heumann, K. G. *Analytica Chimica Acta* **1993**, *283*, 230.

(114) Tarnovsky, A. N.; Wall, M.; Gustafsson, M.; Lascoux, N.; Sundstrom, V.; Akesson, E. *Journal of Physical Chemistry A* **2002**, *106*, 5999.

(115) Butler, L. J.; Hintsa, E. J.; Shane, S. F.; Lee, Y. T. *Journal of Chemical Physics* **1987**, *86*, 2051.

(116) Man, S. Q.; Kwok, W. M.; Phillips, D. L. *Journal of Physical Chemistry* **1995**, *99*, 15705.

(117) Man, S. Q.; Kwok, W. M.; Phillips, D. L.; Johnson, A. E. *Journal of Chemical Physics* **1996**, *105*, 5842.

(118) Zheng, X. M.; Kwok, W. M.; Phillips, D. L. *Journal of Physical Chemistry A* **2000**, *104*, 10464.

(119) Kwok, W. M.; Ma, C. S.; Parker, A. W.; Phillips, D.; Towrie, M.; Matousek, P.; Zheng, X. M.; Phillips, D. L. *Journal of Chemical Physics* **2001**, *114*, 7536.

(120) Kwok, W. M.; Ma, C. S.; Phillips, D.; Parker, A. W.; Towrie, M.; Matousek, P.; Phillips, D. L. *Chemical Physics Letters* **2001**, *341*, 292.

(121) Anderson, C. a. A., N.; University of Michigan: Ann Arbor, 2010.

(122) Spears, K. G. a. S., J.; 1.8 ed. 1999.

(123) Jeffrey I. Steinfeld, J. S. F., William L. Hase *Chemical kinetics and dynamics*; Second ed.; Prentice-Hall, Inc., 1998.

(124) Stickrath, A. B.; Carroll, E. C.; Dai, X. C.; Harris, D. A.; Rury, A.; Smith, B.; Tang, K. C.; Wert, J.; Sension, R. J. *Journal of Physical Chemistry A* **2009**, *113*, 8513.

(125) Rice, S. A.; Kenneywallace, G. A. *Chemical Physics* **1980**, *47*, 161.

(126) Tyrrell, H. J. V. *Butterworth* **1984**, *ISSU*.

(127) Akgerman, A.; Gainer, J. L. *Journal of Chemical and Engineering Data* **1972**, *17*, 372.

(128) Akgerman, A.; Gainer, J. L. *Industrial & Engineering Chemistry Fundamentals* **1972**, *11*, 373.

(129) Gainer, J. L., Metzner, A. B., A.I.Ch.E.-Int. Chem. Eng. Symp. Ser. 6 (6), 74 *A.I.Ch.E - International Chemical engineering symposium* **1965**, *6*, 74.